5-1999

Multispecies contaminant transport in undisturbed columns of weathered fractured saprolite

Melanie A. Mayes

To the Graduate Council:

I am submitting herewith a thesis written by Melanie A. Mayes entitled "Multispecies contaminant transport in undisturbed columns of weathered fractured saprolite." I have examined the final electronic copy of this thesis for form and content and recommend that it be accepted in partial fulfillment of the requirements for the degree of Master of Science, with a major in Geology.

<div align="right">Claudia Mora, Major Professor</div>

We have read this thesis and recommend its acceptance:

Philip Jardine, Larry McKay

<div align="right">Accepted for the Council:
Carolyn R. Hodges</div>

<div align="right">Vice Provost and Dean of the Graduate School</div>

(Original signatures are on file with official student records.)
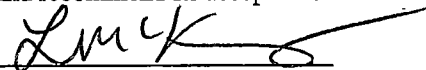
To the Graduate Council:
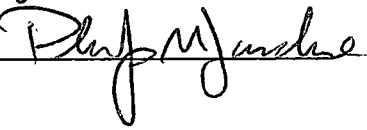
I am submitting herewith a thesis written by Melanie A. Mayes entitled "Multispecies Contaminant Transport in Undisturbed Columns of Weathered Fractured Saprolite." I have examined the final copy of this thesis for form and content and recommend that it be accepted in partial fulfillment of the requirements for the degree of Master of Science, with a major in Geology.

Claudia Mora, Major Professor

We have read this thesis
and recommend its acceptance:

Accepted for the Council:

Associate Vice Chancellor and
Dean of The Graduate School

Multispecies Contaminant Transport in Undisturbed Columns of Weathered Fractured Saprolite

A Thesis
Presented for the
Master of Science
Degree
The University of Tennessee, Knoxville

Melanie A. Mayes
May 1999

Dedication

This thesis is dedicated, with gratitude, to my parents, Mr. John L. Mayes and Mrs. Erma M. Mayes, for their unfailing support and encouragement of my endeavors. To my brother, Mr. Kevin E. Foss, I am grateful always for the influence he has had upon my life, his interest in mineralogy and his appreciation for the geology that surrounds us.

Acknowledgements

Abstract

Laboratory-scale tracer experiments were conducted to investigate the geochemical and hydrological processes that govern the fate and transport of organically-chelated radionuclides in clay-rich residual soils. Undisturbed columns (8.5 cm diameter x 15 cm length) of weathered, fractured shale saprolite were obtained from a proposed waste disposal site at the Oak Ridge National Laboratory. Single and multispecies saturated transport experiments were conducted to determine the rates and mechanisms governing the transport of $^{57,58}Co(II)EDTA^{2-}$, $^{57}Co(III)EDTA^{-}$, $^{109}CdEDTA^{2-}$, and $H^{51}CrO_4^{-}$. The transport of reactive contaminants through undisturbed, heterogeneous materials was affected by nonequilibrium conditions, as a result of physical processes, such as multi-region flow, or chemical processes, such as rate-limited sorption or transformation reactions. Geochemical reactions between soil mineral surfaces and chelated contaminants resulted in redox reactions and chelate dissociation, coupled with dissolution of soil minerals. $Co(II)EDTA^{2-}$ was oxidized to $Co(III)EDTA^{-}$, and a pulse of aqueous Mn suggested that surficial Mn(IV) oxides may have catalyzed the redox reaction. Subsurface Fe and Al oxides dissociated the $CdEDTA^{2-}$ chelate, resulting in the formation of $Fe(III)EDTA^{-}$, $Al(III)EDTA^{-}$, and uncomplexed Cd. The divalent Cd^{2+} was transported as a reactive cation, where stabilization may occur by adsorption to soil surfaces. The transport of Cr(VI) was governed by the reduction to Cr(III) in the presence of soil organic matter, followed by irreversible sorption and/or precipitation of the trivalent cation Cr^{3+}. Both Cr(VI) and Cr(III) were irreversibly sorbed, but the proportion of trivalent Cr was greater in a column amended with organic matter, which suggested that oxidation of organics catalyzed the reduction of Cr(VI). Nonequilibrium conditions during transport were identified using flow interruption, which allowed rate-limited processes to approach equilibrium. Results were modeled with a version of the convective-dispersive equation where flow was segregated into mobile and immobile flow regions. Optimization of the model was completed on the flow interrruption, to estimate the rate of diffusive mass transfer between the two regions. Retardation coefficients were obtained by fitting to the breakthrough curves. The results

indicated that physical nonequilibrium was significant during column transport studies, and that some geochemical reactions between soil and contaminants were rate-limited, which has implications for predictions of contaminant migration.

Table of Contents

List of Tables

List of Figures

1. Introduction

Weapons production and subsequent decontamination over the past four decades at Department of Energy (DOE) facilities has resulted in the production and disposal of complex mixtures of organically-chelated radionuclides and toxic metals. Decontamination efforts utilized organic chelating agents, particularly ethylenediaminetetraacetate (EDTA) salts, to remove the metals by forming stable, water-soluble complexes (Ayres, 1971). The contaminants were historically disposed in shallow burial trenches, but their migration into stream and ground water has been attributed to the enhanced mobility of chelated complexes (Means et al., 1978a; Means et al., 1978b; Olsen et al., 1986). The ^{60}Co radionuclide and the toxic metals Cd and Cr have been classified as priority pollutants in soils and groundwater because of their high toxicity, mobility and capacity for incorporation by plants and animals. Additionally, large inventories are present at many industrial and government waste sites (NRC, 1974; U.S. EPA, 1978). Prediction of contaminant mobility may be inhibited by poorly constrained stability of anionic chelate-metal complexes in the presence of the trench mineralogy. Trench excavations were typically in the residual of the Conasauga group, which consists of extensively weathered and fractured interbedded shales, siltstones, and limestones with secondary precipitates of reactive Mn, Fe, and Al hydroxides and oxides (Arnseth and Turner, 1988). The weathered bedrock, or saprolite, has a high capacity to adsorb metal cations, but reactions with the oxides/hydroxides may alter contaminant mobility. Subsurface migration of chelated contaminants, ^{60}Co(II)EDTA^{2-} and CdEDTA^{2-}, and anionic chromate (HCrO$_4^-$) may be affected by physical processes such as preferential flow and matrix diffusion, and chemical processes such as sorption, redox, and dissociation/complexation reactions. Understanding the rates and mechanisms of these pathways is paramount to remediation strategies, as well as preventing future contaminant migration.

Previous work

Geochemistry of Cd, Co, and Cr

The transport of CdEDTA^{2-} in the subsurface is not well characterized, and the behavior of Cd may be dependent upon specific interactions with soil minerals. The organic complexant, EDTA^{4-}, forms a strong bond with the metal, and thus, an exceedingly stable aqueous complex, which could accelerate its migration in the environment (Elliott and Denneny, 1982). The adsorption of Cd^{2+} has been observed to decrease in the presence of EDTA^{4-} (Chubin and Street, 1981; Elliott and Denneny, 1982). In addition, EDTA^{4-} does not readily degrade, and may therefore be persistent in the environment (Girvin et al., 1993; Li and Shuman, 1996). Therefore, the stability of the CdEDTA^{2-} complex may promote the migration of Cd in the subsurface. However, these effects may be counteracted by surface-mediated dissociation of CdEDTA^{2-}, and subsequent stabilization of the divalent Cd^{2+} cation by adsorption. Complex dissociation by soil Fe- and Al-oxides has been observed for other divalent metals, such as SrEDTA^{2-} (Jardine et al., 1993), as well as other metal-EDTA complexes, including Ca, Zn, Pb, and Ni (Nowack and Sigg, 1997). Thus, the EDTA^{4-} complex may enhance the migration of Cd^{2+} in the groundwater environment, while soil minerals may dissociate the complex, thus allowing Cd to participate in adsorption reactions as a divalent cation. However, the relative importance of these reactions in undisturbed materials has not been investigated, therefore, the rates and mechanisms governing the transport of CdEDTA^{2-} are relatively unknown.

The transport of ^{60}Co(II)EDTA^{2-} from waste disposal sites has been observed, and attributed to reactivity with subsurface minerals (Means et al., 1978a; Means et al., 1978b; Olsen et al., 1986). Subsurface Fe- and Al-oxides can dissociate the Co-EDTA complex, resulting in stabilization of Co^{2+} by adsorption (Girvin et al., 1993; Szecsody et al., 1994; Zachara et al., 1995; Nowack and Sigg, 1997). In the presence of Mn-oxides, however, dissociation of the Co-EDTA complex is inhibited by the production of Co(III)EDTA^{-}. It is believed that the oxidation of Co(II)EDTA^{2-} is controlled by a surface-mediated

reaction with MnO_2 (Jardine et al, 1993; Jardine and Taylor, 1995b; Zachara et al., 1995). Iron oxides can also catalyze the production of Co(III)EDTA·, but to a much lesser extent than MnO_2 (Brooks et al., 1996). These mechanisms may accelerate the transport of ^{60}Co from disposal sites, because of the high aqueous stability Co(III)EDTA· (Jardine et al., 1993; Jardine and Taylor, 1995a). The transport of Co(II)EDTA^{2-} was investigated to quantify the relative importance of these reactions through undisturbed columns of heterogeneous soils containing mixed oxides of Fe, Al, and Mn.

The behavior of aqueous Cr is highly dependent upon the state of oxidation, and there are several reactions with soil minerals that may alter the valence of Cr. Cr(VI) is quite mobile in the groundwater environment, because it is present in solution as an anionic complex, typically CrO_4^{2-} or $HCrO_4^-$; while cationic Cr^{3+} may exist in aqueous solution, or in several precipitated hydroxide minerals in association with Fe(III) (Richard and Bourg, 1991). The adsorption of Cr(VI) under oxic conditions has been observed (Zachara et al., 1989; Kent et al., 1995). However, Cr is a redox-sensitive element, and it is known that Cr(VI) may be reduced to the less mobile, and less toxic Cr(III) in the presence of aqueous phase Fe(II), Fe(II) bearing minerals, and organic matter (Bartlett and Kimble, 1976; Eary and Rai 1991; Anderson et al., 1994; Kent et al., 1994; Davis and Olsen, 1995). Davis and Olsen (1995) found that pump-and-treat remediation was successful at removing adsorbed $HCrO_4^-$ from soil surfaces; however, they also observed the stabilization of Cr(III), which was bound in $Cr,Fe(OH)_{3(s)}$ precipitates. The batch studies of Eary and Rai (1991) also observed the reduction of Cr(VI) and precipitation of Cr(III) in acidic soils, in the presence of both Fe(II) and organic matter. However, these studies are flawed by the abnormally low pH used by the authors (e.g., pH 2.8). At pH<3, Fe(II) bearing minerals dissolve and Cr(VI) is spontaneously reduced to Cr(III) in aqueous solution. The oxidation of Cr(III) to Cr(VI) can also occur, and it has been observed to be catalyzed by Mn-oxides (Bartlett and James, 1979; Fendorf and Zasoski, 1992). In the presence of dissolved organics, Cr(III) may remain soluble (James and Bartlett, 1983a) or become oxidized to Cr(VI) (James and Bartlett, 1983b). The behavior of Cr(VI) is complex, and is affected by the presence of organics or mixed oxides. Most studies, however, have been in batch systems or relatively clean sand and

gravel aquifers, thus, the redox and transport of Cr in heterogeneous systems that contain both organic matter and mixed oxides of Fe, Al, and Mn is relatively unknown.

Physical effects of heterogeneous materials

In addition to geochemical interactions, the physical characteristics of weathered and fractured media may exert considerable control on contaminant transport. In heterogeneous media, flow is distributed between pore classes, or between fractures and matrix, resulting in different rates of transport. Advective transport through fractures, bedding planes, and macropores can rapidly transport solutes from contaminated areas, while diffusion along concentration gradients may move solutes into the matrix (Jardine et al., 1990; Solomon et al., 1991). The field tracer experiment of Wilson et al. (1993) recorded a 47% loss of Br$^-$ to the Melton Branch saprolite, presumably due to diffusion into the matrix. The importance of diffusive processes in contaminant transport is further demonstrated by a comparison between the rate of transport of colloidal and solute tracers – the rates of migration of nonreactive tracers ^{18}O and Br$^-$ were two orders of magnitude less than the rate of colloid transport through a weathered and fractured clay till in Ontario (McKay et al., 1993). The difference in the rates of migration was attributed to diffusion of solutes into the matrix, while the colloids were excluded because of their larger size and slower diffusion coefficients. O'Brien et al. (1996) ran dual tracers, Br$^-$ and PFBA, with distinctly different diffusion coefficients, in addition to fluorescent microspheres and bacteriophage colloids through undisturbed Melton Branch columns. They too observed dramatic differences in the rate of migration of the colloids over the solute tracers through fractured media; and further, demonstrated that the observed difference was dependent upon the flow velocity. Experiments performed under lower flow rates resulted in increased diffusion of solute tracers into the matrix. Gaber et al. (1995), using undisturbed soil cores, observed tailing of ^{3}H$_2$O only at faster pore water velocities (greater than 0.74 cm h^{-1}), while tailing of atrazine, an organic pesticide, was observed at all velocities(0.12 to 2.16 cm h^{-1}). The ^{3}H$_2$O pulse exhibited tailing at only the higher flow rates, due to nonequilibrium between the preferential flow features and the matrix. The observed nonequilibrium behavior of atrazine at all velocities, however, was probably indicative of rate-limited sorption processes (Gaber et al., 1995).

4

Nonequilibrium due to flow conditions or rate-limited processes can be identified using a simple technique of flow interruption, because diffusional and chemical processes are allowed to approach equilibrium during the period of suspended flow (Brusseau et al., 1989; Brusseau et al., 1997). Nonequilibrium is identified by a perturbation in concentration of the solute when the flow is resumed. In the absense of advection, diffusive exchange occurs between the macropores and the micropores, resulting in an equilibration of solute concentrations (Reedy et al., 1996). The idea of flow interruption was originally developed in chemical engineering applications to distinguish between film diffusion and intra-aggregate diffusion (Kunin and Myers, 1947; Kressman and Kitchener, 1949). Flow interruption techniques have been applied to miscible displacement experiments to identify physical nonequilibria in heterogeneous media (Koch and Fluhler, 1993; O'Brien et al., 1996; Reedy et al., 1996), as well as chemical nonequilibria due to rate-limited sorption or transformation processes (Murali and Aylmore, 1980; Brusseau et al., 1991). Reedy et al. (1996) used flow interruption to identify physical nonequilibria in undisturbed saprolite columns over several different flow rates, and to subsequently quantify the rate of the diffusive mass transfer of Br$^-$ into the matrix during the interrupt period. Murali and Aylmore (1980) used a flow interruption technique on packed soil columns to identify kinetic limitations in the adsorption of common inorganic ions. Following the resumption of flow, they observed large perturbations in the concentration of phosphate and selenite, while no perturbations were observed in either sulfate or nonreactive ^3H_2O. Therefore, adsorption of phosphate and selenite were kinetically-limited, while adsorption of sulfate had reached equilibrium. Flow interruption has also been used to identify rate-limited partitioning of hydrophobic organic chemicals into soil organic matter (Brusseau et al., 1989; Brusseau et al., 1991). The existence of physical nonequilibrium may be significant during miscible displacement experiments through structured media, which can be identified by the method of flow interruption. In addition, the importance of rate-limited chemical processes, such as sorption or partitioning into organics, can be assessed.

The extent of physical or chemical nonequilibrium can be assessed using transport modeling, however, the assumption of local equilibrium is inherent in the application of the classical convective-dispersive (CD) equation. A viable strategy for the modeling of nonequilibrium transport utilizes a

5

modification of the CD equation that considers dual-region flow, combined with flow interruption, which provides insight about the exchange between regions. The concept of dual porosity assumes that flow through a fractured media can be represented by regions of mobile and immobile water (Selim et al., 1976; Parker and van Genuchten, 1984). It has been shown that the dual-region flow model is mathematically equivalent to an adsorption model, where adsorption on some sites is instantaneous, while on others it is kinetically-limited (Nkedi-Kizza et al., 1984). The CD equation is used to model the regions of mobile water (equilibrium sites), while immobile regions are represented by diffusion-type movement (kinetic sites). It should be noted that the proportion of mobile/immobile sites is dependent upon the pore-water velocity (van Genuchten and Wierenga, 1976; Akratanakul et al., 1983; Smettem, 1984; Lee et al., 1988). Flow interruption provides an opportunity to isolate the exchange of mass between the mobile and immobile regions in the absense of advective flow. During the interruption, the velocity term in the CD equation is eliminated, and the only operative process is the rate of mass transfer between the mobile and immobile regions. Reedy et al. (1996) were able to quantify the rate of transfer of Br⁻ between regions by using a two-region modeling strategy, where optimization of the coefficient of mass transfer was performed on the interruption perturbation. Nonequilibrium processes can be reproduced using a dual-region model, while quantifying the rate of exchange between the macro- and micropores during the interruption.

Objectives

The objective of this investigation is to provide an improved understanding and predictive capability of the coupled geochemical and hydrological processes that govern the fate and transport of chelated radionuclides and toxic metals in heterogeneous subsurface environments, including preferential flow, matrix diffusion, sorption, and oxidation-reduction reactions. A suite of single- and multispecies experiments will be conducted to quantify these effects during transport through undisturbed columns of weathered, fractured saprolite. Single-species transport of $CdEDTA^{2-}$ will be investigated (experiment 1), while that of $Co(II)EDTA^{2-}$ has been characterized by Jardine et al. (1993), with supporting batch experiments by Jardine and Taylor (1995a). Multispecies experiments will be conducted to examined the

6

co-transport behavior of CdEDTA^{2-} with Co(II)EDTA^{2-} (experiment 2), and CdEDTA^{2-}, Co(III)EDTA^{-}, and HCrO$_4^{-}$ (experiment 3). Two additional single-species experiments will be performed to identify the mechanisms governing Cr transport dynamics, a control Cr(VI) experiment (4), and Cr(VI) through an organic-amended column (experiment 5). Effluent breakthrough curves and solid-phase dissolution curves will be examined to determine the mechanisms governing the geochemical reactions between the chelated contaminants and the soil.

The rate of contaminant transport will be quantified using a dual-region version of the convective-dispersive equation capable of reproducing flow interruption (Selim et al., 1976). The breakthrough curve of a nonreactive tracer, Br^{-}, will be used to determine column hydraulic characteristics, including the dispersion coefficient and Peclet number. The rate of contaminant transport will be quantified with the retardation coefficient of the reactive contaminants. The results from the 5 experiments will be examined for consistency to determine the extent of competitive contaminant reactions. A flow interruption will be used to quantify the extent of physical and chemical nonequilibrium during transport, following the methods of Reedy et al. (1996). Physical nonequilibrium between preferential flow features and the matrix will be quantified using a Br^{-} tracer, while expanding the method to quantify chemical nonequilibrium processes as a result of rate-limited sorption or transformation reactions. Determination of the rates and mechanisms of contaminant transport will improve our ability to predict the behavior of chelated metals and radionuclides in the subsurface environment.

2. Materials and Methods

Site Characterization

The saprolite columns were obtained from the Melton Branch Watershed Experimental Station (MBWES), within the proposed solid waste storage area (SWSA-7) on the Oak Ridge Reservation approximately 10 km southwest of Oak Ridge, TN (Figure 1). The bedrock underlying the site is the mid- to late Cambrian Conasauga Group, which consists of six formations of interbedded fine-grained clastics and limestones, that compose a transgressive sequence and alternating carbonate platform (Hatcher et al., 1992). The geology is heterogeneous, as limestone, siltstone, and shale interfinger and grade into one another over very short distances (Hatcher et al., 1992). The reservation is located near the western edge of the Valley and Ridge physiographic province, where the Paleozoic sedimentary sequence has been extensively folded and faulted, as a result of thrusting from the southeast during the Alleghanian orogeny (Hatcher et al., 1992). The numerous folds, faults, and bedding planes have acted as conduits for infiltration, resulting in extensive weathering along fractured zones. The original structure of the parent material, including laminations, bedding planes, and folds, has been well-preserved (Figure 2), thus the weathered material is referred to as saprolite. The saprolite is quite heterogeneous, and consists of alternating thinly-bedded structured material, which was derived from clastic-rich shales, and thickly-bedded massive material, derived from limestone-rich shales (Penfield, 1998). All carbonate has been leached from the weathered zone (Rothschild et al., 1984). There is only a shallow soil profile, which may be a result of excessive soil erosion induced by pre-WWII deforestation and slope farming practices (Hatcher et al., 1992).

The existence of complex weathered and fractured zones exerts the primary control on the local hydrology. The MBWES is a forested catchment characterized by steeply-sloping ridges separated by many small drainages; mean annual precipitation is currently on the order of 1300 mm y^{-1}. During precipitation events, perching of the water table occurs around 2 m depth, and subsequent stormflow occurs

8

Legend:

O_CH Chickamauga Group

OG_K Knox Group

Є_RS Rogersville Shale

Є_C Conasauga Group

Є_R Rome Formation
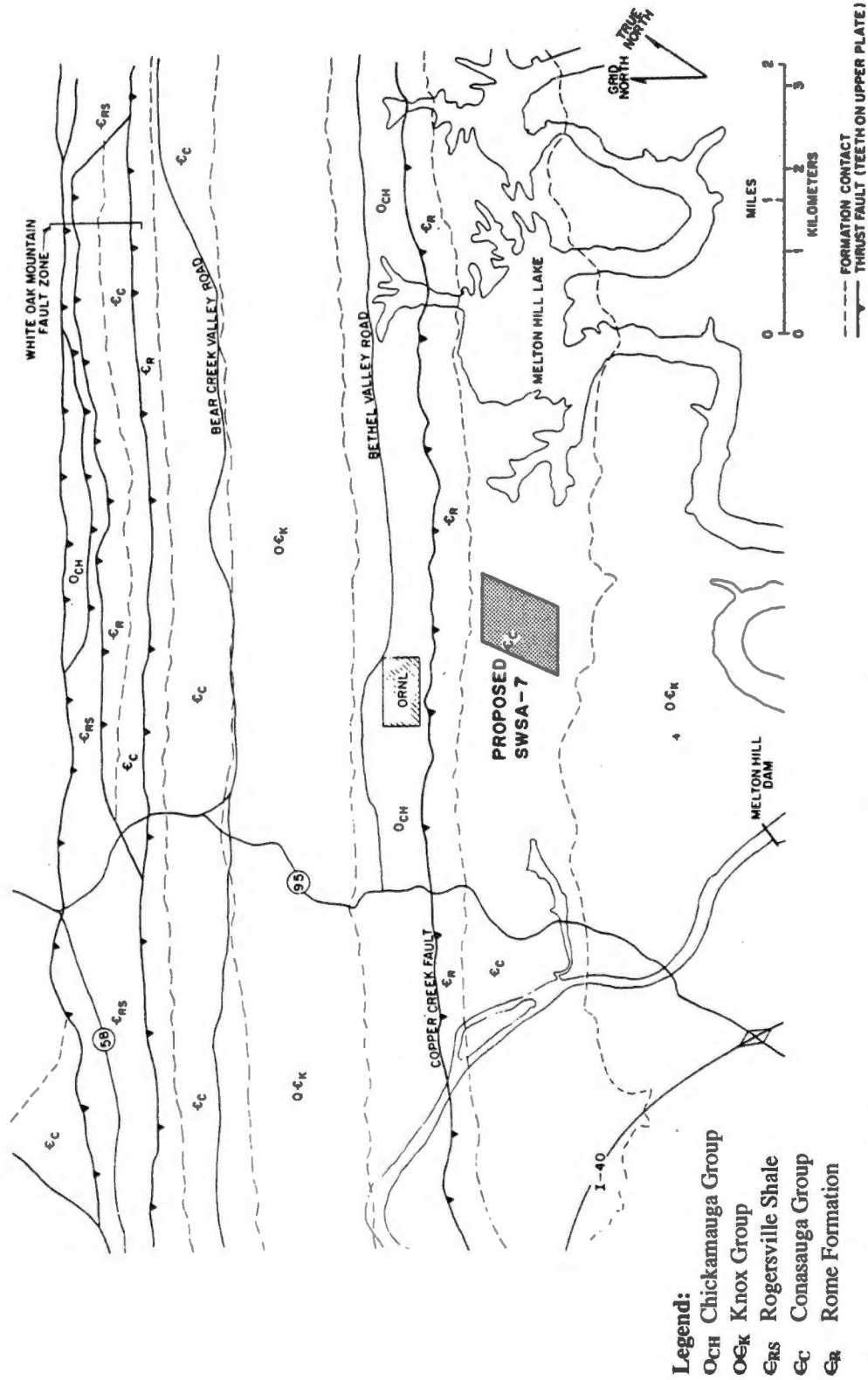
Figure 1. Location of and geologic units within the study area. Solid Waste Storage Area (SWSA) 7, Oak Ridge National Laboratory, Oak Ridge, Tennessee. *Source:* Rothschild, E.R., D.D. Huff, B.P. Spalding, S.Y. Lee, R.B. Clapp, D.A. Lietzke, R.G. Stansfield, N.D. Farrow, C.D. Farmer, and I.L. Munro. 1984. Characterization of soils at proposed solid waste storage area (SWSA) 7. ORNL/TM-9326. Oak Ridge National Laboratory, Oak Ridge, TN. 158 pp.

Figure 2. Saprolite weathered from the Dismal Gap Formation, Conasauga Group. This excavation into the saprolite was near the source of the soil columns, in the Melton Branch Watershed, SWSA-7. The remnant bedding structure of the parent material is apparent, as well as the heterogeneity of the saprolite. Color differences indicate differences in the mineralogy of the layers, either inherited or as a result of differential weathering.

by rapid downslope movement (Moore, 1989). The influence of fracture flow results in a high variability of hydraulic conductivity and infiltration rates over distances of only a few meters (Wilson and Luxmoore, 1988; Wilson et al., 1989). The mean hydraulic conductivities of the surface and subsurface were 9.56 x 10^{-5} m s^{-1} and 0.76 x 10^{-5} m s^{-1}, respectively (Wilson et al., 1993).

Bedding plane and fracture surfaces may be coated with secondary deposits of Fe- and Mn-oxides and translocated clay minerals (Arnseth and Turner, 1988). The Fe and Mn content are highly correlated, suggesting coprecipitation under oxidizing conditions. However, Mn and Fe typically precipitate under different redox conditions, thus a physical mechanism may account for their similar distribution (Arnseth and Turner, 1988). Deposition of oxides from groundwater may be controlled by flow restriction and fluid sequestration, followed by desiccation, oxidation, and co-precipitation (Tardy and Nahon, 1985). The shaly character of the Dismal Gap formation tends to restrict vertical flow, and may provide microenvironments suitable for perching of the water table. The ultimate end of this model is a reduction in the soil permeability by infilling of precipitates. As noted by O'Brien et al. (1996), fluorescent microspheres were not detected on some bedding plane fractures with oxide deposition, suggesting that they were no longer hydraulically active.

The Fe oxide mineralogy is primarily ferrihydrite and amorphous $Fe(OH)_3$, with significant coprecipitated Al, which may compose up to 20 mol % of the Fe-extractable portion (Table 1) (Arnseth and Turner, 1988). Mn-oxide mineralogy is primarily amorphous Mn(IV) oxides as well as pyrolusite. Extractions of aluminosilicates on the Melton Branch soils indicated that the proportions increased with depth, and averaged 2–4 g Al_2O_3 kg^{-1} and 1.4–4.6 g SiO_2 kg^{-1} (Arnseth and Turner, 1988). There are distinct differences in the mineralogy of the thinly-bedded shale saprolite and the massive saprolite, reflected by differences in pH, extractable Fe, organic matter, and clay mineralogy (Table 1) (Kooner et al., 1995). Overall cation-exchange capacity of the soil is high, due to the presence of reactive oxides and exchangeable clays, and is ~ 5 to 20 cmolc kg^{-1} (Rothschild et al., 1984).

Table 1: Select chemical and mineralogical analyses from the Melton Branch midslope.

Soil Type	pH	DCB* extractable Fe$_2$O$_3$ (g kg^{-1})	DCB* extractable MnO$_2$ (g kg^{-1})	DCB* extractable Al$_2$O$_3$ (g kg^{-1})	DCB* extractable SiO$_2$ (g kg^{-1})	MN* extractable MnO$_2$ (g kg^{-1})	MN* extractable Fe$_2$O$_3$ (g kg^{-1})	O.M. (g kg^{-1})	Clay Mineralogy[+]
Structured shale[⊕]	4.6	25	0.36	-	-			0.89	$I_{30}IS_{29}V_{25}S_{10}K_3Q_3$
Massive shale[⊕]	3.8	32		-	-			2.15	$I_{30}IS_{25}K_{20}S_{10}V_{10}Q_5$
Bulk midslope[✧]	5.0	26	0.54	4.8	0.9	0.82	0.37	-	I, V, HIV, (K)

Extraction methods: *DCB = Dithionite-citrate-bicarbonate; *MN = hydroxylamine hydrochloride. Description of extraction methods may be found in Arnseth and Turner, 1988[+].

[+] Mineralogy of the < 2 μm clay fraction. Numerical subscripts refer to weight percentage of each mineral in sample as determined by differential scanning calorimetry and x-ray diffraction. I = illite; V = vermiculite; K = kaolinite; S = smectite; Q = quartz; IS = interstratified (random interstratified kaolinite:smectite); HIV = hydroloxy-interlayered vermiculite.

[⊕] Mineralogic variations observed at the column scale between interbeds of structured siltstone/shale and massive limestone/shale saprolite near the source of columns used in this study. *Source:* Kooner, Z.S., P.M. Jardine, and S. Feldman. 1995. Competitive surface complexation reactions of sulfate and natural organic carbon on soil. J. Environ. Qual. 24: 656-662.

[✧] Mineralogic characterization performed within the Melton Branch watershed. Samples taken from a midslope region (versus ridgetop or drainage) at an equivalent depth as the columns used in this study. *Source:* Arnseth, R.W., and R.S. Turner. 1988. Sequential extraction of iron, manganese, aluminum, and silicon in soils from two contrasting watersheds. Soil Sci. Soc. Am. J. 52: 1801-1807.

Soil Column Excavation and Experimental Configuration

The columns were collected from saprolite formed on the Dismal Gap formation (formerly the Maryville Limestone), the shaly uppermost unit of the Conasauga. Soil columns were obtained by excavating a 2 x 2 m area approximately 1.5 m deep, along the midslope area of a tributary of Melton Branch. Stainless steel cylinders measuring 8.5 x 15 cm were hydraulically pressed into the soil floor. The columns were freed by removing the saprolite around the cylinders, while leaving the undisturbed soil on either end of column. Once in the laboratory, the excess soil was removed from each end. During this procedure, care was taken to prevent smearing of the pores, which could alter the hydraulic conductivity of the columns.

Each end of the column was fitted with a coarse fritted glass plate (8.5 cm diameter and 0.3 cm thick, with a bubbling pressure of -30 cm) to provide a uniform distribution of influent into the column. The porosity of the frits (25-50 μm pore diameter) was such that it did not limit the hydraulic conductivity of solution through the soil. A thin layer of quartz sand (Iota Standard Sand, ~150-250 mm diameter, Unimin Corp., Spruce Pine, NC) was placed between the saprolite and the plates to ensure a good hydraulic connection. The fritted glass endplates were positioned into low volume plexiglass holders (Tempe Cell, Soil Moisture), which were bolted together to hold the frit plates against the soil column ends (Figure 3).

Experimental Approach

The columns were inverted and slowly saturated from the bottom at a flow rate, q, of 1 mL h^{-1} with 0.01 M CaCl$_2$ (reagent grade), using a medical infusion pump (AVI 200A Infusion Pump, 3M, St. Paul, MN). After saturation, the column was flushed with CaCl$_2$ (0.01 M) for several days before the injection of the influent solution began (q = 5 mL h^{-1}). Influent solutions were composed of a nonreactive tracer, Br$^-$ (added as CdBr$_2$) and reactive components (Table 2), for a total ionic strength of I = 0.03 M, which was equivalent to a carrier solution of 0.01 M CaCl$_2$. The flushing solution and the influent solution

Figure 3. Experimental configuration of laboratory columns. The column was inverted to the *in situ* position, with the influent entering the bottom of the column, supplied at a constant rate by the medical pump (3M Corporation). Column dimensions were 15 cm in length by 8.5 cm in diameter. Samples of the effluent were collected in the ISCO fraction collector.

Table 2. Chemical components of influent solutions.

Experiment	Influent pH[§]	Reagent Mixture	Reactive Components	Concentration (M) and Activity (pCi g^{-1})
(1) Cd	3.8	$CdBr_2$ and Ca_2EDTA[▲]	$CdEDTA^{2-}$	1.90×10^{-3}
			^{109}Cd	2393 ± 70
(2) Cd, Co	3.9	$CdBr_2$ and Ca_2EDTA	$CdEDTA^{2-}$	1.95×10^{-3}
			^{109}Cd	1223 ± 31
		$CoCl_2$ and Ca_2EDTA	$Co(II)EDTA^{2-}$	1.80×10^{-3}
			^{57}Co	53.2 ± 0.8
			^{58}Co	93.2 ± 1.6
(3) Cd, Co, Cr	3.7	$CdBr_2$ and Ca_2EDTA	$CdEDTA^{2-}$	1.90×10^{-3}
			^{109}Cd	1165 ± 44
		$KCo(III)EDTA$	$Co(III)EDTA^{-}$	1.05×10^{-3}
			^{57}Co	122.4 ± 2.1
		K_2CrO_4	$HCrO_4^{-}$	0.500×10^{-3}
			^{51}Cr	5894 ± 134
(4) Cr	3.7	K_2CrO_4	$HCrO_4^{-}$	0.500×10^{-3}
			^{51}Cr	5238 ± 55
(5) NOM, Cr	3.7	K_2CrO_4	$HCrO_4^{-}$	0.500×10^{-3}
			^{51}Cr	5095 ± 202

[§] Based on indigenous soil pH in 1:1 mixture of soil and 0.01 M $CaCl_2$, T=25°C.

[▲] EDTA = ethylene-diamine-tetraacetate ($C_{10}H_{16}O_8N_2$).

Structure:

HOOC–CH$_2$ ╲
            N–CH$_2$–CH$_2$–N
HOOC–CH$_2$ ╱   ╲ CH$_2$–COOH
                              ╱ CH$_2$–COOH
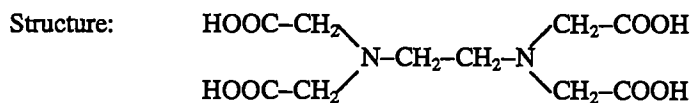
were of equivalent ionic strength, which is essential during reactive contaminant transport studies to maintain the uniqueness of adsorptive characteristics, which are dependent upon ionic strength. The pH of each experiment was equivalent to the indigenous pH of the soil in 0.01 M CaCl$_2$ (1:1 ratio); these were typically 3.6 - 4.0. The experimental setup is shown in Figure 3. Effluent solutions were collected at 7.5 mL intervals using an Isco fraction collector (Figure 3), which was ~2% of a column pore volume.

Chemical analyses centered on a comparison of the influent and effluent solutions as a function of time. Changes in the chemical composition of the effluent were related to chemical interactions during transport through the column, since the influent was monitored for chemical stability. The transport experiments began with the influx of the influent solution and continued until the reduced concentration (effluent/influent concentration, hereafter referred to as C/C_o) of all input components had reached near steady-state. As the system approached steady-state, the flow was interrupted for one week to identify the presence of rate-limited processes. After flow was resumed and the effluent concentrations again reached a steady-state, the influx of tracers was terminated, and the system was continuously flushed with the 0.01 M CaCl$_2$ carrier solution until the reduced concentrations of all components had dropped to <1%. A flow interruption was also performed during the elution, when reduced concentrations of reactive components were ~ 5%. An experimental summary is given (Table 3), listing the duration of each experiment and the timing and duration of each flow interruption.

For investigations involving Cr(VI) transport, the quantity of natural organic matter on Column 5 was increased by about 2.2 times. Freeze-dried NOM from a wetlands pond in Georgetown, SC was dissolved in 0.01 M CaCl$_2$ to produce a 300 mg C L^{-1} solution, and added to the soil at a flux of 0.09 cm h^{-1}. The column was flushed with 0.01 M CaCl$_2$ for several pore volumes before the initiation of the experiment.

Table 3: Summary of experimental events.

Experiment, Metal Contaminant	Porewater Velocity (cm d⁻¹)	Volume of pores (mL)	Influent pulse (PV†)	Influent interrupt (PV†)	Interrupt Duration (days)	Effluent interrupt (PV†)	Interrupt Duration (days)	Total pulse (PV†)
(1) Cd	5.08	342	23.18	18.55	10.04	42.63	7.79	54.56
(2) Cd, Co	5.06	338	8.32	5.32	5.94	18.92	6.88	35.14
(3) Cd, Co, Cr	5.19	329	31.00	20.41	7.08	-	-	82.07
(4) Cr	4.74	367	37.18	22.34	2.67	-	-	92.91
(5) NOM, Cr	4.48	388	55.05	-	-	-	-	90.00

† PV, or dimensionless pore volume. The pore volume represents cumulative sample volume as points along the breakthrough curve, normalized to the volume of pore water (mL) for each column. The formula is as follows: PV = cumulative volume/ (sample volume) (water content)

Chemical Analyses

Chemical analyses are separated into direct methods that quantify ionic species (e.g., $Co(II)EDTA^{2-}$), and indirect methods that quantify elemental concentrations (e.g., total Co, including all ionic species). Direct methods are always preferable, but not always possible due to interference by other species or lack of appropriate methods or equipment for their quantification. Consequently, for complex aqueous solutions, direct methods were supplemented with indirect methods and coupled with the use of a geochemical speciation model to predict chemical complexes.

Direct detection of the reaction products $Co(III)EDTA^-$, $Fe(III)EDTA^-$, and $HCrO_4^-$ was achieved by scanning spectrophotometry. Br^-, $Co(II)EDTA^{2-}$, $Co(III)EDTA^-$, and $CdEDTA^{2-}$ were analyzed using liquid ion chromatography (I.C.) (Dionex model DX-300) using the methods of Taylor and Jardine (1995). $Co(III)EDTA^-$ and $HCrO_4^-$ interfere with the detection of $Fe(III)EDTA^-$ in these methods, therefore in complex solutions the concentration of $Fe(III)EDTA^-$ was predicted using indirect methods and a geochemical speciation model. Other direct methods include monitoring effluent for pH, Eh, and Br^- using the respective ion-specific electrode.

The aqueous concentrations of stable Co and Cd, as well as indigenous cations Ca, Na, Mg, K, Fe, Al, Mn, and Si were determined by Inductively Coupled Argon Plasma Emission Spectrophotometry (Thermo Jarrell Ash Polyscan IRIS ICAP). Analyses were also confirmed by Atomic Adsorption Spectroscopy (Perkin-Elmer 5000 AAS). Total Cr was quantified by AAS, while Cr(VI) was determined using spectrophotometric methods. Finally, the concentration of $EDTA^{4-}$ was determined using a Total Organic Carbon (TOC) furnace (Shimadzu TOC-5000).

The concentrations of Co, Cd, and Cr were also determined by gamma ray spectroscopy of the radioisotope tracers ^{109}Cd, ^{51}Cr, ^{57}Co, and ^{58}Co. Influent solutions containing experimental quantities of the stable metals were spiked with low concentrations of gamma-ray emitting radionuclides (Table 2). The chemical behavior of metals is independent of isotopic composition, thus, radioactive tracers can be used to

monitor the movement of stable metals. The advantages of using radioactive tracers are their low detection limits (10^{-15} M), nondestructive analyses, and quantification of multiple radionuclides in a single analysis. Typically, 5 ml (or 5 grams) of sample were counted in plastic scintillation vials for various time increments, depending on the level of activity present. The sample containers were calibrated using a NIST traceable gamma-ray standard solution (QCY series, Amersham, Inc.) in an aqueous matrix (Larsen and Cutshall, 1981). In addition, the solid phase was sectioned and counted following the experiment, yielding sorbed radionuclide profiles with depth. These data were used to estimate the mass loss by irreversible sorption during the experiment and compared to aqueous phase mass recoveries. Analyses were performed using a high purity Intrinsic Germanium (HPGe) coaxial detector coupled to a Nuclear Data microprocessor (ND 6700) with a peak-search routine programmed to acquire gamma-ray spectra in 4096 channels. Quantification for the radionuclides were based upon the following gamma-ray energies: ^{109}Cd, 88 keV photon, ^{57}Co, 122 keV photon, ^{58}Co, 810 keV photon, and ^{51}Cr, 320 keV photon. Corrections were made for the ambient background, the net sample photopeak count rate, and radionuclide decay to the start of the experiment. Relative precision was approximately $\pm 5\%$ or less along the breakthrough and plateau portions of the experiment. Precision was lower near the end of the experiments (which were on the order of 280 d in length) due to the decay of the short-lived tracers, particularly ^{51}Cr ($t_{1/2} = 27$ d), and precision approached 50% (the detection limit).

Quantification of the ^{109}Cd photon energy in the soils at 88 keV was complicated due to interference of lead X-rays from ^{212}Pb and ^{214}Pb, which have photon energies at 87 keV. The source of these X-rays are daughter product decays associated with the unstable isotopes ^{226}Rd and ^{228}Rd, which exist naturally in the soil. The interfering photon count rates, however, can be estimated and subtracted from the total 88 keV count rate. An additional correction was also performed for soil self-absorption, which can range from 5-20%, of the 88 keV photon in reference to the aqueous standard, using the methods of Cutshall et al. (1983) and Larsen and Lee (1983).

The speciation of solid phase Cr was determined using X-ray Near Edge Spectroscopy (XANES) at the Stanford Synchrotron Radiation Laboratory. The fraction of Cr(III) and Cr(VI) with depth were

obtained for the control Cr and NOM-loaded Cr columns (experiments 4 and 5). The proportion of Cr(VI) was determined using the amplitude of the pre-edge feature relative to the total atomic cross-section, and comparison to standard curves, following the method of Patterson et al. (1997).

Geochemical speciation modeling

The ionic speciation of elements exerts control on solute dynamics, thus, when direct detection of ionic species is not possible, a speciation model may be useful. A thermodynamic equilibrium speciation model, GEOCHEM, (Sposito and Mattigod, 1980; Parker et al., 1987) was used to estimate the chemical speciation of each element using the principles of mass and charge balance. For example, the $EDTA^{4-}$ chelate could be distributed between the metallic complexants as $Co(II)EDTA^{2-}$, $Co(III)EDTA^{-}$, $Fe(III)EDTA^{-}$, $Al(III)EDTA^{-}$, and $CdEDTA^{2-}$. Direct methods yield the ionic concentrations of $Co(II)EDTA^{2-}$, $Co(III)EDTA^{-}$, and $CdEDTA^{2-}$, but the concentrations of $Fe(III)EDTA^{-}$ and $Al(III)EDTA^{-}$ cannot always be quantified due to interference and the lack of appropriate methods, respectively. $Fe(III)EDTA^{-}$ can be directly detected using spectrophotometric methods only in the absense of $Co(III)EDTA^{-}$. These concentrations, however, can be estimated using the geochemical model. Input parameters include total concentration of EDTA, Fe, Al, and Cd, and all other chemical components, including indigenous cations (ICAP results), pH and ionic strength. The model uses intrinsic association constants for all possible metal-ligand complexes, and predictions based on thermodynamic equilbrium are used to determine the distribution of EDTA between metals. Speciation calculations were performed at various times during the course of the experiment to yield breakthrough curves of the modeled ionic species. Such geochemical modeling allows for the quantification of ionic species where direct analyses are not possible, thereby enhancing the chemical resolution of the effluent solutions.

Soil Properties

Following the termination of each experiment, the columns were weighed, then dismantled and sectioned into 1.5-2.0 cm increments. The soils were oven-dried at 55°C, then weighed again. The volumetric water content, θ, was calculated (MM^{-1}, or L^3L^{-3}):

$$(1) \qquad \theta = V_w/V_t$$

where V_t is the volume of the column (L^3) and:

$$(2) \qquad V_w = \text{wet soil (M)} - \text{dry soil (M)}.$$

The parameter V_w is the water content, or pore volume, and one pore volume can be conceptualized as the volume of water contained within a single column length. The advantage of this parameter is that it describes the flow of water through the columns in dimensionless volume, relative to the pore space within each column. Therefore, different columns of varying V_w can be compared with a common x-axis. Breakthrough curves will be presented as a function of pore volume, with the time axis shown for reference. The dimensionless pore volume is calculated from the individual sample and the volume of pore space:

$$(3) \qquad \text{Pore volume} = \text{cumulative volume}/[(\text{sample volume})(\text{water content})]$$

The bulk density of the soil ($M L^{-3}$) was calculated by:

$$(4) \qquad \rho_b = \text{dry soil (M)} / V_t$$

The soil characteristics for these 5 columns are listed in Table 4. The pumping rate for all experiments was 5 mL h^{-1}. The mean pore water velocity ($L T^{-1}$) is calculated with respect to the rate of flow through the open pore space (pore volume) of the column (Table 4):

$$(5) \qquad V = q / (\pi r^2 \theta)$$

where q is the rate of infusion ($L^3 T^{-1}$) and r is the column radius (L^3). Hydraulic conductivity was measured using a constant head permeameter during the experiment (Table 4).

Table 4: Measured physical properties of saprolite columns.

Experiment, Metal Contaminant	Volume of pores (mL)	Water content (θ) $(cm^3\,cm^{-3})$	Bulk density (ρ_b) $g\,cm^{-3}$	Hydraulic[+] conductivity (K) $(m\,s^{-1})$	Peclet Number[+]
(1) Cd	342	0.426	1.428	1.17×10^{-7}	6.30 ± 0.40
(2) Cd, Co	338	0.428	1.483	8.95×10^{-8}	2.69 ± 0.20
(3) Cd, Co, Cr	329	0.417	1.500	4.18×10^{-8}	6.42 ± 1.00
(4) Cr	367	0.457	1.261	2.50×10^{-7}	2.87 ± 0.48
(5) NOM, Cr	388	0.483	1.327	-	9.62 ± 3.37

+ Hydraulic conductivity was obtained from the measurement of hydraulic head using a constant head permeameter.

+ Peclet numbers were best fit to observed Br⁻ data using convective-dispersive equation with the 95% confidence interval shown for the estimated value.

Transport modeling

The mobile-immobile, or two-site conceptual approach was used to model the transport of solutes through the columns. This approach assumes that steady-state flow through the mobile region (macropores and/or fractures) occurs by advective and dispersive flow, while transport within the immobile region (micropores) flow occurs primarily by diffusion (van Genuchten and Wierenga, 1976). Flow in the mobile regions is described by the classic convective-dispersive equation, with regions of mobile and immobile water:

$$(6) \qquad \theta^m (\partial C^m/\partial t) = \theta^m D_{LH} (\partial^2 C^m/\partial x^2) - V\theta^m (\partial C^m/\partial x) - \alpha (C^m - C^{im})$$

and:

$$(7) \qquad \theta^{im} (\partial C^{im}/\partial t) = \alpha (C^m - C^{im})$$

where D_{LH} is the dispersion coefficient in the mobile water region ($L^2 T^{-1}$) reflecting the combined effects of axial diffusion and hydrodynamic dispersion on transport, θ^{im} is the immobile water fraction, ($L^3 L^{-3}$), C^m and C^{im} are the solute concentrations in the mobile and immobile water, respectively, ($M L^{-3}$), x is the depth (L), and t is time (T). An assumption is that θ^{im} is representative of intraaggregate pores where solute transfer occurs by diffusion only, or adsorption is on kinetically-limited adsorption sites. In Equation (7), α is a first-order mass transfer coefficient (T^{-1}) representative of the rate of mass transfer between the mobile and immobile sites, in a manner analogous to diffusion.

The convective-dispersive equations associated with the above mobile-immobile model formulations are subject to the following initial and boundary conditions:

$$(8) \qquad C^m = C^{im} = 0 \qquad\qquad t = 0, \quad 0 < x < L_e$$

$$(9) \qquad VC_o = -\theta^m D_{LH} (\partial C^m/\partial x) + VC^m \qquad x = 0, \quad t < t_p$$

$$(10) \qquad 0 = -\theta^m D_{LH} (\partial C^m/\partial x) + VC^m \qquad x = 0, \quad t > t_p$$

$$(11) \qquad (\partial C^m/\partial x) = 0 \qquad\qquad x = L_e, \quad t > 0$$

where t_p is the duration of an applied solute pulse, C_o is the input concentration in the applied pulse, and L_c is the solute transport length. Equations (6) and (7), subject to the above conditions, were solved numerically using the implicit-explicit finite difference (Crank-Nicholson) method, where a mass balance was maintained as a check on the numerical calculations. The flux-averaged boundary condition was used, as it has been shown to be appropriate for modeling the effluent curves of column displacement studies (van Genuchten and Parker, 1984).

An important parameter within the mobile-immobile concept is the mass transfer between these two regions. The flow interruption technique provides an opportunity to examine the rate and mechanisms controlling the transfer of solutes between the matrix and the macropores, because this is the only process operative in the absense of flow. In effect, the velocity term becomes $V = 0$, and the dispersion term becomes $D_{LH} = D_o = D_e/\tau$, where D_o and D_e are the actual and effective molecular diffusion coefficients, respectively, and τ is a tortuosity factor. Equation (6) becomes reduced to the diffusion equation:

$$(12) \qquad \theta^m (\partial C^m/\partial t) = \theta^m D_o (\partial^2 C^m/\partial x^2) - \alpha (C^m - C^{im})$$

During the flow interruption, it is important that molecular diffusion within the mobile water phase is negligible. This mechanism of transport was minimized by timing the interruptions when there was a minimal concentration gradient within the mobile regions. In the "plateau" region of the breakthrough curve (C/C_o approaches 1), as well as the end of the washout curve (where C/C_o is around 5%, but slowly approaching 0) most of the mobile water should have nearly the same concentration, as exhibited by relatively small change in effluent concentration. During these periods, the exchange of solutes was simplified and controlled by mass transfer between the mobile and immobile phases along concentration gradients, which is described by Equation (7).

The modeling strategy followed that of Reedy et al. (1996). The CD equation was used to model the transport of conservative Br^-, using a curve-fitting routine that operates by minimizing the sum-of-least-squares along the Br^- breakthrough curve (Parker and van Genuchten, 1984). The dispersion coefficient, obtained from fitting to Br^-, is a property of the column heterogeneities and the pore-water velocity. It was used to fit the CD equation to the reactive contaminant curves, solving for the retardation coefficient, R.

The model-fitted values of D and R were the initial input parameters in a two-site simulation code, STOPFLO, modified after Selim et al. (1976). The fraction of mobile sites, F = 0.45, was obtained from Br⁻ column studies on the Melton Branch saprolite (Reedy et al., 1996). The first order rate coefficient, α, which described the mass transfer between the mobile/immobile fractions, was optimized to produce the observed perturbation in Br⁻ or the reactive species as a result of interrupted flow.

Multi-region transport modeling

An additional modeling routine was required to model the transport of Cr(VI) to account for nonlinear and irreversible sorption of Cr(VI) (Selim et al., 1990). The CXTFIT model assumed that the partitioning between the solution and the solid were independent of the solution concentration, and sorption could therefore be described with a constant distribution coefficient (K_d), which is the slope of the partitioning line on a linear isotherm. However, the distribution of solute onto the solid phase may be dependent upon solute concentration, as in the nonlinear isotherm. Different phases of the soil may have different affinities for the solute, indicating that multiple reactions control solute-soil interactions. The governing equations for the Multi-Reaction Transport Model (MRTM) are as follows (Selim et al., 1990).

Adsorption is described by the Freundlich equation:

$$(13) \qquad s_e = K\,C^{\,n}$$

where s_e represents the reversibly sorbed phase that is in local equilibrium with the soil solution phase (C), K is the associated affinity coefficient, and n is a parameter indicative of linear sorption ($n = 1$), or nonlinear sorption ($n < 1$).

The reaction between C and s_{irr}, where s_{irr} represents the irreversibly sorbed phase, can be represented by:

$$(14) \qquad Q = \rho\,(\partial s_{irr}/\partial t) = \theta\,k_s\,C$$

where k_s is the first-order rate coefficient (h^{-1}) for the irreversible retention reaction. Therefore, s_{irr} represents an irreversible sink term which can account for the loss of mass to the soil. The parameter Q is the rate of solute removal (or supply) from soil solution (mg cm⁻³ h⁻¹).

25

The equation governing the transport of reactive solutes was a modification of the classic convective-dispersive equation, assuming one-dimensional, steady-state flow through homogenous soils, and can be expressed as:

$$(17) \qquad \theta \, (\partial C/\partial t) = \theta D_{LH} \, (\partial^2 C/\partial x^2) - V \, (\partial C/\partial x) - \rho \, (\partial s/\partial t) - Q$$

with all terms previously defined. The change in concentration with time, $\theta \, (\partial C/\partial t)$, is expressed as a function of these parameters: $\theta \, D_{LH} \, (\partial^2 C/\partial x^2)$, a term considering two-dimensional dispersion along the flow path, $V \, (\partial C/\partial x)$, which represents advective flow, $\rho \, (\partial s/\partial t)$, represents reversible kinetic sorption, and Q represents the rate of irreversible sorption.

3. Results and Interpretation

Hydraulic and lithologic properties of soil columns

The physical characteristics of the five soil columns were measured using standard techniques. Hydraulic conductivity, obtained using a constant head permeameter, ranged from 4×10^{-8} to 2×10^{-7} m s^{-1} (Table 4). The hydraulic conductivities were around two orders of magnitude lower than previous Melton Branch column studies, which ranged from 10^{-4} to 10^{-6} m s^{-1} (Harton, 1996; Cropper, 1998; Haun et al., 1998), and field studies, which were 0.76×10^{-5} m s^{-1} (Wilson et al., 1993). The difference may be related to the method of obtaining the columns, since the previous columns were excavated so that flow was parallel to bedding planes. The columns in this study were hydraulically pressed so that flow was generally across bedding planes, and the angle of column length to bedding ranged from $45°-80°$. The saturated hydraulic conductivity of the matrix was predicted to be between 4×10^{-8} m s^{-1} and 6×10^{-9} m s^{-1} by Wilson et al. (1992), therefore, the measured hydraulic conductivities of these columns were within an expected range. The low hydraulic conductivity, as well as the Peclet number of the columns (Table 4), suggested that preferential flow along the sidewall of the column did not occur. Following the experiments, the columns were dismantled, sectioned, and weighed. The soils were dried, and weighed again to obtain the volumetric water content and the bulk density of the soil (Table 4).

Distinct lithologic variations were observed between the columns, though they were taken from an equivalent depth, over an area of only 4 m^2. The Dismal Gap formation consists of heterogeneous and finely interbedded silty and limey shales, with some fine sandstone (Hatcher et al., 1992). Previous workers (Kooner et al., 1995; Penfield, 1998), have observed two distinct Melton Branch lithologies which closely correspond to the observations of this study. Mineralogic characterizations of each lithology are provided in Table 1 (Kooner et al., 1995), as well as a bulk characterization of the midslope region (Arnseth and Turner, 1988). Column 2 was characterized by highly structured and fractured, thinly bedded silty-shale saprolite, with visible Mn- and Fe-oxide staining and mottling. Columns 4 and 5 were capped at the top and

27

bottom by structured saprolite, but the middle region was characterized by massive, red clayey saprolite, with considerably less visible structure and fractures. Columns 1 and 3 were intermediate, being mostly structured and finely bedded, with some massive layers. The current interpretation is that the structured saprolite was weathered from finely interbedded clastic-dominated shales, while the massive units were weathered from less structured limestone shales (Penfield, 1998). Decaying roots as large as 5 grams, as well as several smaller rootlets, were observed only in the structured material (columns 1, 2, and 3), perhaps as a result of root penetration along the larger fractures.

Single-species transport of CdEDTA^{2-}

A single-species experiment (experiment 1) was conducted to characterize the transport of CdEDTA^{2-}. The mobility of ^{109}Cd was significantly retarded relative to nonreactive Br$^-$, and exhibited extensive tailing, indicating the prevalence of time-dependent interfacial geochemical processes influencing the transport of Cd. The complete breakthrough required 16 pore volumes, while that of Br$^-$ took 3 pore volumes (Figure 4). The absence of a perturbation of Br$^-$ as a result of flow interruption (18.55 pore volumes) indicated that physical equilibrium was attained. The perturbation in the concentration of ^{109}Cd, however, suggested it had not reached equilibrium, thus kinetically-limited chemical processes may be responsible. Differences in the diffusion coefficients of Br$^-$, ^{109}Cd, and CdEDTA^{2-} could also be responsible for this behavior, but there is considerable geochemical evidence to suggest that chemical processes are responsible for the observed nonequilibrium.

Transport modeling was performed to characterize the transport of ^{109}Cd, and quantify the extent of nonequilibrium. Because the transport of Br$^-$ was conservative, its breakthrough curve (BTC) was used to assess dispersion along the column flowpath. The equilibrium convective-dispersive (CD) equation was applied to the Br$^-$ BTC (Figure 4), assuming a retardation of one. The mean pore-water velocity, pulse duration (Table 3), and physical soil parameters (Table 4) were directly measured, and tortuosity was estimated as 0.60, from previous column studies (Reedy et al., 1996). The model-fitted dispersion coefficient was equal to 11.75 ± 0.75 cm^2 d^{-1}, which measured the spreading along the solute front due to
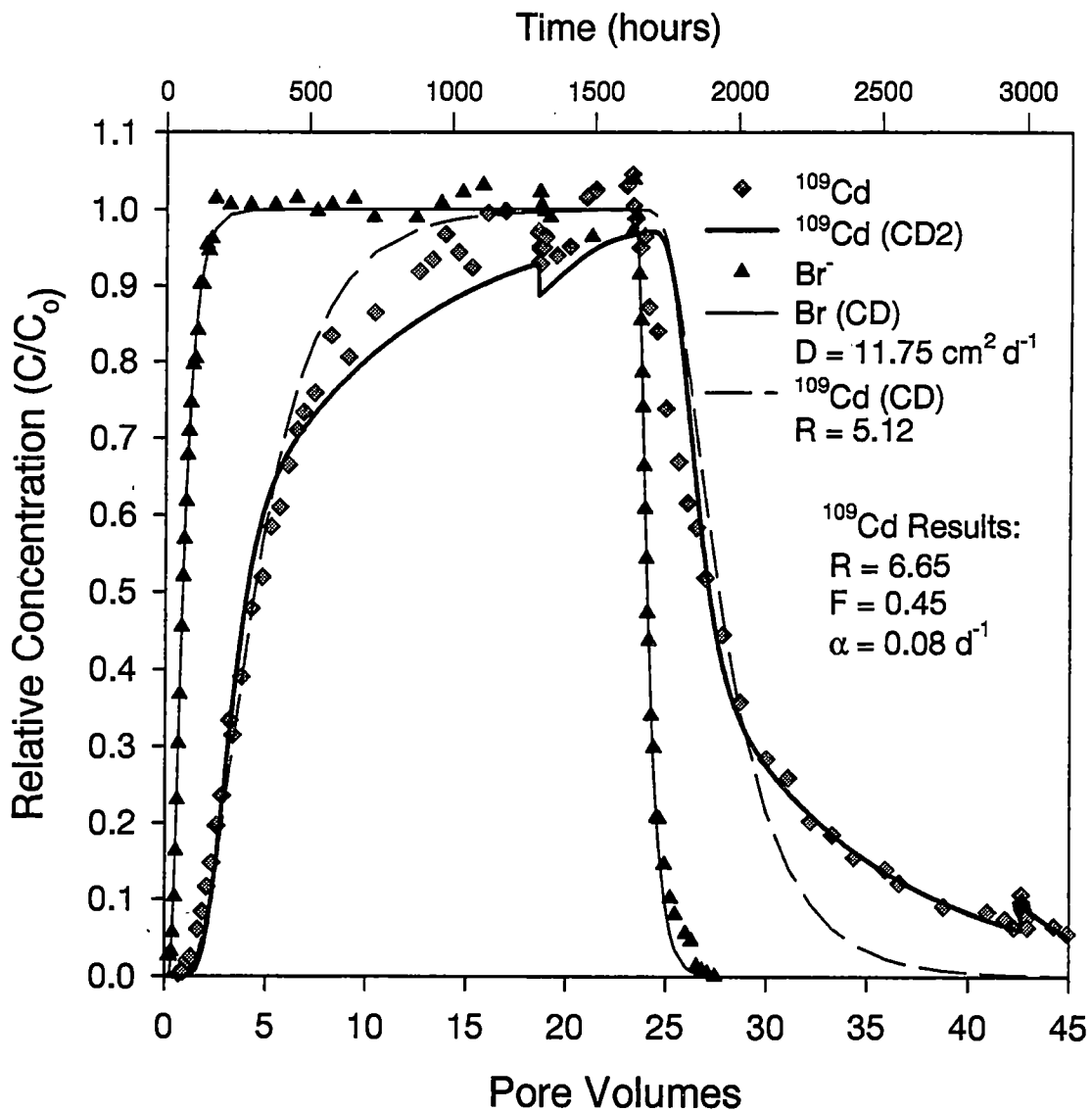
Figure 4. Experimental and modeled breakthrough curves for Br⁻ and ^{109}Cd for the single-species CdEDTA^{2-} experiment (1). The breakthrough and washout portions of the ^{109}Cd curve exhibited considerable tailing, compared to the nonreactive Br⁻. The fit to the Br⁻ curve was from the application of the convective-dispersive (CD) equation to the data. ^{109}Cd was tested with the CD equation, but the fit was inadequate due to the tailing along the breakthrough and washout portions, which was indicative of nonequilibrium conditions. The fit to the ^{109}Cd curve was improved by using the two-site CD equation, STOPFLO code (CD2). Two-site modeling assumed a fractional distribution between equilibrium and kinetically-limited sorption sites, F, with equilibrium sites modeled with the CD equation, and α representative of the rate of mass transfer between the equilibrium and kinetically-limited sites.

29

the physical characteristics and heterogeneities of the column. The Peclet number is a dimensionless indicator of column hydraulic characteristics, as it is calculated from D by the removal of the velocity and length terms: $P = VL / D_{LH}$. A Peclet number of 6.30 ± 0.40 was obtained, suggesting that heterogeneous flow through the saprolite column was significant (Table 5).

The [109]Cd BTC exhibited considerable asymmetry and tailing, which may be indicative of geochemical nonequilibrium conditions (Figure 4). The flow interruptions, however, confirmed the existence of nonequilibrium, as indicated by a decrease in the [109]Cd concentration during the influent interruption, and an increase following the desorption interruption. During the influent interruption, the adsorption of [109]Cd continued, striving to reach equilibrium with the solid phase, resulting in a decrease in the aqueous [109]Cd concentration upon resumption of flow. During the effluent interruption, the desorption of [109]Cd was not at equilbrium, therefore desorption into solution continued in the absence of flow. Overall mass balance indicated that there was a 99.9% mass recovery of [109]Cd, therefore, time-dependent desorption was complete when the experiment was terminated (Table 6). As might be expected from the interruption results, transport modeling with the CD equation, which assumed equilibrium conditions, was unsuccessful, and the model overestimated the rate of breakthrough and underestimated the observed tailing during the washout (Figure 4).

The two-site CD equation was used to model the transport of [109]Cd and quantify the extent of nonequilibrium. Input parameters consisted of the dispersion coefficient D, which was obtained from Br-, and the fractional distribution of equilibrium (mobile) and kinetic (immobile) sites, $F = 0.45$, obtained from Reedy et al. (1996). While other F values were tested, 45% consistently resulted in the most adequate fit. The initial retardation coefficient was obtained from the application of the CD model (Table 5). These parameters, D, R, and F, were used to match the shape of the breakthrough curve, while optimization of the model was completed on the flow interruption. In the absence of flow, the only operative process was the transfer of mass between the mobile and immobile regions. The first order coefficient of mass transfer, α, was varied to provide the best observable fit to the concentration perturbation following the flow interrupt

Table 5: Results of application of the convective-dispersive equation to tracer breakthrough curves

Experiment, Metal Contaminant	Dispersion Coefficient (D) (cm² d⁻¹)	D: r²‡	Peclet Number (P)	Metal	Model	Retardation Coefficient (R)	R: r²‡	Distribution Coefficient (K_d) (cm³ g⁻¹)	Fraction of mobile sites (F)§	First-order rate coefficient (α) (d⁻¹)§
(1) Cd	11.75±0.75♦	0.997	6.30±0.40♦	Br⁻	CD‡	1.00				
				¹⁰⁹Cd	CD	5.12±0.26♦	0.962	1.23±0.07♦		
				¹⁰⁹Cd	CD2§	6.65		1.69	0.45	0.08
(2) Cd, Co	27.45±2.02	0.993	2.63±0.20	Br⁻	CD	1.00				
				Br⁻	CD	1.00				
				¹⁰⁹Cd	CD	3.83±0.25	0.943	0.82±0.07		
				¹⁰⁹Cd	CD2	4.98		1.15	0.45	0.04
				⁵⁷Co	CD	1.83±0.14	0.930	0.24±0.07		
				⁵⁷Co	CD2	3.52		0.73	0.45	0.08
(3) Cd, Co, Cr	12.01±1.85	0.991	6.42±1.00	Br⁻	CD	1.00				
				¹⁰⁹Cd	CD	4.88±0.31	0.94	1.08±0.08		
				¹⁰⁹Cd	CD2	7.56		1.66	0.45	0.06
				⁵⁷Co	CD	2.35±0.09	0.988	0.375±0.03		0.03
				⁵¹Cr	MRTM†	12.65±0.83	0.97	2.85±0.23		

‡ Application of the 1-D convective-dispersive (CD) equation (CXTFIT), assuming reversible sorption that is at equilibrium. Model parameterization is accomplished with a linear, least-squares fit to the curve (r² is shown). *Source:* Parker, J.C., and M. Th. van Genuchten. 1984. Determining transport parameters from laboratory and field tracer experiments. Virginia Agric. Exp. Stn. Bull. 84-3.

♦ 95% confidence interval is shown for CXTFIT parameters.

§ Application of the STOPFLO simulation code (CD2). STOPFLO uses the 1-D CD equation, with reversible sorption on two sites -- one equilibrium, and one kinetically-limited. F controls the distribution between sites, and α the rate of mass transfer between sites. Model parameterization is accomplished using CXTFIT results in the STOPFLO simulation routine, with some adjustments to R, and matching α to the flow interruption data. Thus, no confidence intervals are given. *Source:* Selim, H. M., J. M. Davidson, and R.S. Mansell. 1976. Evaluation of a two-site adsorption model for describing solute transport in soils. p. 444-448. *In* Summer Comput. Simul. Conf., Washington, D.C. 12-14 July 1976. Simulation Councils, La Jolla, CA.

† Application of the Multi-Reaction Transport Model, assuming linear sorption. See also Table 7. *Source:* Selim, H.M., M.C. Amacher, and I.K. Iskandar. 1990. Modeling the transport of heavy metals in soils. U.S. Army Corps of Engineers Monograph 90-2.

Table 6: Mass balance of influent tracers from solution and solid.

Experiment, Metal Contaminant	Metal	Effluent mass Activity (µCi)/ Conc. (moles)	*Solution Recovery (%)	Mass on Solid (µCi)	^Solid Recovery (%)	Total Recovery (%)
(1) Cd	^{109}Cd	17.82 µCi	99.86	N/A		
	Cd	15.0e-3 moles				
(2) Cd, Co	^{109}Cd	3.36 µCi	96.00	0.131	3.74	99.74
	Cd	5.26e-3 moles				
	^{57}Co	0.146 µCi	96.05	0.0027	1.78	97.83
	Co	4.86e-3 moles				
(3) Cd, Co, Cr	^{109}Cd	11.8±0.4 µCi	100.9	0.03	0.26	101.1
	Cd	19.6e-3 moles				
	^{57}Co	1.24 µCi	100.8	0.004	0.33	101.0
	Co	10.8e-3 moles				
	^{51}Cr	24.7 µCi	41.8	30.2	51.0	92.7
	Cr	1.92e-3 moles				
(4) Cr	^{51}Cr	45.14 µCi	57.5	32.64	41.6	99.0
· ·	Cr	3.92e-3 moles				
(5) NOM, Cr	^{51}Cr	36.52 µCi	33.6	58.95	54.2	87.9
	Cr	3.59e-3 moles				

✶ Solution recovery obtained by integration of the area beneath the effluent curve and comparison with the area beneath the influent pulse.

⅄ Solid recovery obtained from counting the radiotracer decays on the dissected column following the experiment.

N/A Solids not counted from this experiment.

(Figure 4). The simulation that best reproduced the experimental interruptions (adsorption and desorption) was with the transfer coefficient equal to 0.08 d^{-1}, F = 0.45, R = 6.65 (Table 5).

Geochemical controls on the transport of CdEDTA^{2-}

The breakthrough of ^{109}Cd exhibited considerable retardation, and direct measurements of CdEDTA^{2-} show that much of the effluent Cd^{2+} was not associated with EDTA^{4-}, particularly early in the experiment (Figure 5). Both total Cd (as ^{109}Cd) and CdEDTA^{2-} exhibited a decrease associated with the flow interruption, which was indicative of adsorption. The greater perturbation exhibited by the chelated complex, however, indicated that some adsorbed CdEDTA^{2-} was dissociated during the interruption.

The dissociation of the chelated complex was accompanied by dissolution of the soil surface. A large pulse of iron was produced during the experiment, and identified as Fe(III)EDTA$^-$ with spectrophotometric methods (Figure 6). This, in addition to the adsorption of CdEDTA^{2-} during the interruption, is direct evidence that the CdEDTA^{2-} complex was dissociated by interactions with the solid phase during transport. This idea is supported by the fact that the concentration of Fe(III)EDTA$^-$ increased three-fold following the interrupt, indicating that it had been released from the solid surface and accumulated in the solution pathways (Figure 6). The perturbation in Fe(III)EDTA$^-$ was much larger than that of CdEDTA^{2-}, which may indicate slow production or desorption relative to the adsorption of CdEDTA^{2-}. The time-dependent release of structurally bound Fe(III)EDTA$^-$ has been documented by Chang and Matejevic (1983). These results suggested that the transport of CdEDTA^{2-} through Melton Branch soils was controlled by multiple rate-limited steps or reactions; first, the initial adsorption onto the soil surface, followed by scavenging of the EDTA^{4-} ligand by surficial Fe(III) and dissociation of CdEDTA^{2-}, and finally the release of Fe(III)EDTA$^-$ from the soil surface. This process is successful since the Fe(III)EDTA$^-$ log K is 27.7, while that of CdEDTA^{2-} is 18.2 (Sposito and Mattigod, 1980).

Evidence suggests that soil aluminum may also affect the stability of the CdEDTA^{2-} complex. At the experimental pH (3.8), Al was mobile and leached from the soil surface at a steady-state concentration due to natural weathering processes (Figure 6). In the presence of CdEDTA^{2-}, however, a distinct pulse of
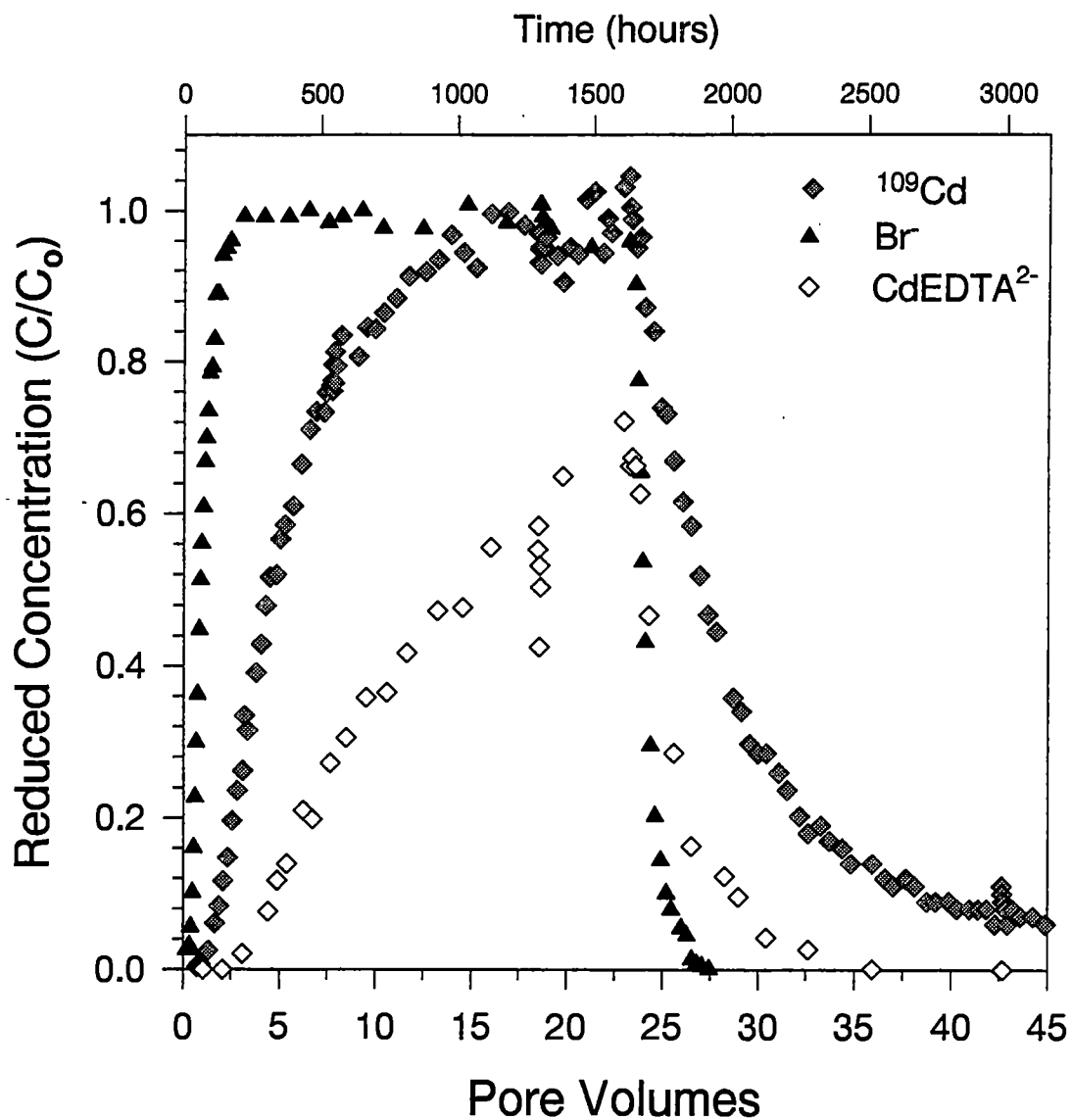
Figure 5. The breakthrough of Br⁻, ^{109}Cd, and CdEDTA^{2-} for the single-species CdEDTA^{2-} experiment (1). The breakthrough of CdEDTA^{2-} was greatly retarded compared to total Cd, as ^{109}Cd, indicating dissociation of the CdEDTA^{2-} complex during transport. Dissociation was particularly apparent during the flow interruption (18.55 pore volumes), as evidenced by the larger perturbation in CdEDTA^{2-}.

Time (hours)

0   500   1000   1500   2000   2500   3000

▼ Fe(III)EDTA⁻
▣ Al

Absolute Concentration (mM)

1.2

1.0

0.8

0.6

0.4

0.2

0.0

0   5   10   15   20   25   30   35   40   45

Pore Volumes
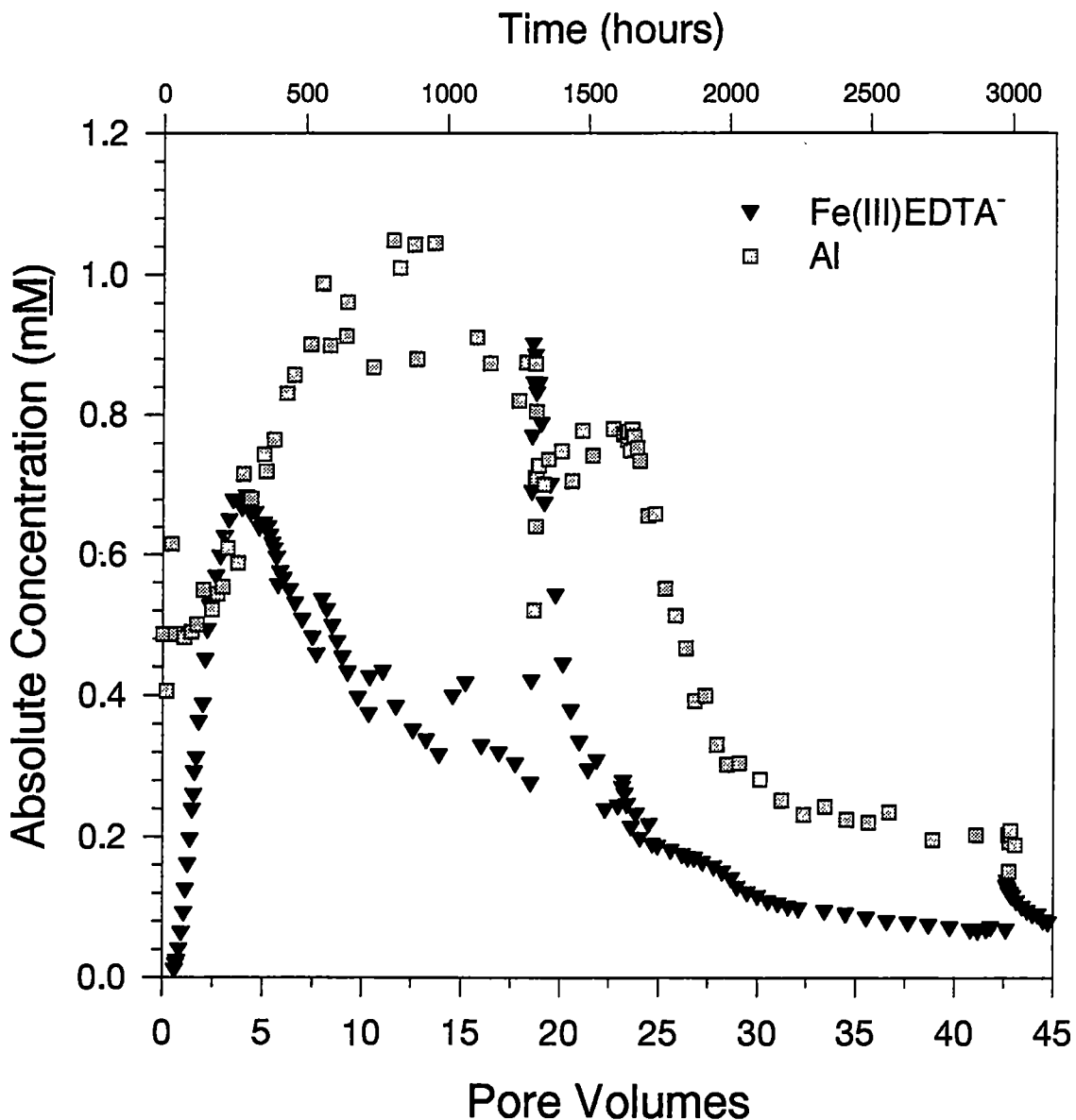
Figure 6. The breakthrough of Fe and Al, released by dissolution of and desorption from the solid phase (experiment 1). The production of Fe(III)EDTA⁻ is direct evidence for dissociation of influent CdEDTA²⁻ by Fe-oxide/hydroxide surfaces. The large perturbation produced during the flow interrupt (18.55 pore volumes), indicated that the production and/or release of Fe(III)EDTA⁻ from the solid surface may have been kinetically-limited. Al was mobile and leaching from the soil surface at the initiation of the experiment, but the increase in Al concentrations during the influent pulse probably indicates that production of Al(III)EDTA⁻ from soil surfaces was enhanced. The sharp decrease in Al concentrations during the flow interruption may be due to competition by Fe(III) for the EDTA⁴⁻ ligand.

35

Al was produced, a clear indication of enhanced dissolution or desorption as a result of a surface-mediated reaction. The formation of Al(III)EDTA$^-$ was possible since the stability constant (log K) of Al(III)EDTA$^-$ is 19.1, relative to 18.2 for CdEDTA^{2-} (Sposito and Mattigod, 1980). Since Al was mobile at the initiation of the influent, the formation of Al(III)EDTA$^-$ may occur in solution and/or on the soil surface. The Al source may be as an exchangeable ion on clays, or in coprecipitation with Fe-oxides, where the proportion of Al in the latter can approach 20 mol % (Amseth and Turner, 1988). Fe(III)EDTA$^-$ and CdEDTA^{2-} were both directly quantified, and we hypothesized that the excess EDTA^{4-} was associated with Al. Mass recovery of EDTA^{4-} was complete, so it is unlikely that EDTA^{4-} remained associated with the solid surface. The concentration of Al decreased dramatically following the flow interruption, which could be a result of competition for the EDTA^{4-} ligand by Fe oxides, since the stability of Fe(III)EDTA$^-$ (log K = 27.7) is greater than that of Al(III)EDTA$^-$ (log K = 19.1). Because direct detection of Al(III)EDTA$^-$ was not feasible, a geochemical speciation model, GEOCHEM (Sposito and Mattigod, 1980) was used to determine the distribution of EDTA^{4-} between metal cations (Figure 7). According to model predictions of thermodynamic equilibrium, EDTA^{4-} was distributed between Al, Fe, and Cd, as we had surmised. However, the model slightly but consistently, underpredicted the concentration of CdEDTA^{2-} and overpredicted that of Al(III)EDTA$^-$. This discrepancy may be due to a number of factors, including inaccurate characterization of the aqueous solution. However, several analytical techniques were used, including IC, ICAP, spectrophotometry, radioactive tracers, and AA, which provided a check on instrument accuracies. A more plausible explanation may be due to the simple limitation of using an equilibrium speciation model to predict the speciation of a solution that is actually not at equilibrium. The flow interruption demonstrated the presence of nonequilibrium, as well as the progression towards dissociation of CdEDTA^{2-} during the experiment. Thus, if the system had not reached equilibrium with respect to the dissociation of CdEDTA^{2-}, the experimental measurements of CdEDTA^{2-} may be higher than equilibrium predictions. More EDTA^{4-} may have been allocated to Al because of the high concentrations of leached Al. The GEOCHEM results provided an estimate of the effluent speciation, however, it is important to note that reaction kinetics may limit the accuracy of equilibrium models and predictions based on those estimates.
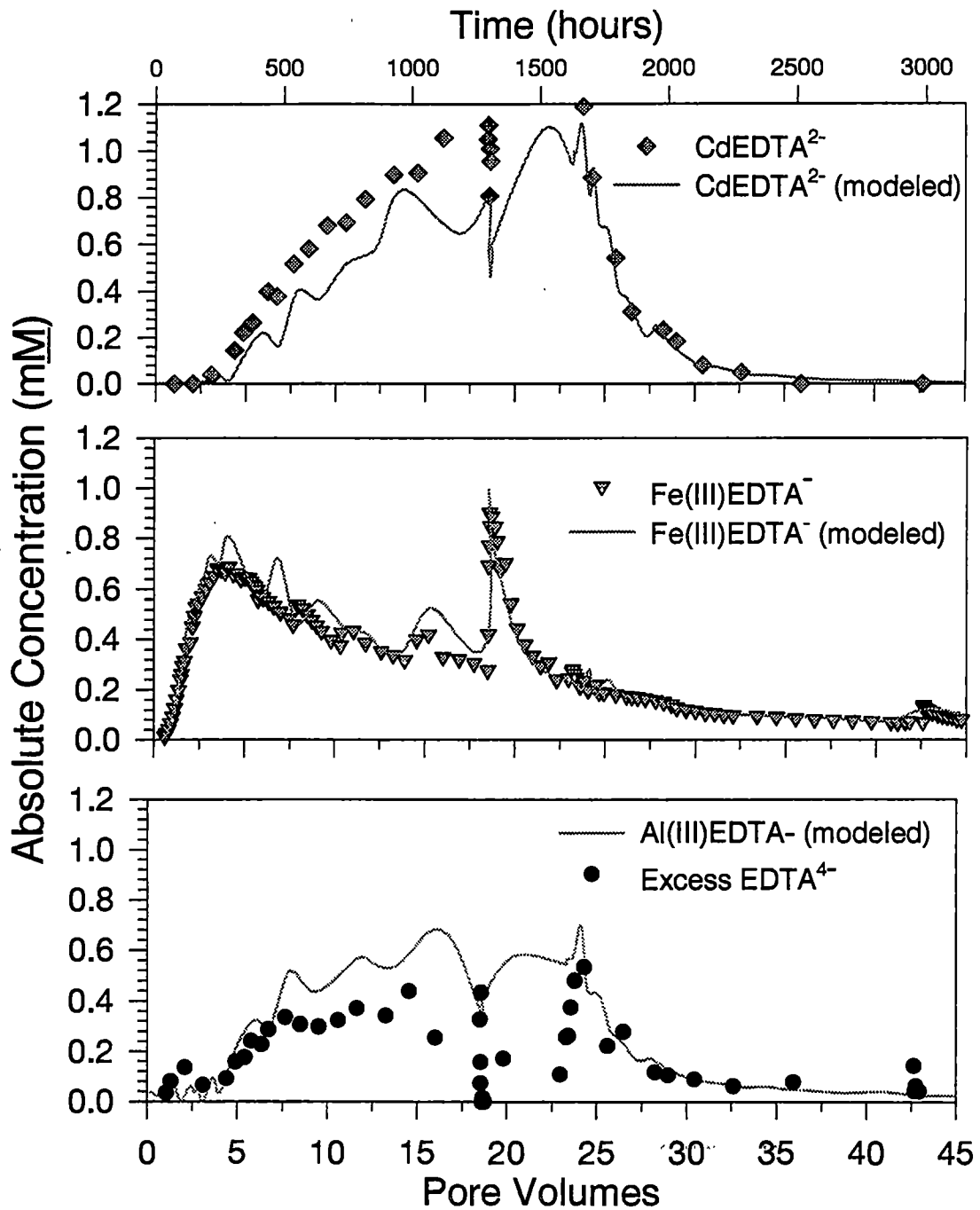
Figure 7. The distribution of EDTA^{4-}, observed, and predicted using a geochemical speciation model (experiment 1). The predicted concentrations were generally very close to observed, particularly for Fe(III)EDTA$^-$. However, the predictions of CdEDTA^{2-} were somewhat lower than observed. Al(III)EDTA$^-$ was not directly detected, but it is likely that excess EDTA^{4-}, that was not associated with Fe or Cd was chelated with Al. The discrepancies between model predictions and observed concentrations may be related to nonequilibrium conditions during transport through undisturbed media.

Multispecies transport of Co(II)EDTA^{2-} and CdEDTA^{2-}

A multispecies experiment (experiment 2) demonstrated that there were significant differences in the behavior of the influent contaminants, Co(II)EDTA^{2-} and CdEDTA^{2-}. The breakthrough of Br$^-$ was followed by ^{57}Co, and then by ^{109}Cd, with the latter two metal complexes exhibiting a significant degree of retardation (Figure 8). Tailing was extensive in the breakthrough of ^{57}Co and ^{109}Cd, as the effluent ^{57}Co reached a maximum of 90% of the influent, while ^{109}Cd only reached 80%. The ^{57}Co and ^{58}Co curves were nearly identical, suggesting that isotopic composition did not affect chemical behavior (data not shown). Influent and effluent flow interruptions resulted in significant perturbations in all three components.

Adsorption of ^{109}Cd and ^{57}Co was mostly reversible, as effluent recovery was 96% of the influent (Table 6). A profile of adsorbed ^{109}Cd and ^{57}Co was generated by sectioning the columns into 1.5-2.0 cm intervals, and counting the decays from the soil (Figure 9). The ^{109}Cd recovered from the soil was 3.74%, for a total influent recovery of 99.74%. The soil profile exhibited an enrichment in the middle of the column, which may be related to a large root. The solid phase recovery of ^{57}Co was 1.78%, for a total mass recovery of 97.8% (Table 6).

A major difference between experiment 2 and the others was that the flow interruption was performed earlier in the experiment (5.32 pore volumes), resulting in significant physical nonequilibrium, as evidenced in the transport of Br$^-$ (Table 3). Nonequilibrium with respect to sorption of reactive species was also observed, due to the combined effects of physical, and perhaps chemical, nonequilibrium. The observed perturbation in ^{109}Cd was considerably larger than in the single-species experiment.

Transport modeling was performed on the Br$^-$ BTC to quantify dispersion through the column, and the extent of physical nonequilibrium. Though the decrease in Br$^-$ during the flow interruption indicated the existence of physical nonequilibrium, the transport of Br$^-$ was initially modeled with the CD equation, assuming R = 1, to obtain an estimate of the dispersion coefficient of 27.5 ± 2.02 cm^2 d^{-1} (Table 5). The Peclet number was 2.63 ± 0.20, which indicated that preferential flow was a dominant mechanism in this
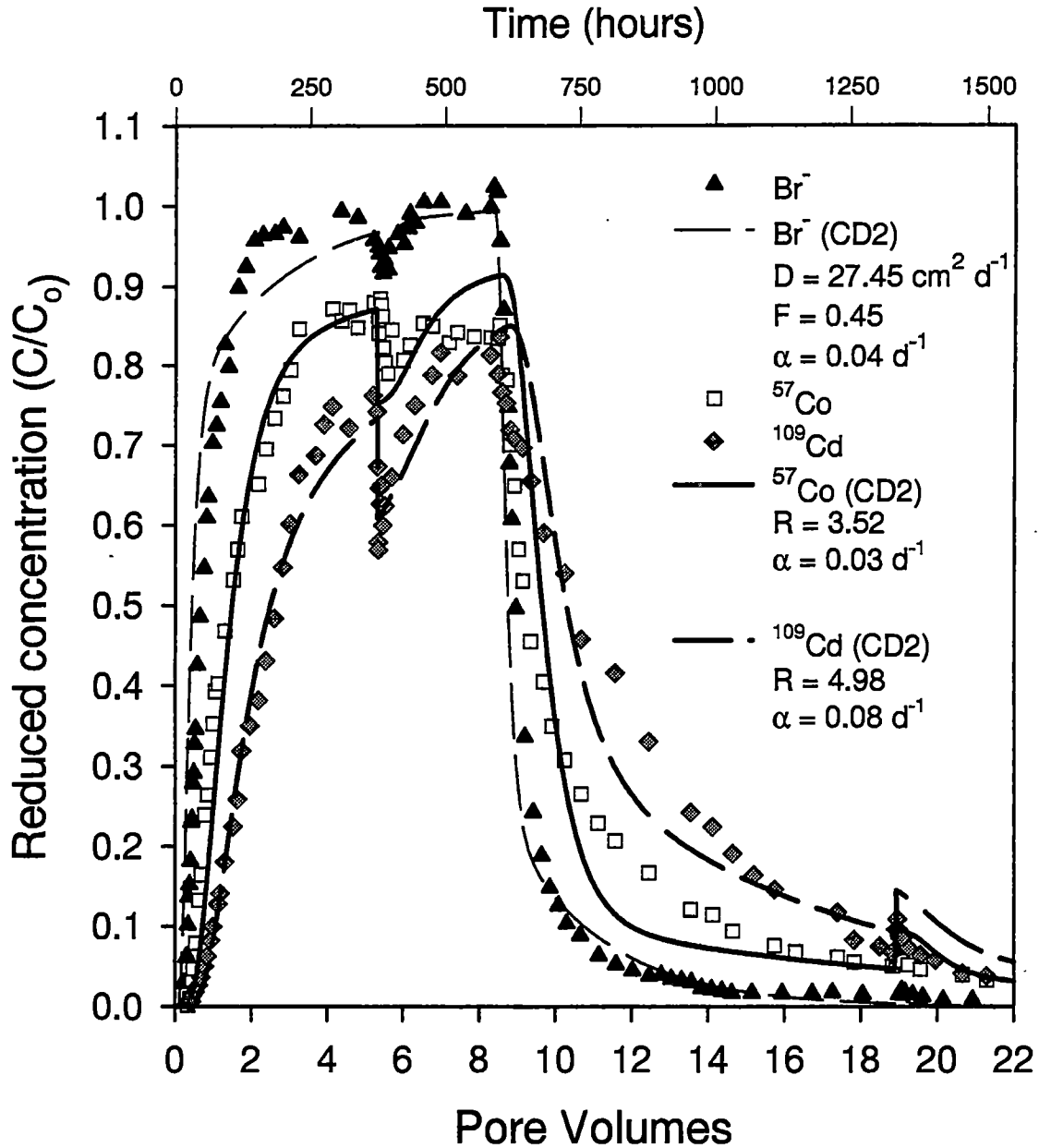
Figure 8. Experimental and modeled breakthrough curves of Br$^-$, ^{57}Co, and ^{109}Cd for the chelated multispecies experiment (2). The reactive species exhibited retardation relative to Br$^-$, and considerable tailing in the breakthrough and washout. All three species exhibited perturbations associated with the flow interruption (5.32 pore volumes), indicating the prevalence of nonequilibrium conditions. Transport modeling assumes a distribution of equilibrium and kinetically-limited sites, F, with equilibrium sites modeled with the CD equation, and α representative of the rate of mass transfer between the equilibrium and kinetically-limited sites. The equilibrium CD equation was applied to Br$^-$ to determine dispersion during transport, then the two-site model was applied to determine the fraction of mobile water (sites), F. These parameters were applied to modeling of the reactive species, with optimization of R and α.
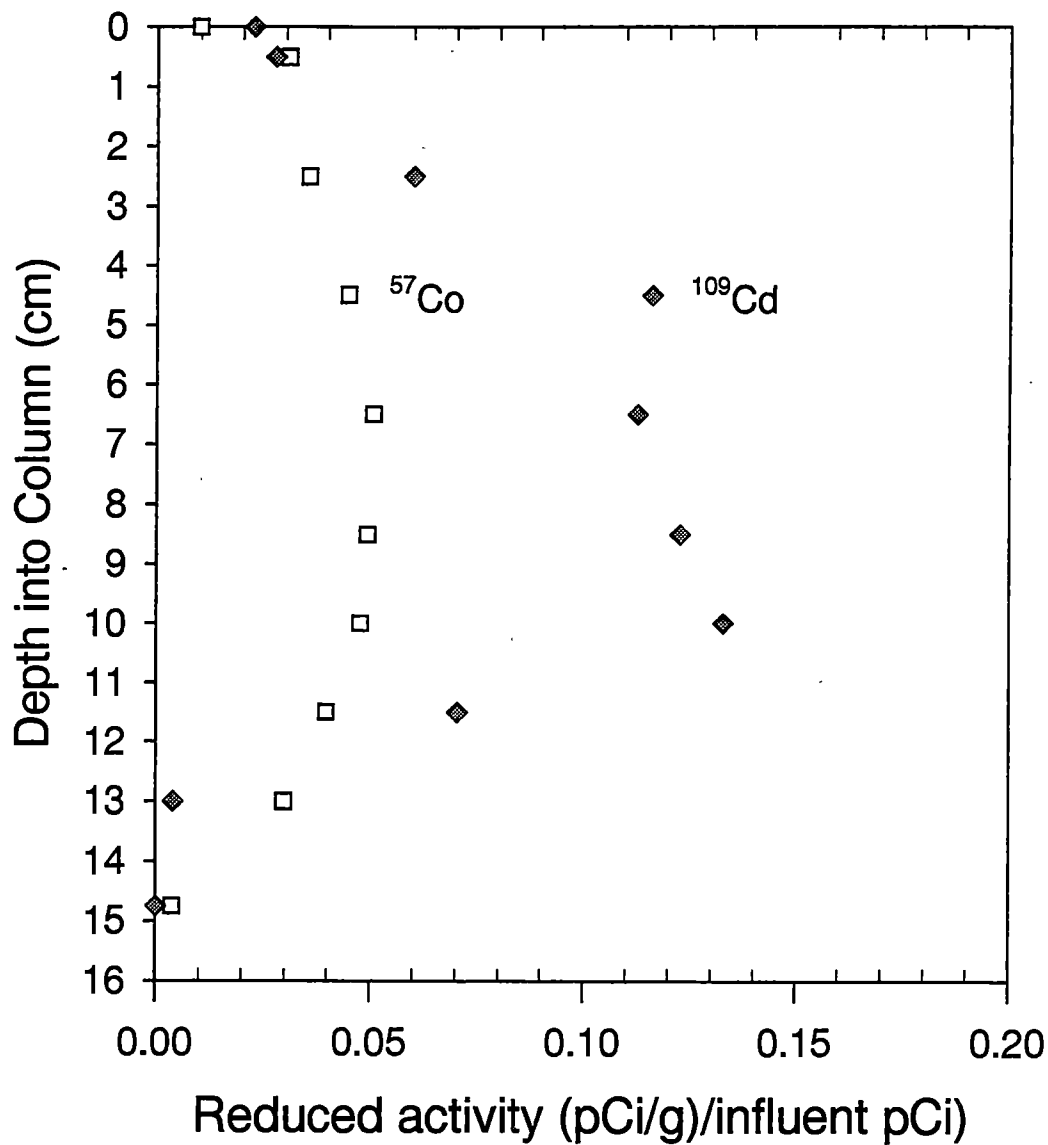
Figure 9. Profile of adsorbed ^{57}Co and ^{109}Cd within soil column 2. Following the termination of the experiment, the columns were sectioned and counted for adsorbed radiotracers. Recovery of ^{57}Co was 1.78% of the influent concentration, and 3.74% of ^{109}Cd. The enrichment of ^{109}Cd in the midsection may be related to a large decaying root and associated reduced clays.

column. Dissection of the column at the end of the transport experiment revealed that it was distinctly structured and fractured relative to the other columns, which may account for the lower Peclet number and greater observed tailing and dispersion of the tracers. Because of the significant perturbation following both flow interruptions, the two-site CD model was applied to the transport of Br^-. The estimate of dispersion from the CD equation was used, with retardation equal to one. The BTC was best simulated with $F = 45\%$ mobile water and $\alpha = 0.04$ d^{-1}, which adequately reproduced the magnitude of the interruptions (Figure 8). A 45% fraction of mobile water was also determined by Reedy et al. (1996), in their investigation of Br^- transport through the same column material. Values of α were nearly identical to those predicted by Reedy et al. (1996) for the pore water velocity of these studies.

Transport modeling was also performed on the BTCs of the reactive contaminants [109]Cd and [57]Co to determine transport characteristics, including retardation and the rate of mass transfer between the mobile-immobile regions. The two-site CD model was used to reproduce the perturbations produced by interrupting flow (Figure 8). The mass transfer coefficient, α, was compared to those of Br^- to determine the extent of chemical nonequilibrium. The conventional CD equation was also applied to the [109]Cd and [57]Co BTC, and the following discussion centers on comparisons of the CD equation with the two-site CD model (Figures 10 and 11).

The transport of [109]Cd was adequately modeled using the CD equation, which provided a good fit to the data (Figure 10). The two-region simulation, however, best described the data with $\alpha = 0.08$ d^{-1}, $R = 4.98$, $F = 0.45$ (Figure 10). The retardation was lower than the single-species experiment, which may related to differences in the reactivity of the saprolite, or physical processes, related to the greater dispersion through this column (Table 5). The mass transfer coefficient, though similar to the single-species experiment, included the additional effects of physical nonequilibrium. The rate of physical mass transfer was 0.04 d^{-1}, as determined from the Br^- simulations. The faster rate of [109]Cd transfer indicated that it was far from equilibrium, probably due to additional, rate-limited chemical processes.

The equilibrium CD model did not adequately model the transport of [57]Co for this experiment, primarily because of the high degree of tailing was observed in the breakthrough of [57]Co (Figure 11). The

Figure 10. Comparison of the equilibrium (one-site) and two-site (equilibrium and kinetic) versions of the CD equation on [109]Cd (experiment 2). The equilibrium fit was close, but the large perturbation following the flow interruption indicated that nonequilibrium processes affected the breakthrough of [109]Cd, thus the two-site model was appropriate. The two-site model closely approximated the breakthrough curve and the flow interruption.
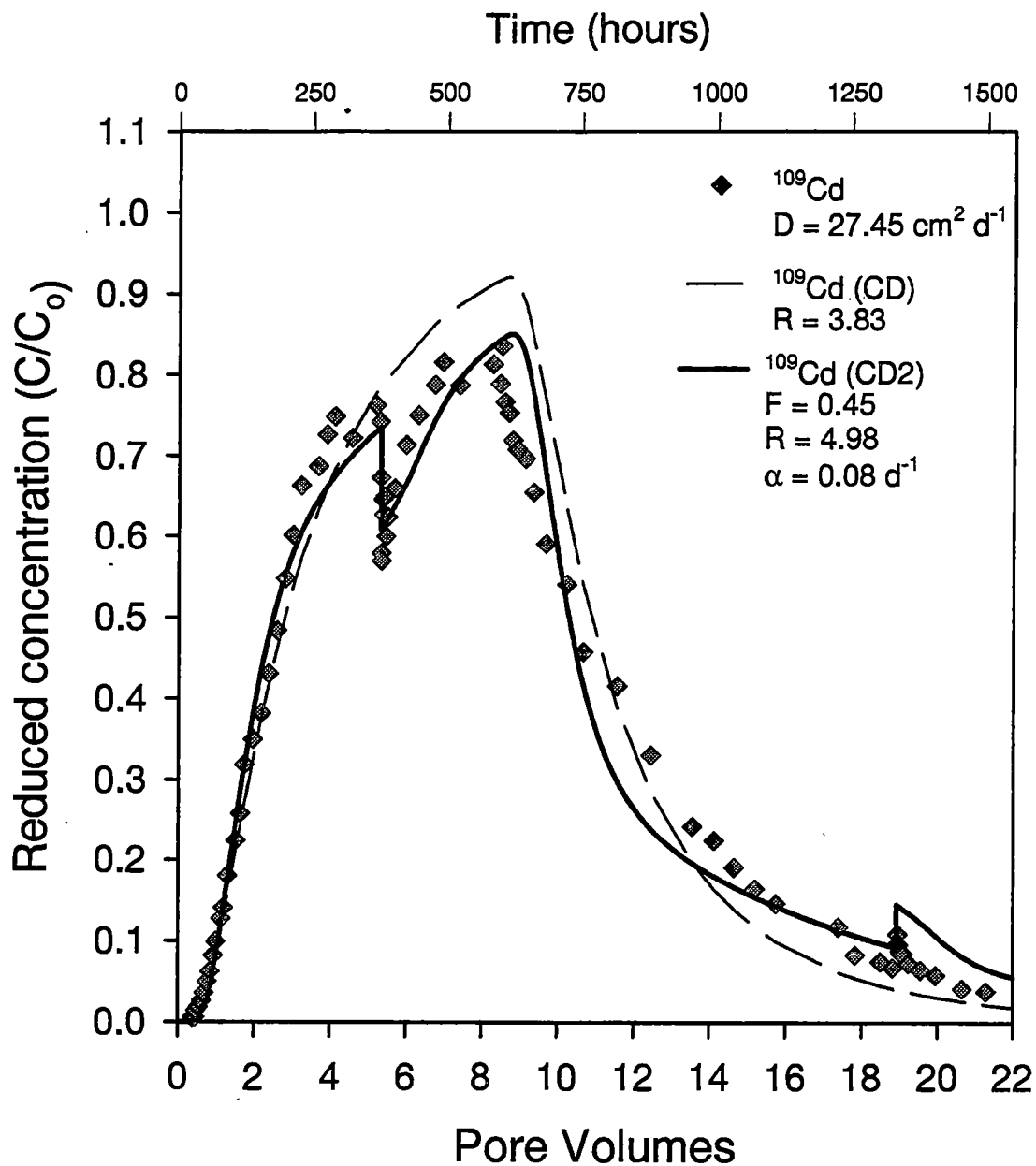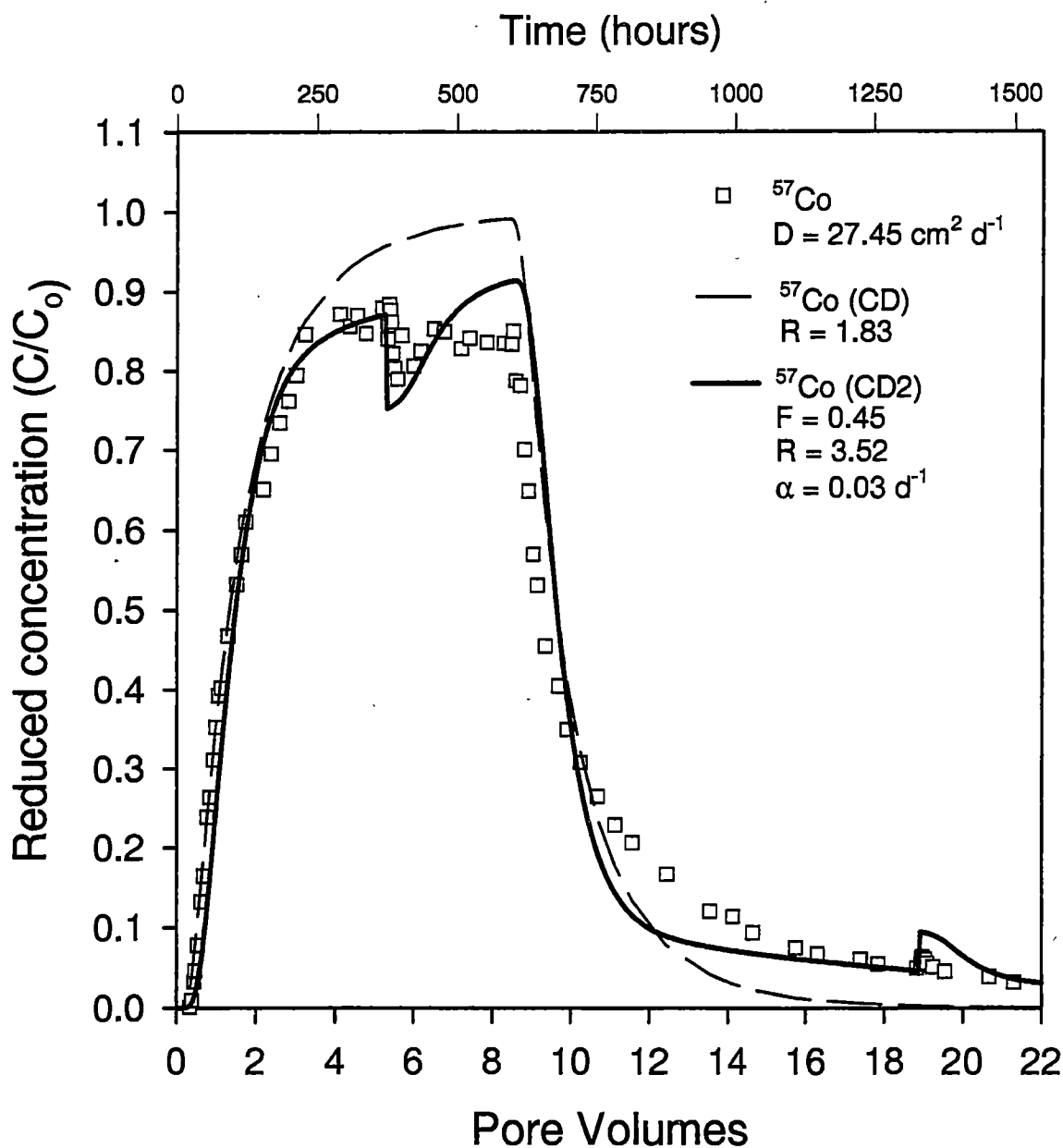
Figure 11. Comparison of the one-site, equilibrium and two-site (equilibrium and kinetic) versions of the CD equation on [57]Co (experiment 2). The equilibrium version could not fit the observed tailing in the breakthrough and washout of [57]Co. The two-site model closely approximated the tailing, as well as the large interruption perturbation.

2-site CD model, however, proved more successful (Figure 11). The best simulation of the flow

interruption and breakthrough curve were obtained with the mass transfer coefficient, α, equal to 0.03 d^{-1}, a

retardation coefficient of 3.52, and 45% mobile water (Table 5). The rate of mass transfer was very close to

the rate of physical transfer determined from Br^- simulations. This indicated that the transport of ^{57}Co was

not limited by the rate of sorption or chemical reaction.

Geochemical controls on the transport of Co(II)EDTA^{2-} and CdEDTA^{2-}

The transport of CdEDTA^{2-} again appeared to be controlled by a surface-mediated dissociation

reaction. Dissociation of the CdEDTA^{2-} complex was prevalent, and there was considerable production of

Fe(III)EDTA$^-$ and Al(III)EDTA$^-$ (Figure 12). A pulse of Fe was produced during the experiment, and there

was a large increase, from 0.77 mM to 1.48 mM, as a result of nonequilibrium during the flow interruption.

Though Fe(III)EDTA$^-$ cannot be detected in the presence of Co(III)EDTA$^-$, aqueous Fe(III) was probably

associated with EDTA^{4-}, since Fe(III) is not soluble under oxidizing conditions, except as colloidal particles

or within a strong ligand. Speciation modeling also predicted 100% complexation of Fe^{3+} with EDTA^{4-}.

Though the Al curve did not exhibit a pulse, its aqueous concentration was high and there were prominent

perturbations during the interruption and the initial breakthrough of Cd and Fe, which suggested the

formation of Al(III)EDTA$^-$ (Figure 12). The absence of a distinct Al pulse, combined with the high

aqueous Al concentrations, suggested that Al may effectively compete for the ligand of CdEDTA^{2-} in

solution. The stability constant of Al(III)EDTA$^-$ (log K = 19.1) was slightly greater than that of CdEDTA^{2-}

(log K = 18.2), thus the former would be more thermodynamically stable given appropriate time. However,

equilibrium thermodynamics could not adequately predict the distribution of EDTA^{4-}, due to the kinetic

limitations present during transport (data not shown). The results of speciation modeling were similar to the

single-species experiment – the predicted concentration of CdEDTA^{2-} was lower than measured, probably

as a result of excess allocation to the thermodynamically favored Al(III)EDTA$^-$.

Influent Co(II)EDTA^{2-} was oxidized to Co(III)EDTA$^-$ during transport through the Melton Branch

saprolite (Figure 13). Oxidation of Co(II)EDTA^{2-} to Co(III)EDTA$^-$ was dominant, based on the fact that

44
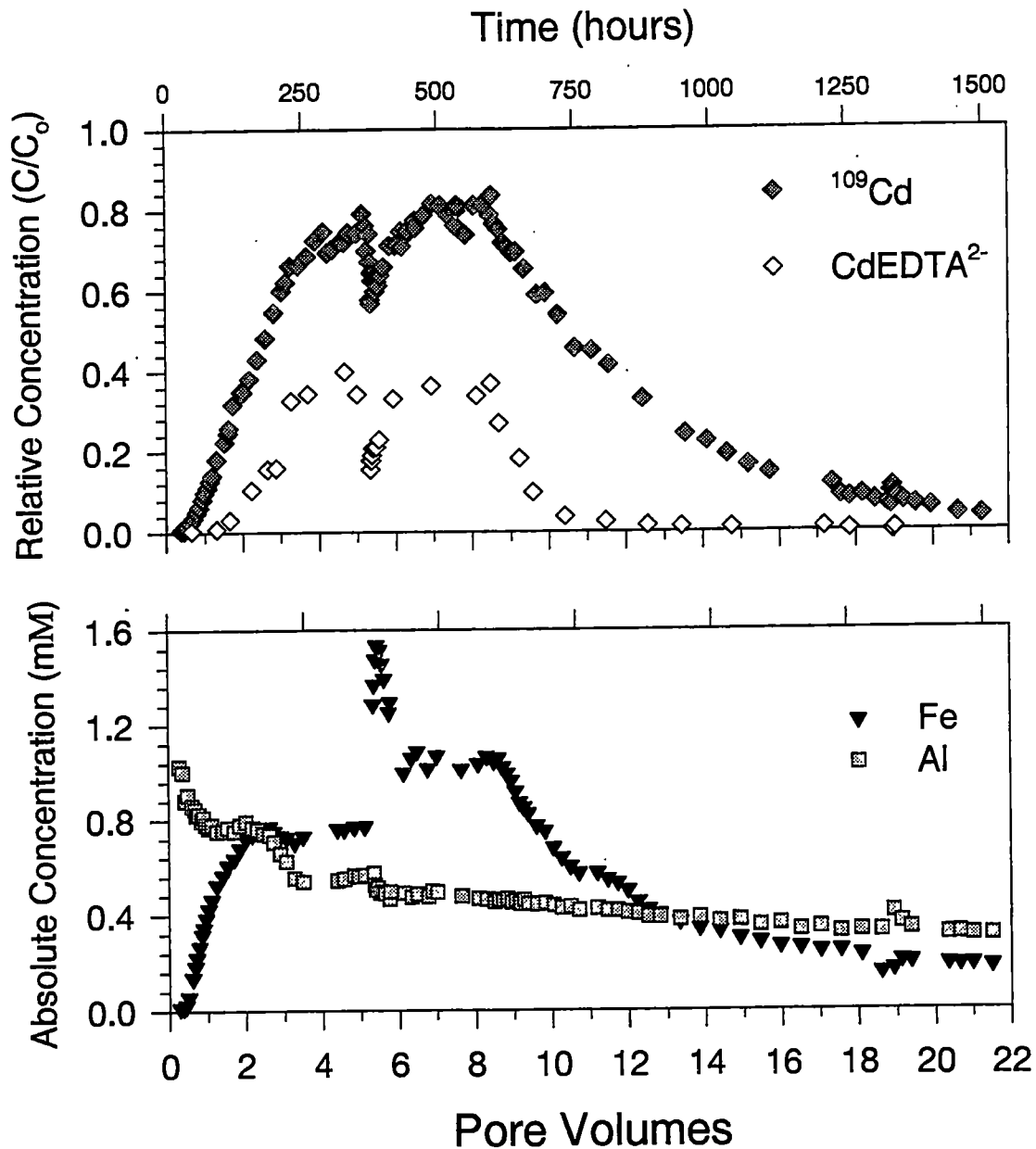
Figure 12. The behavior of CdEDTA^{2-}, and the subsequent distribution of EDTA^{4-} in the dual-chelate experiment (2). **a).** The breakthrough of ^{109}Cd and CdEDTA^{2-}. Dissociation of the CdEDTA^{2-} complex is evident. There was a large perturbation associated with the flow interruption in both species, indicative of nonequilibrium conditions in the adsorption and dissociation of the complex.

b). The breakthrough of Fe and Al, released by dissolution of the solid phase. Fe(III)EDTA$^-$ was not detectable due to interference, but speciation calculations indicated that all aqueous Fe(III) was chelated. The production of Fe(III)EDTA$^-$ is clear evidence of the dissociation of the influent CdEDTA^{2-} complex. The large perturbation associated with the interruption (5.32 pore volumes) indicated that significant production and/or release of Fe(III)EDTA$^-$ occurred during this period, suggesting kinetic limitations during flow. Al was leaching from the exchangeable surface complex, and there was no apparent pulse of Al. However, perturbations in the Al curve during the breakthrough of Fe at ~ 3 pore volumes, and during the interruption indicated that Al dynamics probably also affected the distribution of EDTA^{4-}. The decreasing Al concentrations in the presence of Fe may indicate competition by Fe for EDTA^{4-}.

45
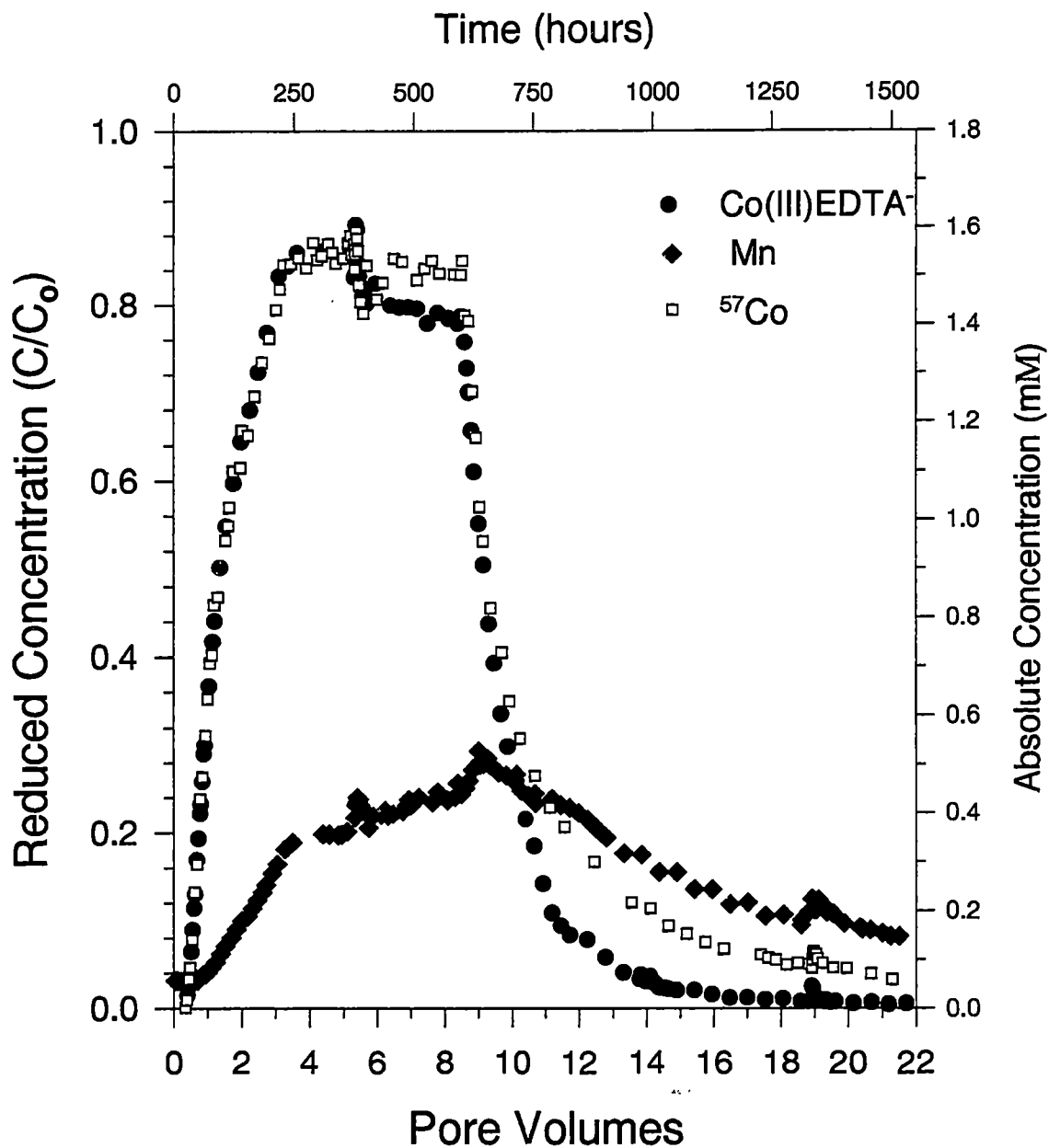
Figure 13. The production of Co(III)EDTA⁻ and Mn(aq) from influent Co(II)EDTA²⁻ (experiment 2). Eluted ⁵⁷Co has been oxidized to Co(III)EDTA⁻, with concurrent production of Mn(II), evidence of a surface-mediated oxidation/reduction reaction. Plots of ⁵⁷Co and Co(III)EDTA⁻ are shown in both reduced (left axis) and absolute (right axis) concentrations, while Mn(aq) is referenced only to absolute concentrations (right). The separation between ⁵⁷Co and Co(III)EDTA⁻ is evidence of dissociation of the Co-EDTA complex following the interruption.

the Co(III)EDTA$^-$ and ^{57}Co curves were nearly identical (within analytical error) during the first 10 pore volumes. Previous work has shown that oxidation of Co(II)EDTA^{2-} may occur in a surface-mediated redox reaction with Mn-oxides (Jardine et al., 1993; Jardine and Taylor, 1995a; Jardine and Taylor, 1995b). Secondary Mn-oxides along bedding and fracture planes in the Melton Branch saprolite (Arnseth and Turner, 1988) may be the source of the pulse of Mn(II) liberated during this experiment. The reaction scheme may occur as suggested by Jardine and Taylor (1995a), where Co(II)EDTA^{2-} becomes adsorbed to the soil surface, and it is subsequently oxidized to Co(III)EDTA$^-$, while surficial Mn(IV) is reduced to aqueous Mn^{2+}. The stoichiometry of this reaction assumes two electrons are required to reduce Mn(IV), while one is produced during the oxidation of Co(II)EDTA^{2-} to Co(III)EDTA$^-$. Mass balance can be used to test this hypothesis, where the mass is obtained by integrating the area beneath the effluent Mn(II) and Co(III)EDTA$^-$ curves. The quantity of Mn produced was 0.080 meq, while that of Co(III)EDTA$^-$ curve was 0.094 meq, which confirms the 2:1 stoichiometry. In addition, the tailing of Mn suggested that its elution was not complete at the termination of the experiment, and this may account for the slightly lower meq of observed Mn(II). Also, reduced Mn is generally unstable in solution, and re-adsorption and/or reoxidation may also be occurring (Jardine and Taylor, 1995b).

The flow interrupt in Experiment 2 suggested that physical and/or chemical nonequilibrium affects the transport of ^{57}Co. Since there was also a perturbation in the Br$^-$ curve, and also because of the similar rate of mass transfer, it is difficult to isolate chemical nonequilibrium. Unusual dynamics were associated with the flow interrupt. Before the interruption, all Co eluted from the columns was Co(III)EDTA$^-$, which was confirmed by direct I.C. analyses. However, following the interrupt, there was a 5% decrease in amount of Co(III)EDTA$^-$ exiting the column, while the total Co curve flattened (Figure 13). The difference between these two curves indicated that some Co^{2+} was liberated from the EDTA^{4-} complex, because it could not be accounted for in direct analyses for Co(II)EDTA^{2-}. The flow interrupt may have passivated the MnO$_2$ surfaces due to O$_2$ consumption. The subsequent lack of reoxidation of surface-bound Mn^{2+} may have therefore decreased the capacity for reduction by regenerated Mn(IV), and allowed other mineral surfaces to interact with Co(II)EDTA^{2-}. Previous work has shown that Fe and Al oxides may dissociate the

Co-EDTA complex (Girvin et al., 1993; Szecsody et al., 1994). Mass balance calculations indicate that around 85% of the Co(II)EDTA^{2-} influent was oxidized to Co(III)EDTA$^-$, therefore this reaction appears to dominate the transport of chelated cobalt. The dissociation of Co-EDTA may account for the remaining 15%, which indicates that this reaction may be important in the absense of Mn-oxides.

Transport of Br$^-$, ^{57}Co(III)EDTA$^-$, ^{109}CdEDTA^{2-}, and H^{51}CrO$_4^-$

The transport of three anionic complexes, ^{109}CdEDTA^{2-}, ^{57}Co(III)EDTA$^-$, and H^{51}CrO$_4^-$ were investigated in a multispecies system (experiment 3). Co(III)EDTA$^-$ was used to characterize the transport of Co, because Co(II)EDTA^{2-} would be readily oxidized to Co(III)EDTA$^-$ in the presence of Cr(VI) in the aqueous influent solution. The breakthrough of Br$^-$ was followed by ^{57}Co and ^{109}Cd, as in the previous experiments. However, the breakthrough of ^{51}Cr was significantly retarded, and the eluted concentration reached a maximum of only 60%, indicating significant mass loss to the soil (Figure 14). The eluted ^{51}Cr was entirely Cr(VI), within analytical error. A flow interruption was performed, but no perturbation was apparent in the concentration of Br$^-$, suggesting that physical equilibrium had been attained. There were decreases in the concentrations of ^{109}Cd and ^{51}Cr, and an increase in the concentration of ^{57}Co, suggesting that the reactive contaminants had not reached chemical (and perhaps physical) equilibrium at the time of the interruption. Soil profiles of ^{57}Co and ^{109}Cd were similar to those of column 2, but the influent recovery was lower, 0.33% and 0.26%, respectively (Figure 15). ^{51}Cr was distributed through the column, and soil counting determined that 51% of the influent Cr(VI) remained associated with the soil (Table 6). A large (4-6 grams) root surrounded by a gray, reduced clay was found in the immediate influent region of this column (20 grams). ^{109}Cd activity in both the roots and the clays was 4-5 times as high as the surrounding matrix, on a per gram basis, while only the root was enriched in ^{51}Cr. Another large root with associated clays was found in column 2, that also exhibited enrichment in ^{109}Cd. The affinity of Cd for dissolved organics has been observed in column studies by Dunnivant et al. (1992), which should also translate to organics associated with the solid phase.
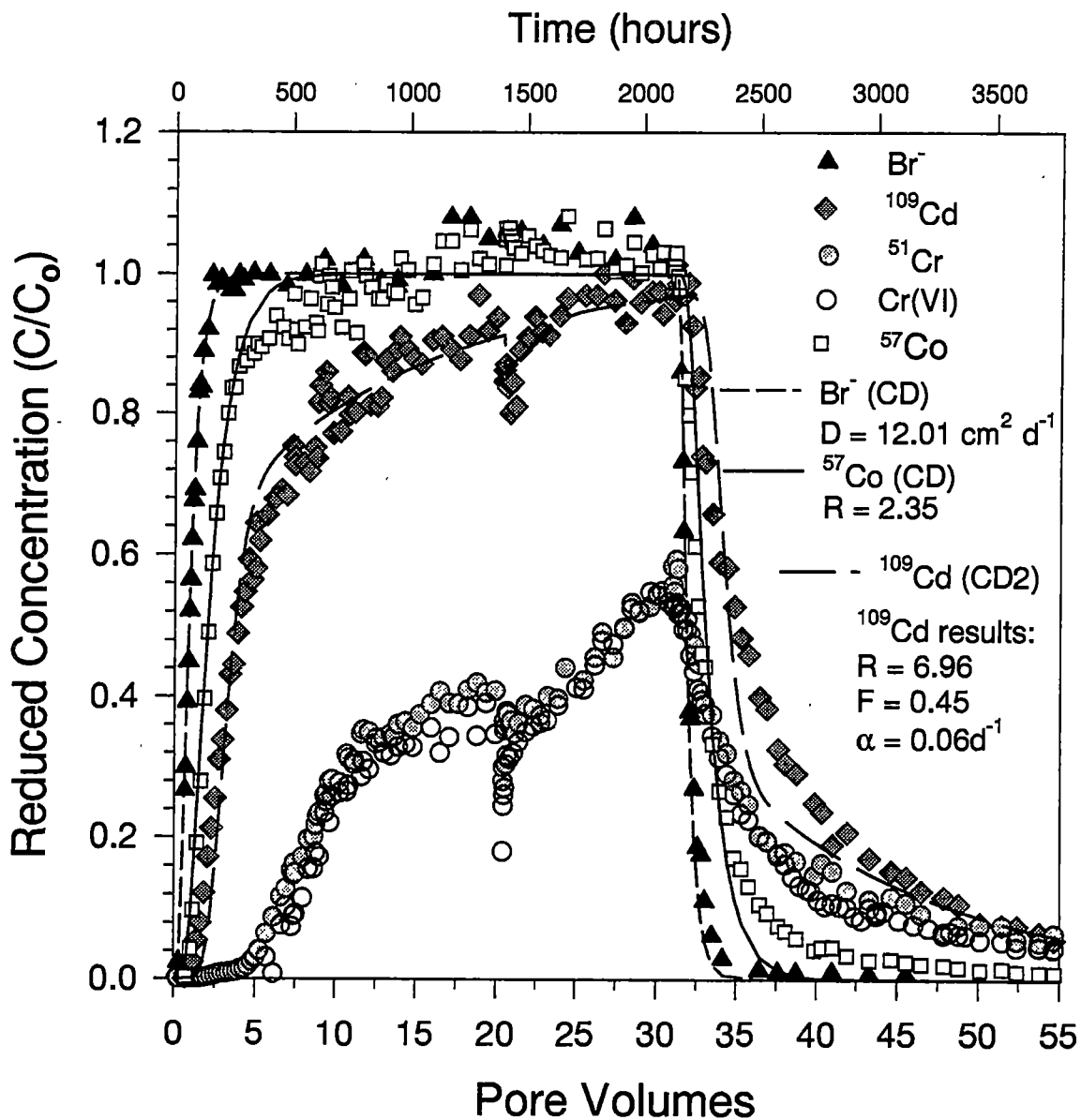
Figure 14. Experimental and modeled breakthrough curves of Br⁻, ^{57}Co, ^{109}Cd, and ^{51}Cr, triple multispecies experiment (3). The retardation of ^{57}Co and ^{109}Cd observed was consistent with that observed in the single and dual-species experiments. Considerable retardation and mass loss were apparent in the ^{51}Cr curve, and all eluted ^{51}Cr was identified as Cr(VI), as in the influent solution. The flow interruption (20.41 pore volumes) produced no perturbation in Br⁻, a 5% increase in ^{57}Co, and observable decreases in ^{109}Cd and ^{51}Cr, indicating the prevalence of chemical nonequilibrium for these species. The equilibrium CD equation was used to model ^{57}Co and Br, while the two-site model was applied to ^{109}Cd.
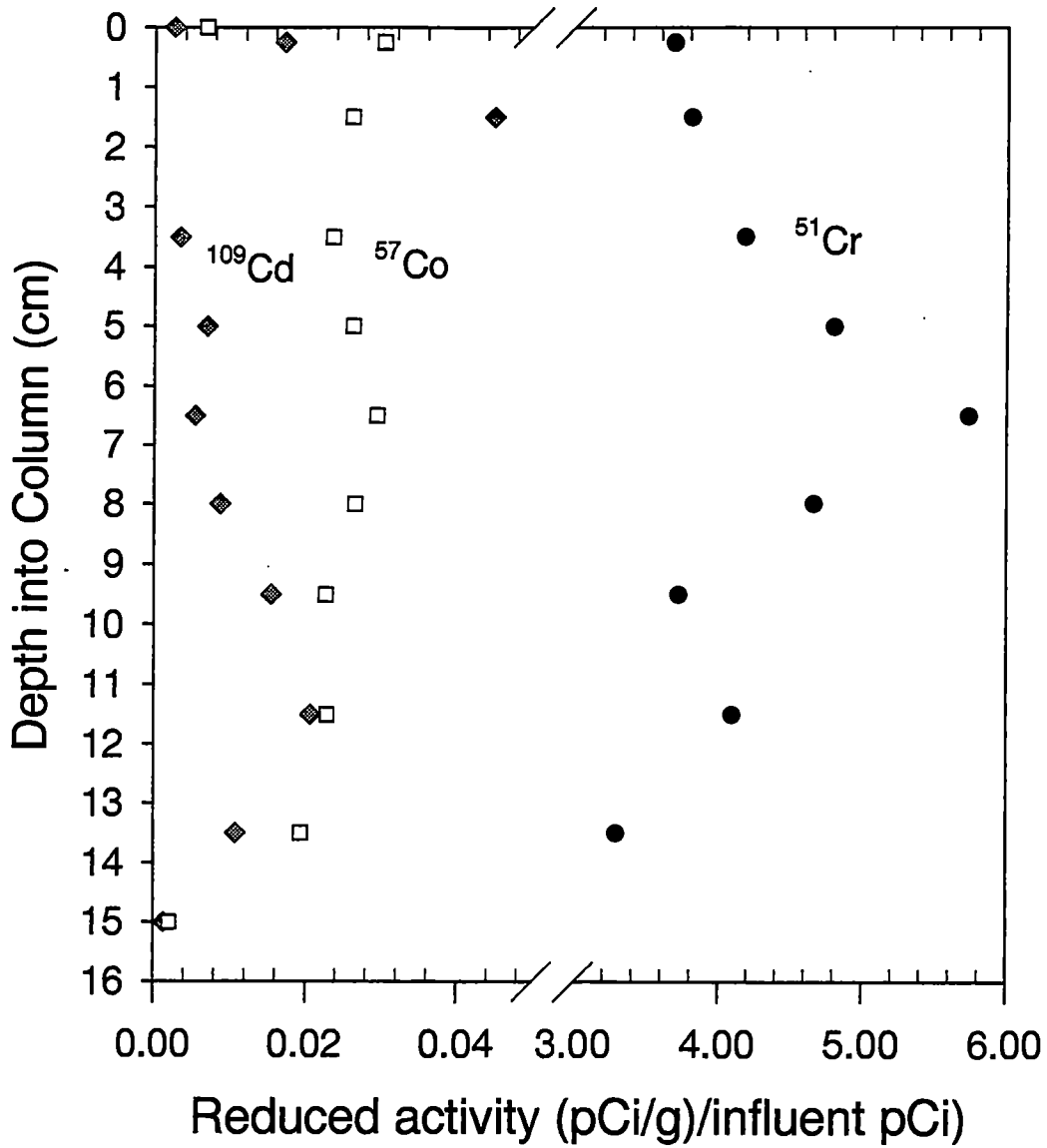
Figure 15. Profile of adsorbed ^{57}Co, ^{109}Cd, and ^{51}Cr within soil column 3. Irreversible sorption of ^{51}Cr is clearly more significant, accounting for 51% of the influent concentration. Irreversible sorption of ^{57}Co and ^{109}Cd accounted for 0.33%, and 0.26%, respectively. An enrichment of ^{109}Cd is apparent at 2 cm depth, perhaps associated with a large decaying root and associated reduced clays.

The observed loss of Cr mass in the mutlispecies experiment (3) suggested that irreversible sorption, or perhaps chemical precipitation, prevented the elution of Cr from these columns. Previous investigations have suggested that Fe(II), as well as organic matter, may catalyze the reduction of Cr(VI) to Cr(III). While aqueous Cr(VI) is anionic, aqueous Cr^{3+} is a trivalent cation, and thus may undergo strong or irreversible sorption to soil surfaces. Since our soils were devoid of Fe(II) bearing minerals, it was hypothesized that organic matter was catalyzing the reduction of Cr(VI) to Cr(III). An initial test of this hypothesis involved a batch experiment containing dissolved organic matter from the Georgetown, SC wetlands pond and Cr(VI). The aqueous solution was monitored for the concentrations of Cr(VI) and total Cr. Over 140 days, the concentration of Cr(VI) was reduced by 50% (Figure 16). Thus, organic matter apparently affected the stability of Cr(VI), and therefore may be important in catalyzing the transformation of Cr(VI) to Cr^{3+}.

Therefore, two additional single-species experiments were performed to quantify the effects of organics in controlling the transport of $H^{51}CrO_4^-$. Transport through a control soil column (experiment 4), with influent $H^{51}CrO_4^-$, was compared to transport through an NOM-amended column (experiment 5), where the soil was loaded with natural organic matter before the initiation of the experiment. In the control experiment, the initial breakthrough of Cr(VI) occurred at around 5 pore volumes (Figure 17), nearly identical to the timing observed in the multispecies Cr(VI). Irreversible sorption accounted for 41.6% of the influent solution, as determined from counting the decays of ^{51}Cr in the soil sections (Table 6). However, dramatic retardation was observed in the NOM-amended column, as the initial breakthrough of ^{51}Cr began around 16 pore volumes (Figure 18). Irreversible sorption accounted for 54.2% of the influent solution, as determined from solid phase counting (Table 6). Therefore, organics were very effective in stabilizing Cr(VI) within the soil columns.
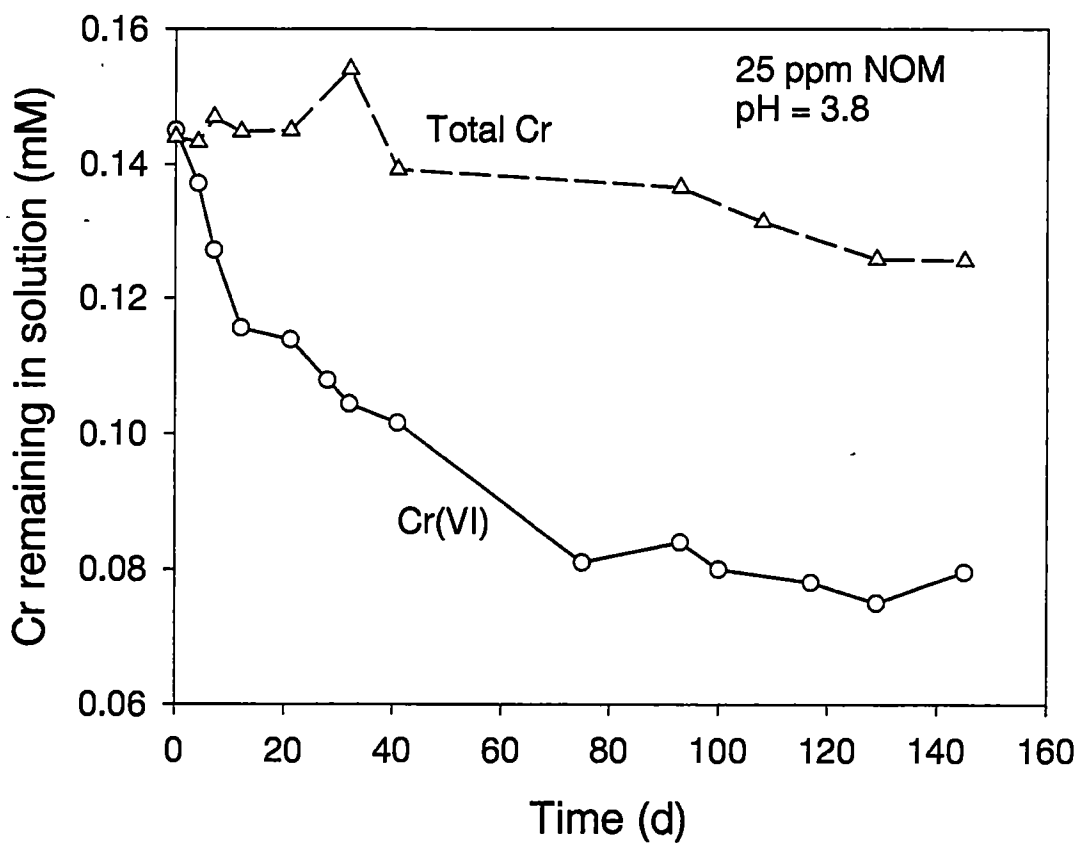
Figure 16. Batch experiment with Cr(VI) and dissolved natural organic matter (NOM). A decrease in Cr(VI) with time is apparent, presumably due to the reduction of Cr(VI) to Cr(III), catalyzed by the organic matter.
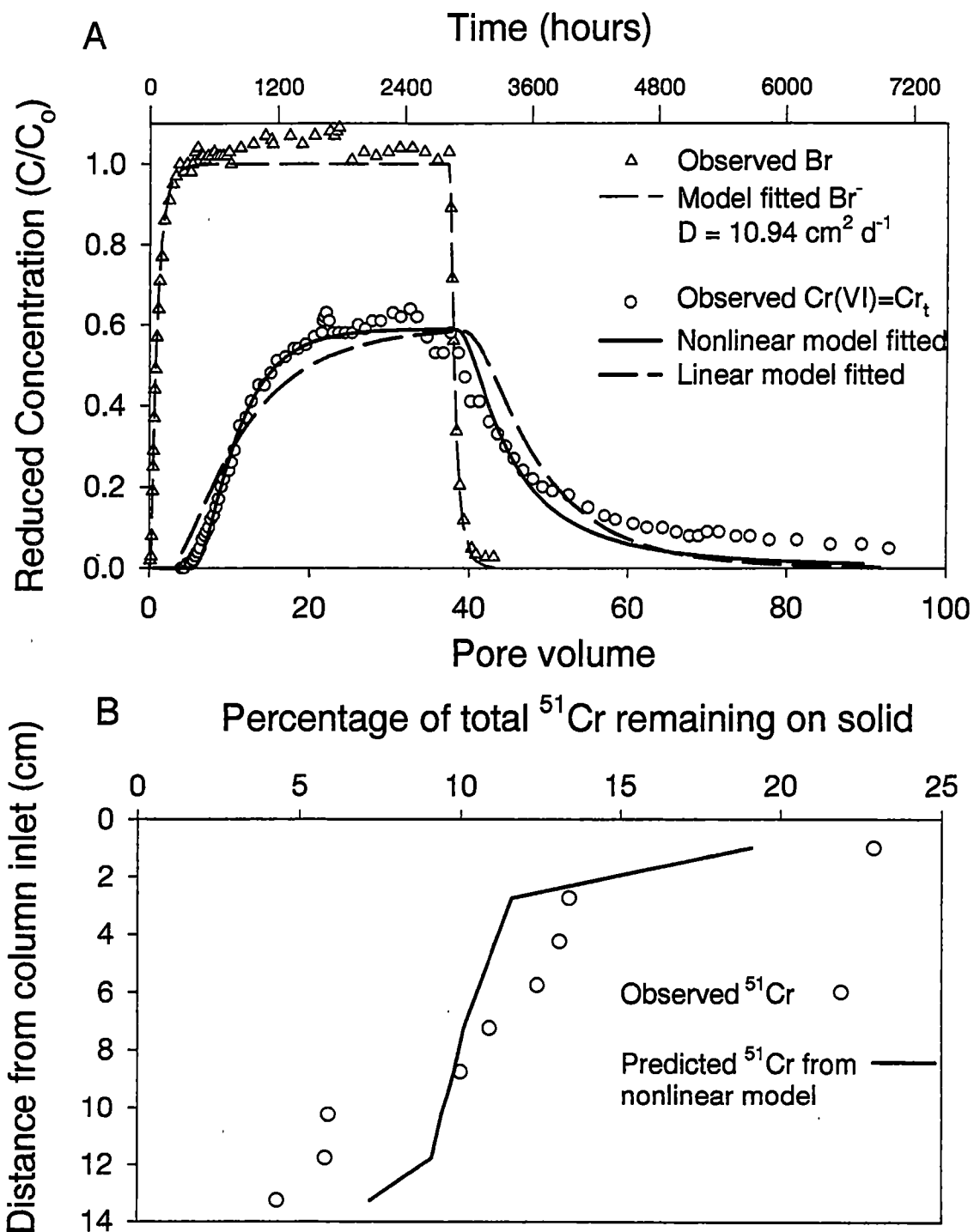
Figure 17. Experimental and modeled breakthrough curve of Br⁻ and ⁵¹Cr from the (control) single-species Cr experiment (4). **a)** Modeling of Br⁻ with the CD equation, while the Multi-Reaction Transport Model (MRTM) was applied to ⁵¹Cr, to reproduce the observed irreversible sorption of Cr. Irreversible sorption was modeled with a rate coefficient, k_s. Linear and nonlinear fits were both attempted, though the nonlinear fit is improved. **b)** Observed and predicted distribution of ⁵¹Cr irreversibly sorbed to the dissected column. Observed data was obtained from radiotracer soil counting following the termination of the experiment.

53
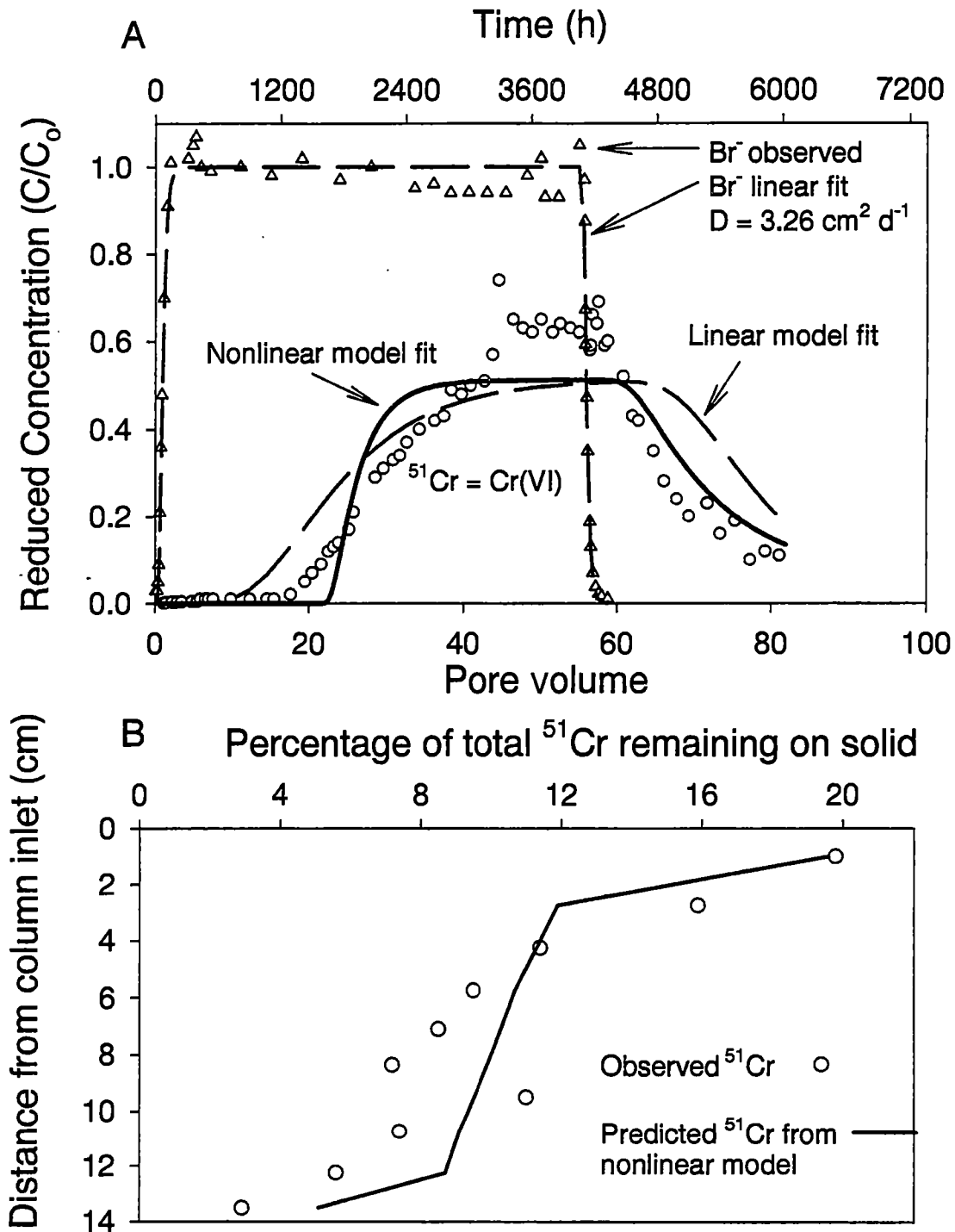
Figure 18. Experimental and modeled breakthrough curve of Br⁻ and ^{51}Cr from the NOM-amended Cr experiment (5). a) Modeling of Br⁻ with the CD equation, while the Multi-Reaction Transport Model (MRTM) was applied to ^{51}Cr, to reproduce the observed irreversible sorption of Cr. Linear and nonlinear fits were both attempted, though the nonlinear fit is probably more appropriate. b) Observed and predicted distribution of ^{51}Cr irreversibly sorbed to the dissected column. Observed data was obtained from radiotracer soil counting following the termination of the experiment.

Transport modeling of Br⁻, ⁵⁷Co(III)EDTA⁻, and ¹⁰⁹CdEDTA²⁻

Transport modeling was performed on the multispecies experiment (3) to quantify the transport of reactive contaminants through the soil columns, but it also tested the validity of the single-species modeling routine in the presence of several reactive species. Transport modeling of $Cr(VI)$ was addressed separately using a multi-reaction model capable of considering irreversible sorption. The transport of Br⁻ was adequately modeled with the CD equation, which assumed local equilibrium (Figure 14). The absence of a concentration perturbation during the interruption suggested that physical equilibrium had been attained. The dispersion coefficient was very similar to the single-species Cd experiment (Table 5). There was a perturbation in the concentration of ⁵⁷Co, however, the observed 5% increase suggested that desorption of ⁵⁷Co was occurring, perhaps as a result of competition for surface sites by $HCrO_4^-$. Therefore, the CD equation was used to model the breakthrough of ⁵⁷Co, resulting in a retardation coefficient of 2.35 ± 0.09 (Figure 14). This was less than that obtained for ⁵⁷Co(II)EDTA²⁻ in experiment 2 (Table 5), but distinct differences would be expected between the two species of Co-EDTA. This was consistent with field observations of ⁶⁰Co contaminated sites, where transport was believed to be accelerated due to the formation of Co(III)EDTA⁻ (Means et al., 1978a, Means et al, 1978b; Olsen et al., 1986). Co(II)EDTA²⁻ was adsorbed and oxidized, while only adsorption governed the transport of Co(III)EDTA⁻. In addition, the stability of Co(III)EDTA⁻ ($\log K = 39.8$) in solution is much greater than that of Co(II)EDTA²⁻ ($\log K = 18.2$), therefore, it should have less interaction with soil surfaces.

The modeling of ¹⁰⁹Cd was first attempted with the CD equation, though the significant perturbation following the flow interruption indicated the existence of nonequilibrium conditions. As expected, two-site modeling provided a better description of the breakthrough curve (Figure 14). Model output parameters obtained were similar to the single-species experiment (Table 5), with the retardation coefficient equal to 6.96, 45% mobile water, and a mass transfer coefficient, $\alpha = 0.06$ d⁻¹. The consistency of the modeling results between the three experiments suggested that interterractions between contaminants

55

was minimal. These investigations have further demonstrated that different mechanisms of geochemical interaction with the saprolite governed the transport of each species, thus, interfering reactions were minimal.

Transport modeling of $H^{51}CrO_4^-$

The transport of Cr(VI) was governed by retardation and irreversible sorption/ precipitation onto the soil surface, therefore multiple reaction types must be considered during the modeling routine. This type of modeling was considerably more complex than the two-site reversible model, which satisfactorily described the transport of chelated Cd and Co. Multiple retention mechanisms were parameterized in the Multi-Reaction Transport Model (MRTM), which was applied to the transport of Cr(VI) (Selim et al., 1990). Recall from the methods, that the partitioning between the solution and the solid was described by the Freundlich isotherm. The fitting routine was used to determine the linearity of sorption by optimizing parameters n, K, and k_s to the observed data. Linear sorption was also investigated by fixing n at unity, and optimizing k_s and K (which is equivalent to K_d when the adsorption isotherm is linear) to the observed data.

Irreversible sorption of ^{51}Cr was modeled using a first order rate of transfer, k_s. The proportion of mass remaining in the column was predicted by the model (Table 7), and the resultant profiles were close to the observed ^{51}Cr profiles, which measured irreversibly bound ^{51}Cr to the solid phase (Figures 17b and 18b).

Nonlinear sorption ($n < 1$) provided the best match to the data for the control and for the NOM-amended experiments (Figures 17a and 18a). This was consistent with batch studies showing the nonlinear sorption of behavior of Cr(VI) to these soils (Jardine et al., in review). Sorption in the organic-amended column was strongly nonlinear ($n = 0.39$), while the affinity coefficient K was very large; conditions which were indicative of the dramatic retardation and mass loss of Cr(VI) observed in this experiment (Table 7). In the control (experiment 4), the nonlinear fit closely matched the breakthrough curve (Figure 17a), and the fitted n was clearly indicative of nonlinear behavior ($n = 0.61$).

Table 7: Results of the application of the Multi-Reaction Transport Model (MRTM)[†] to the Cr(VI) displacement experiments.

Nonlinear sorption[♦]

Experiment	K^* (cm^3 g^{-1})	n	k_s (h^{-1})	$r^{2¶}$	Irreversibly Sorbed (%) Observed	Irreversibly Sorbed (%) Predicted[♦]
(3) Multi	$5.36 \pm 1.67^*$	$0.800 \pm 0.134^*$	$0.0111 \pm 0.0008^*$	0.95	51.0	48.2
(4) Control	15.6 ± 2.0	0.610 ± 0.047	0.0081 ± 0.0004	0.98	41.6	42.1
(5) NOM	65.0 ± 15.4	0.391 ± 0.080	0.0083 ± 0.0008	0.90	54.2	55.9

Linear sorption

Experiment	K^* (cm^3 g^{-1})	k_s (h^{-1})	$r^{2¶}$
(3) Multi	$2.85 \pm 0.23^*$	$0.0111 \pm 0.0008^*$	0.97
(4) Control	5.38 ± 0.35	0.0082 ± 0.0008	0.91
(5) NOM	9.91 ± 1.06	0.0093 ± 0.0011	0.81

♦ Uses Freundlich isotherm; K^* and n, empirical parameters from Freundlich equation; where $n = 1$ (linear sorption), K^* is the distribution coefficient; k_s is the irreversible first-order rate coefficient; * indicates 95% confidence interval; ¶ indicates the sum-of-least-squares (r^2) between the observed data and model-fitted curves.

† *Source:* Selim, H.M., M.C. Amacher, and I.K. Iskandar. 1990. Modeling the transport of heavy metals in soils. U.S. Army Corps of Engineers Monograph 90-2.

The fit to the multispecies (experiment 3) curve was slightly closer assuming linear sorption (Figure 19). Nonlinear sorption, however, also closely matched the shape of the initial breakthrough, and optimization of n yielded a value of 0.80 ± 0.135. The higher n may indicate more tendency toward linear behavior, compared to the other Cr(VI) experiments. It is possible that the unusual shape of the BTC in the multispecies experiment interferred with the fitting routine, and the subsequent determination of sorption linearity. The best indication of Cr(VI) sorption behavior was from the results of the control experiment, which were adequately described by nonlinear sorption, while the NOM experiment suggested that nonlinear adsorption may be enhanced in the presence of organics. Overall, the multiple reaction modeling was successful, and generally consistent. It appears that the assumption of nonlinear adsorption, with a high component of irreversibility, closely described the behavior of Cr(VI) through Melton Branch soils.

Lithologic variations may be responsible for the differential behavior of Cr(VI) between the multispecies and the other two single-species Cr experiments. During column dissection, lithologic differences were observed – the soils of columns 4 and 5, the control and NOM-amended columns, were dominated by unstructured clayey material, probably produced from weathering of the massive limestone-shale units, while structured shale saprolite was only present near the influent and effluent region. In addition, the clays were red, presumably indicative of a high oxidized iron content (Table 1). Column 3 (multispecies), however, was mostly fractured saprolite, with considerable black mottling along the bedding planes, which was probably Mn-oxide precipitates (Arnseth and Turner, 1988).

The shape of the Cr(VI) breakthrough curve in the multispecies experiment is quite unusual, which could have interfered with the fitting routine (Figure 19). The shape of the curve changes following the flow interruption, however, a direct relationship is difficult to support. A possible explanation for this behavior was the presence of a large root (5 grams), surrounded by a gray reduced clay (15 grams), immediately at the influent region of column 3. The root and clays were counted for radioactive decays separately; and while the clays did not have excessive ^{51}Cr, the root was enriched, on a per gram basis,
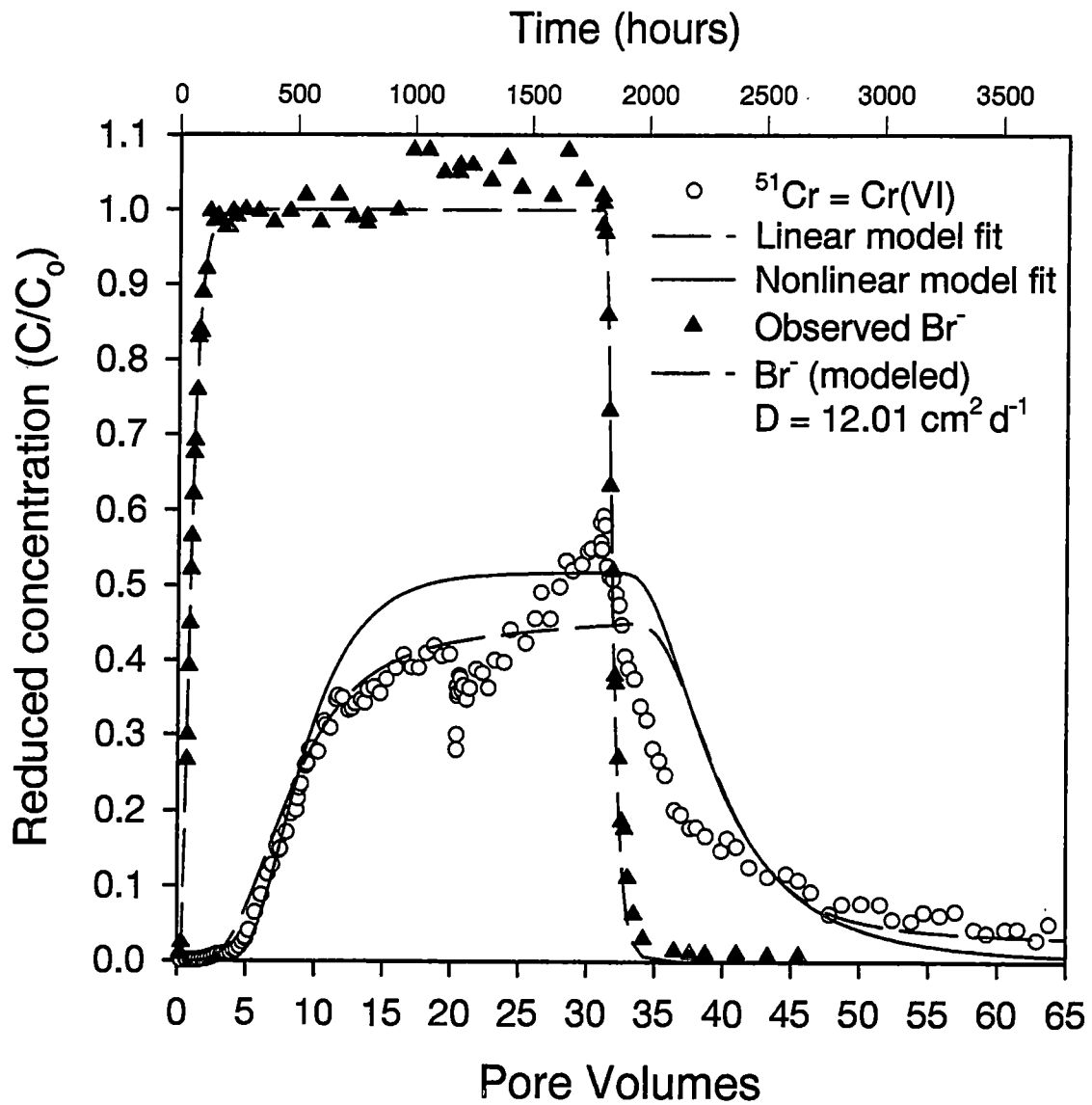
Figure 19. Experimental and modeled breakthrough curve of Br⁻ and ⁵¹Cr from the (triple) multispecies experiment (3). Modeling of Br⁻ was accomplished using the CD equation, while the Multi-Reaction Transport Model (MRTM) was applied to ⁵¹Cr to reproduce the observed irreversible sorption of Cr. Linear and nonlinear fits were both attempted, though the nonlinear fit was probably more appropriate. Irreversible sorption was modeled with a rate coefficient, k_s.

relative to the surrounding matrix. It seems plausible that unevenly distributed, *in situ* organic matter could affect the behavior of Cr(VI).

Geochemical controls on the transport of $H^{51}CrO_4^-$

The transport of chromate ($H^{51}CrO_4^-$) was dramatically retarded compared to that of co-contaminants Co(III)EDTA$^-$ and CdEDTA^{2-}, in addition to exhibiting considerable loss mass to the saprolite (Figure 14). A high degree of chemical nonequilibrium was also evident from the flow interruption. The irreversible sorption of ^{51}Cr may be a result of a reduction of Cr(VI) to $Cr^{3+}_{(aq)}$, where organic matter provided the necessary electrons for the reduction of Cr(VI). The enhanced retardation and loss of mass exhibited by the organic-amended column suggested that a mechanism of irreversible sorption was important, however, neither reduced Cr(III) nor organic carbon were detected in the effluent.

Direct evidence for the reduction of Cr(VI) was obtained using X-Ray Absorption Near-Edge Structure (XANES) on the dissected columns at the Stanford Synchrotron Radiation Laboratory (SSRL). XANES was used to identify the valence state of adsorbed ions, which confirmed the presence of Cr(III) on soil surfaces (Figure 20). In the influent region of the NOM-amended column, all of the adsorbed Cr was present as Cr(III), while in the control experiment, 60% of Cr near the influent was Cr(III), but both columns exhibited decreases in Cr(III) with depth, indicating the contribution of Cr(VI) adsorption. Mass balance with the ^{51}Cr profiles indicated that in the organic-amended column, 84.5% of the adsorbed ^{51}Cr was Cr(III), and 45.8% of the total influent Cr(VI) was reduced to Cr(III). In the control experiment, 58.8% of adsorbed ^{51}Cr is Cr(III), and a total of 24% of influent Cr(VI) was converted to Cr(III). The addition of organic matter to Column 5 clearly resulted in increased reduction of Cr(VI) to Cr(III). TOC extractions of the NOM-loaded and control soils demonstrated that organic carbon (OC) was enriched in the amended column by about 2.2 times; this implied that OC was also significant in the control experiment (Figure 21). XANES analyses have not yet been performed on the multispecies column 3. These results should provide an interesting comparison with those of Columns 4 and 5, due to the observed lithologic differences between the columns, even with the proximity of their *in situ* positions.
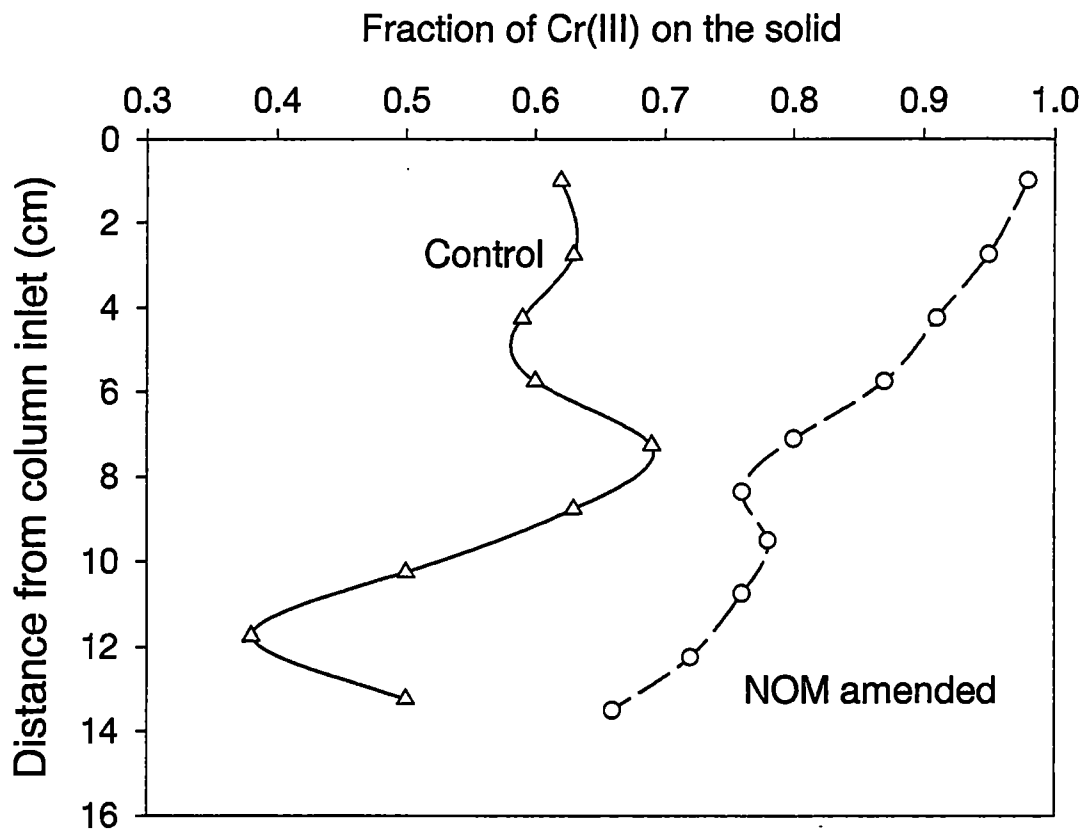
Figure 20. Fraction of Cr(III) on soil columns 4 and 5. X-ray Adsorption Near-Edge Spectroscopy (XANES) was used to determine the valence of adsorbed ^{51}Cr on dissected control and NOM-loaded columns (4 and 5, respectively). The NOM-amended column exhibited enhanced production of Cr(III), particularly in the influent region, which is clear evidence that Cr(VI) is reduced to Cr(III) in the presence of organic matter. Cr(III) may reside on soil surfaces as a tightly-held trivalent cation, or incorporated into Fe,Cr(OH)$_3$ solids. It is also apparent that sorption of Cr(VI), as HCrO$_4^-$ or CrO$_4^{2-}$ was prevalent.

Percent organic carbon on solid phase
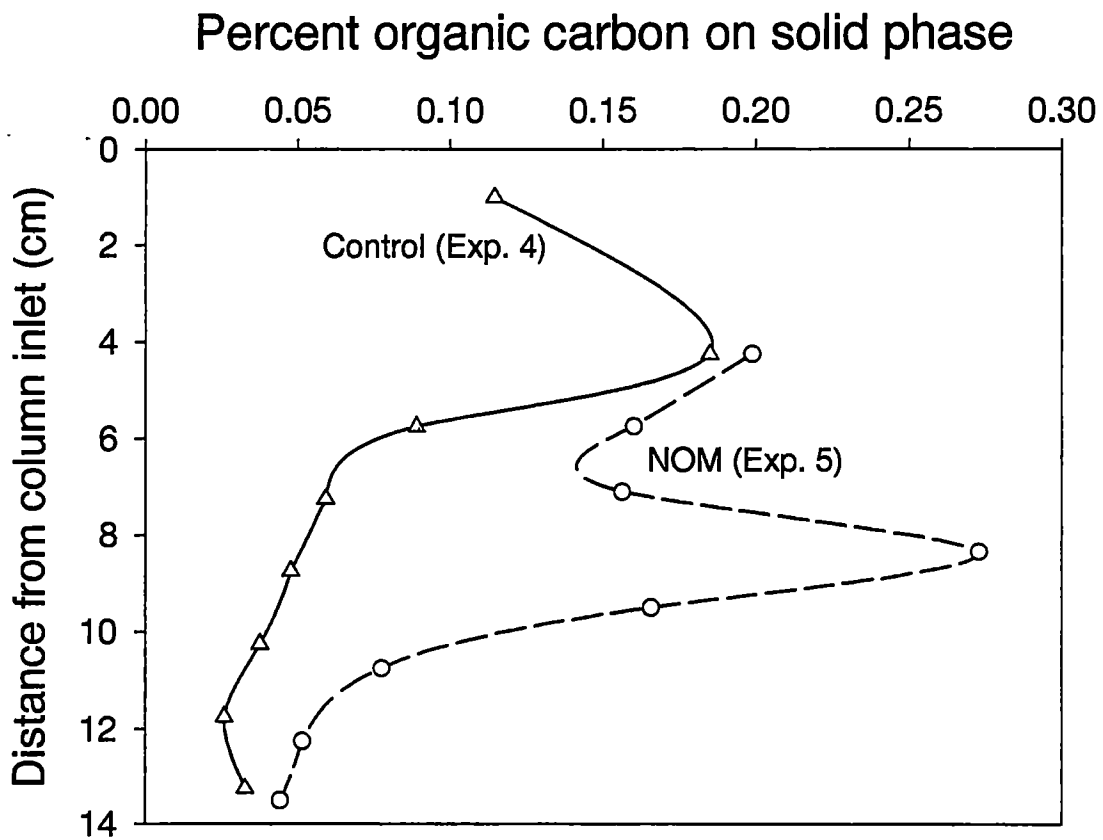
Figure 21. Fraction of organic carbon on soil columns 4 and 5. Extractions of organic carbon from solid phase indicate that the NOM-amendment was successful in enhancing the organics present in the soil (the total increase was 2.2 times greater than the ambient NOM). It is also apparent that significant organic carbon was already present in these soils (the control experiment 4). Therefore, it is probable that NOM also catalyzed the reduction of Cr(VI) to Cr(III) in the control experiment.

Solid-phase dissolution curves also provided insight into the behavior of $H^{51}CrO_4^-$. The dissolution curves for the control experiment were dominated by Al; the initial concentration of leached Al was 0.35 mM, which increased to 0.6 mM over 5 pore volumes, then dropped throughout the rest of the experiment (Figure 22). There was also an insignificant amount of Mn, similar to that observed in the Cd control, which was eluted early in the experiment. In the NOM-amended experiment, Mn (0.25 mM) was mobile at the initiation of the experiment, and increased to 0.38 mM, before dropping to zero by 25 pore volumes (Figure 23). This may be a result of reduction of surficial Mn(IV) oxides to aqueous Mn^{2+} in the presence of the added organic matter. Aqueous Al concentrations increased slightly and continued to leach throughout the experiment. Fe was immobile in both of these experiments.

A peak of Al (0.20 to 0.90 mM) was liberated early in the multispecies experiment, similar to that observed in the other Cr experiments (Figure 24). The liberation of Al(III) may be related to competition for exchangeable surface sites by Cr^{3+}. Al(III) is strongly adsorbed via cation exchange on soil surfaces, however, the relative affinity for the surface may be greater for Cr^{3+}, resulting in the displacement of Al(III). Al concentrations peaked early in the experiment, then decreased rapidly. The decrease, however, continued until only 15 pore volumes, when its mobility subsequently increased to again approach 1.0mM. The elution of the second pulse of Al may be a result of ligand exchange with $CdEDTA^{2-}$, as suggested by the similarity of this Al curve to that observed in the single-species $CdEDTA^{2-}$ experiment (1). The two distinct pulses of Al may indicate multiple sources of reactive soil Al, mobilized as a result of different contaminant interactions. Al is present on exchangeable surface sites, in phyllosilicates, and as coprecipitation products in Fe-oxides (Arnseth and Turner, 1988); therefore, it seems plausible that different rates and mechanisms would control their release. The exchange of the $EDTA^{4-}$ ligand between Al(III) and Cd^{2+} may be a result of any and all of these sources. Al on exchangeable surface sites may be readily available for ligand exchange and Al should also be liberated by the ligand-enhanced dissolution of Fe-oxides. The mobility of Si in these experiments could also suggest dissolution of phyllosilicates, or liberation of Si associated with Fe-oxides (Table 1).
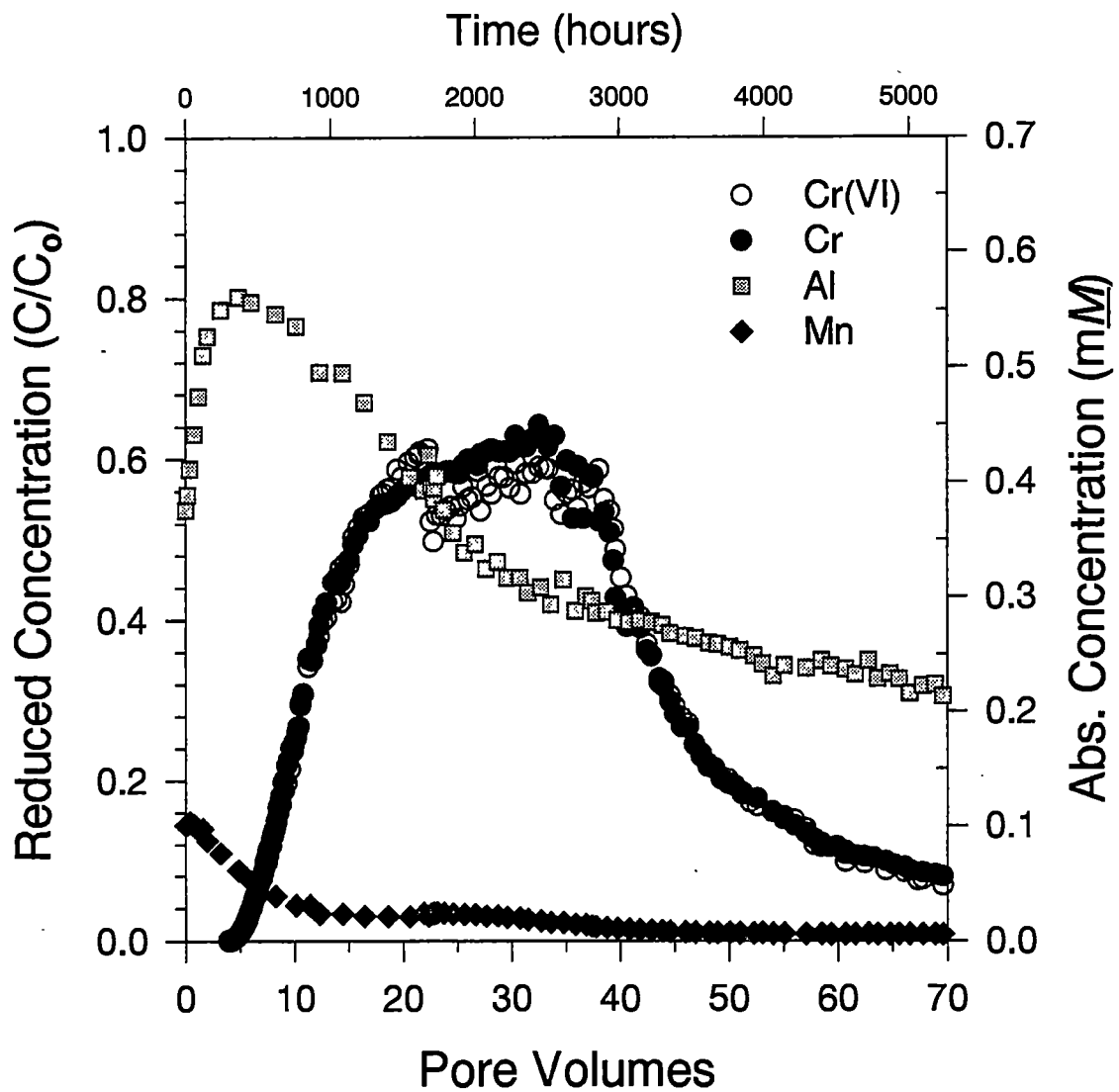
Figure 22. Solid phase dissolution/desorption in the Cr(VI) control experiment (4). Cr and Cr(VI) are shown for reference (left axis). Enhanced leaching of Al occurs in the early portion of the experiment (right axis). The reduction of Cr(VI) to Cr(III) may have dislodged adsorbed Al(III) from soil surfaces, producing the large peak early in the experiment. Only minor Mn, and essentially no Fe or DOC were liberated during the course of this experiment.
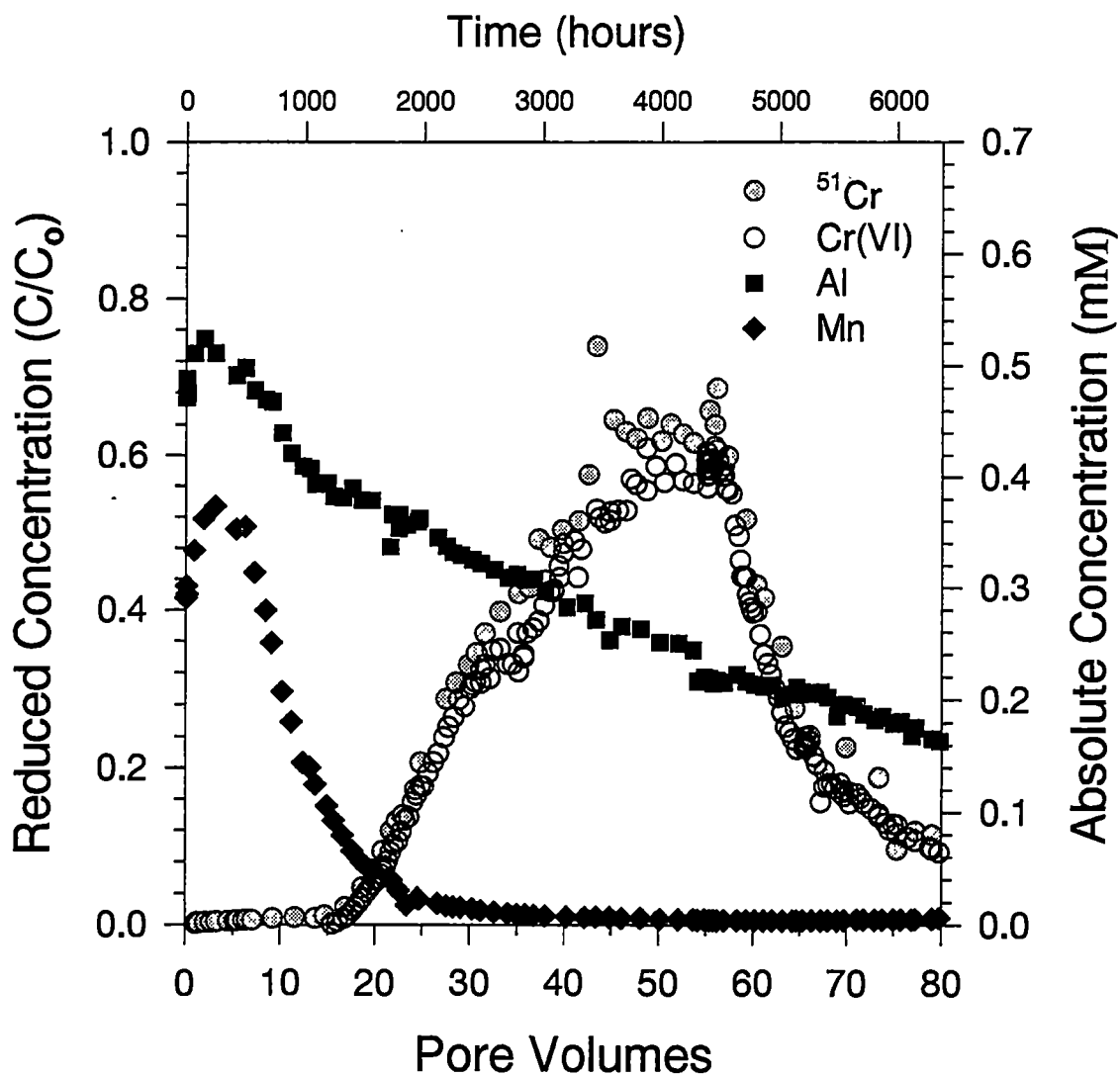
Figure 23. Solid phase dissolution/desorption in the NOM-amended Cr(VI) experiment (5). ^{51}Cr and Cr(VI) are shown for reference (left axis). Leaching of Al was prevalent throughout the experiment (right axis). A pulse of Mn was produced, perhaps due to reduction of surficial $Mn^{(IV)}O_2$ to $Mn^{2+}_{(aq)}$ in the presence of added organic matter. The concentrations of DOC and Fe were minimal in the effluent.
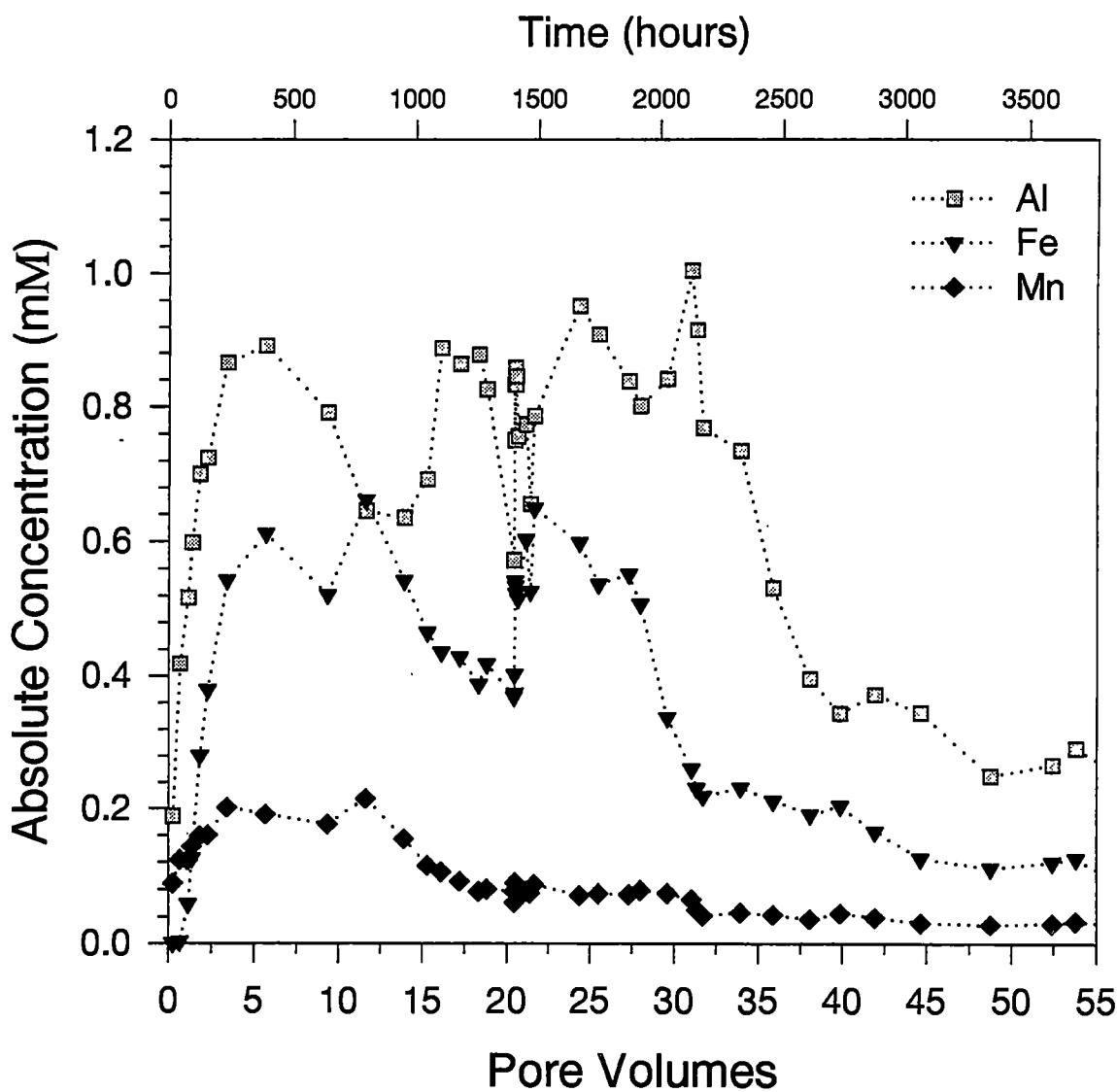
Figure 24. Solid phase dissolution/desorption in the multispecies experiment (3). The dissolution of Fe(III) was a result of the dissociation of CdEDTA^{2-} and production of Fe(III)EDTA$^-$. The positive perturbation associated with the flow interruption (20.41 pore volumes) indicated that this was a rate-limited process. The Al curve exhibited a sharp initial peak, which may be related to competition for surface adsorption by Cr(III). An additional pulse of Al was produced, which may be a result of the formation of Al(III)EDTA$^-$ from the dissociation of CdEDTA^{2-}. The decrease in Al during the interruption may be a result of competition by Fe for the EDTA^{4+} chelate. Dissolution of Mn was minor in the presence of influent Co(III)EDTA$^-$, which does not undergo significant adsorption or reaction with the solid surface.

As in the CdEDTA^{2-} experiment, a pulse of Fe was produced as a result of scavenging of the EDTA^{4-} ligand by surficial Fe and subsequent dissolution of the oxide, promoted by the greater aqueous stability of Fe(III)EDTA$^-$ over CdEDTA^{2-}. The flow interruption resulted in a drop in the concentration of mobile Al, and an increase in the concentration of Fe(III), probably due to competition for EDTA^{4-} by Fe, due to the greater stability of Fe(III)EDTA$^-$ (log K = 27) over Al(III)EDTA$^-$ (log K = 19). The patterns of Al and Fe dissolution suggest that the surface-mediated dissociation of CdEDTA^{2-} occurred even in the presence of Co(III)EDTA$^-$ and Cr^{3+}/HCrO$_4^-$. The dissolution curves from the multispecies experiment (Figure 24) were a combination of those observed during the CdEDTA^{2-} experiments, where the dissociation of CdEDTA^{2-} resulted in pulses of Fe and Al during the influent (Figure 6); and those observed in the Cr experiments, where a large pulse of Al was produced very early in the experiment (Figure 22). There was little evidence of dissociation or reactivity of Co(III)EDTA$^-$, likely due to the high aqueous stability (log K = 39.8) of Co(III)EDTA$^-$, and competition for surface sites by strongly-adsorbed HCrO$_4^-$. Eluted ^{57}Co was present exclusively as Co(III)EDTA$^-$.

4. Discussion

Heavy metal contamination from radionuclides and a variety of other toxic metals is common in government and industrial facilities. Organic solvents have been extensively used to remove surface metal contamination because they form strong anionic aqueous complexes. As indicated by this study and others, however, these types of solvents tend to accelerate the migration of metals into ground and surface waters. The behavior of divalent metals, such as Co^{2+} and Cd^{2+} is dramatically different as $EDTA^{4-}$ chelates.

$Co(II)EDTA^{2-}$ was oxidized to $Co(III)EDTA^-$ in the Melton Branch soils by a surface-mediated reaction (Figure 13). It was likely that the redox couple included Mn(VI) oxides, which are present as secondary deposits along relict bedding planes of the Melton Branch saprolite. A pulse of Mn was observed, and mass balance calculations indicated that the amount of Mn produced was nearly enough to account for the electron transfer as a result of this redox reaction. These calculations assume a simple stoichiometry, with two moles of $Co(III)EDTA^-$ produced from every mole of Mn(IV) reduced to $Mn^{2+}_{(aq)}$. The ratio was greater in batch experiments with saprolite (Jardine and Taylor, 1995a), and in packed pyrolusite columns (Jardine and Taylor, 1995b), which was attributed to the reoxidation of Mn^{2+} on reactive mineral surfaces. Regeneration of the solid surface was less important in these experiments, because reaction products were removed under flowing conditions. It is likely that the fresh, synthetic MnO_2-coated surface in the packed pyrolusite columns was very reactive to reoxidation and re-precipitation. The dominance of the redox reaction in the presence of Mn-oxides has important environmental implications, because of the high aqueous stability of the reaction product, $Co(III)EDTA^-$ (log K — 39.8), which may promote its migration from contaminated sites.

Further evidence exists in the accelerated rate of transport of $^{57}Co(III)EDTA^-$ observed in experiment 3 (R = 2.35 ± 0.09), compared with that of $^{57}Co(II)EDTA^{2-}$ in experiment 2 (R = 3.52). The single negative charge on $Co(III)EDTA^-$ should be less reactive with charged soil surfaces than that of $Co(II)EDTA^{2-}$, however, structural differences in the chelated complex dictates this behavior. Adsorption of anionic chelates is ligand-mediated, as evidenced by increased adsorption at lower pH, as the surface

charge becomes more positive (Girvin et al., 1993; Szecsody et al., 1994; Nowack and Sigg, 1997). The smaller ionic radius of Co^{3+} allows for complete sexidentate coordination with the ligand – Co(III) is coordinated to 4 carboxylate O and 2 ethylenediamine N (Table 2) (Girvin et al., 1993). The larger ionic radius of Co^{2+} does not allow for complete encirclement, and coordination is quinquedentate – a carboxylate O is free to completely bond with surface hydroxyls, resulting in stronger adsorption (Girvin et al., 1993). The flow interruption during the breakthrough of $^{57}Co(III)EDTA^-$ demonstrated the affinity for the surface by this complex (Figure 14). Though the interruption occurred on the adsorption limb of the BTC, the concentration of $^{57}Co(III)EDTA^-$ increased, which was indicative of desorption. The weak association of $^{57}Co(III)EDTA^-$ with the soil surface may have made it susceptible to desorption as a result of competition by the more strongly adsorbed $HCrO_4^-$ complex.

The migration of ^{60}Co from contaminated sites can be accelerated by the formation of $Co(III)EDTA^-$, therefore knowledge of the governing reaction rates is necessary to make accurate predictions of contaminant behavior. The flow interruption provided information about chemical and hydrologic controls on the rate of oxidation of $Co(II)EDTA^{2-}$ to $Co(III)EDTA^-$. A negative perturbation in both the ^{57}Co and reaction product $Co(III)EDTA^-$ curves indicated that the contaminant had not reached equilibrium with respect to transport through the column (Figure 13). A dual-region transport model was applied to the BTCs to estimate the rate of nonequilibrium exchange processes. The rate of the oxidation of $Co(II)EDTA^{2-}$ to $Co(III)EDTA^-$ may be limited by the rate of sorption and subsequent reaction, however, the perturbation in the Br^- BTC confirmed that (physical) nonequilibrium existed between preferential flow features and the matrix. Transport modeling resulted in similar estimates of the rate of mass transfer, 0.04 d^{-1} for Br^- and 0.03 d^{-1} for ^{57}Co, which suggested that the observed perturbations were a result of physical processes, rather than chemical. Other studies have shown that the oxidation of $Co(II)EDTA^{2-}$ to $Co(III)EDTA^-$ was rapid, and may occur on the time scale of minutes (Zachara et al., 1995; Jardine and Taylor, 1995a, b). There was also evidence of dissociation (around 15%) of the $Co(II)EDTA^{2-}$ complex (Figure 13), which could stabilize $^{60}Co^{2+}$ by adsorption in the subsurface environment. Dissociation of the $Co(II)EDTA^{2-}$ complex in the presence of Fe- and Al-oxides has been demonstrated (Girvin et al., 1993;

Szecsody et al., 1994; Zachara et al., 1995; Nowack and Sigg, 1997). However, the oxidation of $Co(II)EDTA^{2-}$ to $Co(III)EDTA^-$ in the presence of Mn-oxides was clearly the dominant process in the Melton Branch soils. Reaction with Mn oxides was rapid, and the affinity of $Co(III)EDTA^-$ for the solid surface was low, therefore disposal of ^{60}Co in chelated complexes has resulted in accelerated migration away from contaminated sites (Means et al., 1978a; Means et al., 1978b; Olsen et al., 1986). Careful consideration should therefore be given to disposal of metal-chelate complexes, due to the dramatic effects of chelates in promoting solubility (and mobility) of contaminants.

While the oxidation of $Co(II)EDTA^{2-}$ was rapid, rate-limited processes were prevalent in the transport of $CdEDTA^{2-}$. Migration of this complex can be stabilized by dissociation, but kinetic limitations in the governing reactions may result in an underestimation of predicted contaminant migration, when nonequilibrium processes are not considered. The rate of mass transfer of ^{109}Cd during transport, determined from the 2-site CD model, was within a narrow range $(0.06 - 0.08\ d^{-1})$ for separate undisturbed columns with different influent solutions. The flow interruptions were exclusively indicative of chemical nonequilibrium in two of the experiments (1 and 3), since there was no observed perturbation in the concentration of Br^- (Figures 4 and 14). However, the Co-Cd experiment (2), also exhibited physical nonequilibrium $(\alpha = 0.04\ d^{-1})$, which was included in the rate of mass transfer of ^{109}Cd $(0.08\ d^{-1})$ (Figure 8). The transport of ^{109}Cd exhibited significant retardation, with estimates from 6.5 - 7 for two experiments (1 and 3), while it was lower (R = 5) for Experiment 2 (Table 5), which may be related to the observed physical nonequilibrium, or column lithologic differences. The large perturbation in ^{109}Cd during the flow interruptions was indicative of kinetically-limited geochemical reactions with soil surfaces, an interpretation supported by greater R observed for ^{109}Cd versus ^{57}Co. The overall consistency of these results suggested that single-species transport modeling was appropriate, due to minimal interference during multispecies transport. Distinct chemical interactions with different soil minerals governed the transport of the different contaminants, thus circumventing competitive effects.

The dissociation of $CdEDTA^{2-}$ during transport was a result of adsorption and subsequent interactions with reactive oxide coatings in the Melton Branch saprolite (Figure 5). Because Cd^{2+} is a large

ion, it is likely that the CdEDTA^{2-} complex exists in quinquedentate coordination, as was hypothesized for the Co(II)EDTA^{2-} complex (Girvin et al., 1993). Adsorption occurs by exchange between surface hydroxyls and the uncoordinated carboxylate group, which is present in the quinquedentate coordination of EDTA^{4-} with metals. Adsorption of the CdEDTA^{2-} complex to reactive Fe-oxide surfaces in the saprolite resulted in the formation of Fe(III)EDTA$^-$. At the pH of this soil (4.0), Fe(III) was immobile, therefore the observed pulse of Fe indicated that the formation of Fe(III)EDTA$^-$ occurred specifically via a surface-mediated reaction (Figure 6). Adsorption of the EDTA^{4-} ligand to oxide surfaces resulted in the formation of a ternary surface complex, due to the affinity of Fe(III) for EDTA^{4-}, and the tendency to form an exceedingly stabile aqueous complex (log K $-$ 27. 7) (Nowack and Sigg, 1997). Surface-coordinated carboxylates reduce the charge on the metal, and thus weaken bonds to distal oxygens, resulting in enhanced rates of water exchange (Ludwig et al., 1995), and ultimately, dissolution and release of the complex into solution (Szecsody et al., 1994; Nowack and Sigg, 1997). This reaction occurs in several steps, any of which may be rate-limiting, including the adsorption of CdEDTA^{2-}, the rate of formation and release of the Fe(III)EDTA$^-$ complex, or the dissociation of Cd^{2+} from the complex. In a comparison of dissolution rates of hydrous ferric oxides (HFO) using several divalent metal-EDTA complexes, Nowack and Sigg (1997) inferred that the dissociation of the metal-EDTA complex was rate-limiting. They observed nonequivalent rates of Fe(III)EDTA$^-$ formation, which were proportional to the equilibrium constant of the divalent metal-chelate complex. Conversely, if the dissolution and release of surficial Fe was the rate-limiting step, then the rate of formation of Fe(III)EDTA$^-$ would be identical. This was observed for dissociation on crystalline geothite surfaces, where the rate-limiting step was a function of the greater bond strength of the ordered structure of geothite over the poorly crystalline to amorphous structure of HFOs (Nowack and Sigg, 1997). These relationships could have important positive implications for the predictability of contaminant dissociation reactions from thermodynamic equilibrium constants, when combined with well-constrained soil mineralogy. However, heterogeneities in the subsurface media may cause departure from predictions of thermodynamic equilibrium due to multi-region flow (Figure 7). The behavior of CdEDTA^{2-} and Fe(III)EDTA$^-$ during the flow interruption in this study provided information about rate-limiting processes.

The concentration perturbation suggested that the process occurred in two stages, the adsorption of CdEDTA^{2-}, followed by the formation and release of Fe(III)EDTA$^-$ from the soil surface. The consistently larger perturbation in Fe(III)EDTA$^-$, compared with CdEDTA^{2-}, suggested that the rate of formation and release of Fe-complexes was slower than the adsorption and dissociation of CdEDTA^{2-} (Figure 12).

The dissociation of CdEDTA^{2-} may have also been affected by interactions with soil Al. The mass of effluent EDTA^{4-} was greater than that associated with CdEDTA^{2-} and Fe(III)EDTA$^-$, and the pulse of Al$_{(aq)}$ produced during the experiments suggested that Al(III)EDTA$^-$ was also formed (Figure 6). Al, however, was mobile and leaching from the exchangeable surface complex before the initiation of the experiment, therefore, the exchange of EDTA^{4-} may have occurred in aqueous solution. The Al(III)EDTA$^-$ complex is thermodynamically favored (log K – 19.1) over CdEDTA^{2-} (log K – 18.2). However, the increasing concentration of Al$_{(aq)}$ throughout the influent pulse suggested that this reaction was also surface-mediated. Adsorption of the EDTA^{4-} ligand may have promoted desorption of Al from the surface complex, due to the greater aqueous stability of Al(III)EDTA$^-_{(aq)}$, which has been observed by Girvin et al. (1993). The source of soil Al is multivariate, and as much as 20% of Fe-oxides may be in the form of coprecipitated Al (Table 1), therefore it is likely that dissolution of oxides promoted by the EDTA^{4-} ligand may have liberated Al, as well as Fe(III). The mobility of Si in these experiments also suggests the possibility of phyllosilicate dissolution, though Si may also be associated with Fe-oxides (Table 1). All of these reactions have important remediation implications, because the dissociation of CdEDTA^{2-} on soil surfaces may inhibit the migration of Cd from waste disposal sites by the adsorption of Cd^{2+} as a divalent reactive cation. The high aqueous stability of Fe(III)EDTA$^-$, in particular, suggests that Fe can be very effective at stabilizing metals under acidic conditions.

These experiments demonstrated that Cr(VI), present as anionic chromate (HCrO$_4^-$), was very reactive with the Melton Branch soils. The transport of Cr(VI) was greatly retarded, and resulted in irreversible sorption or precipitation of around 50% of the influent in all experiments (Figure 17, Table 6). Further evidence of kinetically-limited geochemical interactions was provided by the flow interruptions, which exhibited dramatic perturbations in the concentration of [51]Cr (Figures 19 and 17). A redox reaction

72

resulted in the formation of Cr(III), which as a trivalent cation, was irreversibly sorbed to the solid surface. A column amended with natural organic matter, which increased its OC content by 2.2 times, exhibited significant additional retardation and irreversibility (Figure 18), suggesting that organic matter provided the electrons to reduce Cr(VI) to Cr(III). XANES analyses indicated that 54% of influent ^{51}Cr remained associated with the organically-amended solid surface, of which 85% was Cr(III), while in the control experiment, 42% remained on the solid, of which 59% was Cr(III) (Figure 20). The reduction of Cr(VI) was therefore enhanced in the presence of additional organic matter, and TOC analyses of the control and amended soils demonstrated that the organic fraction was also significant in the control experiment (Figure 21). The release of surficial Al(III) observed during these experiments may be a result of cation exchange induced by the greater affinity for the surface by Cr(III) (Figure 22). The XANES analyses demonstrated that irreversible adsorption of HCrO$_4^-$ was also important during transport through the Melton Branch soils.

Multi-reaction transport modeling (MRTM) successfully reproduced experimental results. The shape of the breakthrough curve was reproduced using a constant rate of irreversible mass transfer, resulting in an estimate of adsorbed ^{51}Cr, which was close to that observed from radioactive counting of the soil sections (Figures 17b and 18b). Sorption was best represented by the nonlinear Freundlich isotherm, assuming equilibrium conditions. Adsorption of Cr(VI) and reduction to Cr(III) in the presence of organics controlled the transport of HCrO$_4^-$ even in the presence of reactive mixed oxides and hydroxides. Organics were very effective at reducing and stabilizing the highly mobile and toxic Cr(VI), as there was no evidence of recovery of Cr(III) in the eluted samples. These results have implications toward simple remedial strategies, such as the use of charcoal barriers to catalyze the reduction of mobile Cr(VI) to the less toxic Cr(III).

5. Conclusions

These studies characterized multispecies contaminant reactions with soil minerals, all of which resulted in the alteration of reactive soil surfaces due to exchange and desorption of surface cations, ligand-promoted dissolution, or dissolution as a result of redox reactions with contaminants. The reactive minerals in the Melton Branch saprolite were secondary oxides of Fe, Al, and Mn along bedding planes and fracture zones, which were deposited during previous groundwater interactions and/or weathering processes. The clay mineralogy may have also contributed Al and Si to the system. Effluent curves of reactive soil metals, Fe, Mn, and Al were used to characterize governing reactions. The adsorption of $CdEDTA^{2-}$ resulted in the dissolution of soil oxides of Fe^{3+} and Al^{3+} to form complexes with the $EDTA^{4-}$ chelate, due to the greater stability of these complexes over $CdEDTA^{2-}$. The formation of $Al(III)EDTA^{-}$ is probably also a result of aqueous and surficial exchange reactions. These reactions may aid in the stabilization of Cd^{2+}, because uncomplexed, divalent Cd^{2+} is more likely to become adsorbed onto soil minerals. An association between Cd and organic matter in the form of large roots within the columns, as well as with surrounding reduced clays, may indicate that adsorption of Cd to organics may be significant. These studies could have applications to remediation strategies, since a simple iron wall may effectively retard the migration of chelated Cd, due to the high stability of the $Fe(III)EDTA^{-}$ complex. However, significant retardation of Cd was observed, indicative of kinetic limitations in the rate of geochemical reactions, which were also observed during the flow interruptions. Therefore, it is important to quantify the extent of nonequilibrium to constrain predictions of Cd migration. The behavior of Cd may be similar to other chelated divalent metals, therefore, this strategy may also be successful for their stabilization. The Melton Branch soil mineralogy is well-characterized, which should help to extrapolate between this experiment and other results from the literature, and thus improve future predictions of contaminant migration.

The oxidation of organics was dominant in catalyzing the reduction of toxic, mobile Cr(VI) to Cr(III) in a mixed, heterogeneous system with Mn oxides and other soil minerals. Trivalent Cr^{3+} was irreversibly sorbed and/or precipitated, thus, Cr was stabilized as a result of these interactions with organic

matter. Significant irreversible sorption of anionic $HCrO_4^-$ was also observed. Kinetic limitations were present in the transport of Cr(VI), which should be considered to adequately predict the stabilization of Cr. In addition, the observed nonlinear sorptive characteristics may also interfere with the accuracy of predictions of contaminant migration.

The transport of Co(II)EDTA^{2-} resulted in rapid oxidation to Co(III)EDTA$^-$ in a reaction with surficial Mn(IV), which was liberated as $Mn^{2+}_{(aq)}$. Fe and Al oxides may have dissociated around 15% of the Co-EDTA complex. However, the redox reaction with Mn-oxides was dominant, and occurred rapidly, which may cause accelerated transport of ^{60}Co from waste disposal sites, due to the high aqueous stability of Co(III)EDTA$^-$.

The behavior of environmental contaminants was dependent upon interactions with the local mineralogy and soil organic matter, therefore, adequate characterization of these interactions is paramount to accurately predict the transport of chelated contaminants. The presence of soil organic matter governed the stabilization of Cr(VI), while Mn-oxides resulted in accelerated migration of Co. An additional consideration is kinetic limitations on the rate of contaminant/soil reactions, due to either chemical processes, or physical interaction during flow through structured media, which were demonstrated by the interruption of flow during the experiments. Solute segregation into micropores is known to account for slow leaching of contaminants during pump-and-treat remediation techniques. It was also apparent that chemical nonequilibrium as a result of rate-limited sorption or transformation reactions can affect predictions of contaminant transport. In the case of CdEDTA2-, kinetic limitations on the rate of contaminant dissociation could result in faster transport than would be predicted, assuming equilibrium conditions. Kinetic limitations were also observed in the transport of Cr(VI), in addition to nonlinear sorption, which may complicate predictions of contaminant stabilization.

References

References

Akratanankul, S., L. Boersma, and G.O. Klock. 1983. Sorption processes in soils as influenced by pore water velocity: 2. Experimental results. Soil Science 135 (6): 331-341.

Anderson, L.D., D.B. Kent, and J.A. Davis. 1994. Batch experiments characterizing the reduction of Cr(VI) using suboxic material from a mildly reducing sand and gravel aquifer. Environ. Sci. Technol. 28: 178-185.

Arnseth, R.W., and R.S. Turner. 1988. Sequential extraction of iron, manganese, aluminum, and silicon in soils from two contrasting watersheds. Soil Sci. Soc. A. J. 52: 1801-1807.

Ayres, J.A. 1971. Equipment decontamination with special attention to solid waste treatment, survey report. BNWL-B-90, Batelle Northwest Laboratories, Richland, WA.

Bartlett, R., and B. James. 1979. Behavior of chromium in soils: III. Oxidation. J. Environ. Qual. 8: 31-35.

Bartlett, R.J. and J.M. Kimble. 1976. Behavior of chromium in soils: II. Hexavalent forms. J. Environ. Qual. 5: 383-386.

Bowers, A.R., and C.P. Huang. 1986. Adsorption characteristics of metal-EDTA complexes onto hydrous oxides. J. Colloid Interface Sci. 110: 575-590.

Brooks, S.C., D.L. Taylor, and P.M. Jardine. 1996. Reactive transport of EDTA-complexed cobalt in the presence of ferrihydrite. Geochimica et Cosmochimica Acta. 60: 1899-1908.

Brusseau, M.L., P.S.C. Rao, R.E. Jessup, and J.M. Davidson. 1989. Flow interruption: A method for investigating sorption nonequilibrium. J. Contam. Hydrol. 4: 223-240.

Brusseau, M.L., R.E. Jessup, and P.S.C. Rao. 1991. Nonequilibrium sorption of organic chemicals: Elucidation of rate-limiting processes. Environ. Sci. Technol. 25: 134-142.

Brusseau, M.L., Q. Hu, and R. Srivastava. 1997. Using flow interruption to identify factors causing nonideal contaminant transport. J. Contam. Hydrol. 24: 205-219.

Chang, H.C., and E. Matijevic. 1983. Interactions of metal hydrous oxides with chelating agents: III. Dissolution of hematite. J. Colloid Interface Sci. 92: 479-488.

Chubin, R.G., and J.J. Street. 1981. Adsorption of cadmium on soil constituents in the presence of complexing ligands. J. Environ. Qual. 10: 225-228.

Cropper, S.C. 1998. Experimental measurements of capillary pressure-saturation drainage of air and DNAPL in fractured shale saprolite. MS thesis, Dept. of Geological Sciences, University of Tennessee, Knoxville.

Cutshall, N.C., I.L. Larsen, and C.R. Olsen. 1983. Direct analysis of Pg-210 in sediment samples: Self-absorption corrections. Nuclear Instruments and Methods 206: 309-312.

Davis, A., and R.L. Olsen. 1995. The geochemistry of chromium migration and remediation in the subsurface. Ground Water 33(5): 759-768.

Dunnivant, F.M., P.M. Jardine, D.L. Taylor, and J.F. McCarthy. 1992. Cotransport of cadmium and hexachlorobiphenyl by dissolved organic carbon through columns containing aquifer material. Environ. Sci. Technol. 26: 360-368.

Eary, L.E., and D. Rai. 1991. Chromate reduction by subsurface soils under acidic conditions. Soil Sci. Soc. A. J. 55: 676-683.

Elliott, H.A. and C.M. Denneny. 1982. Soil adsorption of cadmium from solutions containing organic ligands. J. Environ. Qual. 11: 658-662.

Fendorf, S.E., and R.J. Zasoski. 1992. Chromium(III) oxidation by δ-MnO_2. 1. Characterization. Environ. Sci. Technol. 26: 79-85.

Gaber, H.M., W.P. Inskeep, S.D. Comfort, and J. M. Wraith. 1995. Nonequilibrium transport of atrazine through large intact soil cores. Soil Sci. Soc. Am. J. 59: 60-67.

Girvin, D.C., P.L. Gassman, and H. Bolton. 1993. Adsorption of aqueous cobalt ethylenediaminetetraacetate by δ-Al_2O_3. Soil Sci. Soc. A. J. 57: 47-57.

Haun, D.B, L.D. McKay, and J.F. McCarthy. 1998. The role of electrostatic attachment on particle trasnport in fractured shale saprolite. Abstract presented at Conference on Mass Transport in Fractured Aquifers and Aquitards, University of Copenhagen, Denmark, May 14-16, 1998.

Harton, A. 1996. Influence of flow rate on transport of bacteriophage in a column of highly weathered and fractured shale. MS thesis, Dept. of Geological Sciences, University of Tennessee, Knoxville.

Hatcher, R.D., Jr., P.J. Lemiszki, R.B. Drier, R.H. Ketelle, R.R. Lee, D.A. Leitzke, W.M. McMaster, J.L. Foreman, and S.Y. Lee. 1992. Status report on the geology of the Oak Ridge Reservation, Oak Ridge National Laboratory, ORNL/TM-12074. pp.

Jabro, J.D., E.G. Lotse, K.E. Simmons, and D.E. Baker. 1991. A field study of macropore flow under saturated conditions using a Br- tracer. J. Soil and Water Conserv. September-October: 376-380.

James, B.R. and R.J. Bartlett. 1983. Behavior of chromium in soils. V. Fate of organically complexed Cr(III) added to soil. J. Environ. Qual. 12: 169-172.

James, B.R. and R.J. Bartlett. 1983. Behavior of chromium in soils. VI. Interactions between oxidation-reduction and organic complexation. J. Environ. Qual. 12: 173-176.

Jardine, P.M., G.V. Wilson, and R.J. Luxmoore. 1988. Modeling the transport of inorganic ions through undisturbed soil columns from two contrasting watersheds. Soil Sci. Soc. Am. J. 52:1252-1259.

Jardine, P.M., G.V. Wilson, and R.J. Luxmoore. 1990. Unsaturated solute transport through a forest soil during rain storm events. Geoderma 46: 103-118.

Jardine, P.M., G.K. Jacobs, and J.D. O'Dell. 1993. Unsaturated transport processes in undisturbed heterogeneous porous media. II. Co-Contaminants. Soil Sci. Soc. Am. J. 57: 954-962.

Jardine, P.M., and D.L. Taylor. 1995a. Fate and Transport of Ethylenediaminetetraacetate Chelated Contaminants in Subsurface Environments. *In* D.L. Sparks (ed.) Soil Environmental Chemistry. Elsevier Science Publishers, The Netherlands (Geoderma 67: 125-140).

Jardine, P.M., and D.L. Taylor. 1995b. Kinetics and mechanisms of Co(II)EDTA oxidation by pyrolusite. Geochimica et Cosmochimica Acta. 59: 4193-4203.

Jardine, P.M., S.E. Fendorf, M.A. Mayes, I.L. Larsen, S.C. Brooks, and W.B. Bailey. Fate and transport of hexavalent chromium in undisturbed heterogeneous soil. *Submitted to* Environ. Sci. Technol., 1998.

Jury, W.A., Gardner, W.R., and W.H. Gardner. 1991. Solute transport in soil. Chapter 7, Soil Physics (5th Edition). John Wiley & Sons, Inc., New York. pp. 218-264.

Kent, D.B., J.A. Davis, L.C.D. Anderson, and B.A. Rea. 1994. Transport of chromium and selenium in the suboxic zone of a shallow aquifer: Influence of redox and adsorptin reactions. Water Resour. Res. 30: 1099-1114.

Kent, D.B., J.A. Davis, L.C.D. Anderson, and B.A. Rea. 1995. Transport of chromium and selenium in a pristine sand and gravel aquifer: Role of adsorption processes. Water Resour. Res. 31: 1041-1050.

Koch, S. and H. Fluhler. 1993. Nonreactive solute transport with micropore diffusion in aggragated porous media determined by a flow-interruption method. J. Contam. Hydrol. 14: 39-54.

Kooner, Z.S., P.M. Jardine, and S. Feldman. 1995. Competitive surface complexation reactions of sulfate and natural organic carbon on soil. J. Environ. Qual. 24: 656-662.

Kressman, T.R.E., and J.A. Kitchner. 1949. Cation exchange with a synthetic phenolsulphonate resin. Discuss. Faraday Soc. 7: 90-103.

Kunin, R., and R.J. Myers. 1947. Rates of anion exchange in ion-exchange resins. J. Phys. Colloid Chem. 51: 1111-1129.

Larsen, I.L. and N.H. Cutshall. 1981. Direct determination of Be-7 in sediments. Earth and Planetary Science Letters 54: 379-384.

Larsen, I.L. and S.Y. Lee. 1983. Nondestructive photon analysis of Am-241 in soils and sediment utilizing self-absorption corrections. Jour. Radioanalytical Chemistry 79(1): 165-169.

Lee, L.S., P.S.C. Rao, M.L. Brusseau, and R.A. Ogwada. 1988. Nonequilibrium sorption of organic contaminants during flow through columns of aquifer materials. Environmental Toxicology and Chemistry 7: 779-793.

Li, Z., and L.M. Shuman. 1996. Extractability of zinc, cadmium, and nickel in soils amended with EDTA. Soil Science. 161: 226-231.

Ludwig, C., W.H. Casey, and P.A. Rock. 1995. Predictions of ligand-promoted dissolution rates from the reactivities of aqueous complexes. Nature 375: 44-47.

McKay, L.D., R.W. Gillham, and J.A. Cherry. 1993. Field experimnets in a fractured clay till. 2. Solute and colloid transport. Water Res. Res. 29: 3879-3890.

Means, J.L., D.A. Crerar, and J.O. Dugiud. 1978a. Migration of radioactive wastes: Radionuclide mobilization by complexing agents. Science (Washington, D.C.) 200: 1477-1481.

Means, J.L., D.A. Crerar, M.P. Borcsik, and J.O. Dugiud. 1978b. Adsorption of Co and selected actinides by Mn and Fe oxides in soils and sediments. Geochimica et Cosmochimica Acta. 42: 1763-1773.

Moore, G.K. 1989. Groundwater parameters and flow systems near Oak Ridge National Laboratory. ORNL/TM-11368. Oak Ridge National Laboratory, Oak Ridge, TN. 93 pp.

Murali, V. and A.G. Aylmore. 1980. No-flow equilibrium and adsorption dynamics during ionic transport in soils. Nature 283: 467-469.

National Research Council. 1974. Committee on Biological Effects of Atmospheric Pollutants. Chromium. National Academy of Science, Washington, DC.

Nkedi-Kizza, P., J.W. Biggar, H.M. Selim, M. Th. van Genuchten, P.J. Wierenga, J.M. Davidson, and D.R. Nielsen. 1984. On the equivalence of two conceptual models for describing ion exchange during transport through an aggregated oxisol. Water Resouce. Res. 20: 1123-1130.

Nowack, B., and L. Sigg. 1997. Dissolution of Fe(III) (hydr)oxides by metal-EDTA complexes. Geochimica et Cosmochimica Acta. 61: 951-963.

O'Brien, R., P.M. Jardine, J.P. Gwo, L.D. McKay, and A. Harton. Quantifying multiregion flow and transport in fractured saprolites. Unpublished report, 1996.

Olsen, C.R., P.D. Lowry, S.Y. Lee, I.L. Larsen, and N.H. Cutshall. 1986. Geochemical and environmental processes affecting radionuclide migration from a formerly used seepage trench. Geochimica et Cosmochimica Acta. 50: 593-607.

Parker, J.C., and M. Th. van Genuchten. 1984. Determining transport parameters from laboratory and field tracer experiments. Virginia Agric. Exp. Stn. Bull. 84-3.

Parker, D.R., L.W. Zelazny, and T.B. Kinraide. 1987. Improvements to the program GEOCHEM. Soil Sci. Am. J. 51:488-491.

Patterson, R.R., S. Fendorf, M. Fendorf. 1997. Reduction of hexavalent chromium by amorphous iron sulfide. Environ. Sci. Technol. 31: 2039-2044.

Penfield, C. Petrographic, mineralogical, and chemical characterization of soil and saprolite at the SWSA-7 site, Oak Ridge National Laboratory, Tennessee. Unpublished report, 1998.

Reedy, O.C., P.M. Jardine, G.V. Wilson, and H.M. Selim. 1996. Quantifying the diffusive mass transfer of nonreactive solutes in columns of fractured saprolite using flow interruption. Soil Sci. Soc. A. J. 60: 1376-1384.

Richard, F.C., and A.C.M. Bourg. 1991. Aqueous geochemistry of chromium: A review. Wat. Res. 25(7): 807-816.

Rothschild, E.R., D.D. Huff, B.P. Spalding, S.Y. Lee, R.B. Clapp, D.A. Lietzke, R.G. Stansfield, N.D. Farrow, C.D. Farmer, and I.L. Munro. 1984. Characterization of soils at proposed solid waste storage area (SWSA) 7. ORNL/TM-9326. Oak Ridge National Laboratory, Oak Ridge, TN. 158 pp.

Selim, H. M., J. M. Davidson, and R.S. Mansell. 1976. Evaluation of a two-site adsorption model for describing solute transport in soils. p. 444-448. In Summer Comput. Simul. Conf., Washington, D.C. 12-14 July 1976. Simulation Councils, La Jolla, CA.

Selim, H.M., M.C. Amacher, and I.K. Iskandar. 1990. Modeling the transport of heavy metals in soils. U.S. Army Corps of Engineers Monograph 90-2.

Smettem, K.R.J. 1984. Soil-water residence time and solute uptake. 3. Mass transfer under simulated rainfall conditions in undisturbed soil cores. J. Hydrology 67: 235-248.

Solomon, D.K., J.D. Marsh, I.L. Larsen, D.S. Wickliff, and R.B. Clapp. 1991. Transport of contaminants during storms in the White Oak Creek and Melton Branch watersheds. Environmental Sciences Publication No. 3395; ORNL/TM-11360. Oak Ridge National Laboratory, Oak Ridge, Tennessee. 127 pp.

Sposito, G. and S.V. Mattigod. 1980. GEOCHEM: A computer program for the calculation of chemical equilibria in soil solutions and other natural water systems. Kearney Foundation of Soil Science. University of CA.

Szecsody, J.E., J.M. Zachara, and P.L. Bruckhart. 1994. Adsorption-dissolution reactions affecting the distribution and stability of Co(II)EDTA in iron-oxide coated sand. Environ. Sci. Technol. 28: 1706-1716.

Tardy, Y., and D. Nahon. 1985. Geochemistry of laterites, stability of Al-goethites, Al-hematite, and Fe^{3+}-kaolinite in bauxites and ferricretes: An approach to the mechanism of concretion formation. Am. J. Sci. 285: 865-903.

Taylor, D.L. and P.M. Jardine. 1995. Analysis of cobalt(II)EDTA and cobalt(III)EDTA in pore water by ion chromotography. J. Environ. Quality 24: 789-792.

U.S. Environmental Protection Agency. 1978. Review of the environmental effects of pollutants: III. Chromium. U.S. EPA Rep. 600/1-78-023. U.S. Dep. Commerce, Springfield, VA.

Van Genuchten, M. Th., and P.J. Wierenga. 1976. Mass transfer studies in sorbing porous media. I. Analytical solutions. Soil Sci. Soc. Am. J. 40: 473-479.

Van Genuchten, M. Th., and J. C. Parker. 1984. Boundary conditions for the displacement experiments through short laboratory soil columns. Soil Sci. Soc. Am. J. 48: 703-708.

Warwick, P., A. Hall, V. Pashley, J. Van der Lee, and A. Maes. Zinc and cadmium mobility in sand: Effects of pH, speciation, cation exchange capacity (CEC), humic acid and metal ions. Chemosphere 36: 2283-2290.

Wilkins, B.J., N. Brummel, and J.P.G. Loch. 1998. Influence of pH and zinc concentration on cadmium sorption in acid, sandy soils. Water, Air, and Soil Pollution 101: 349-362.

Wilson, G.V. and R.J. Luxmoore. 1988. Infiltration, macroporosity, and mesoporosity distributions on two forested watersheds. Soil Sci. Soc. Am. J. 52: 329-335.

Wilson, G.V., J.M. Alfonsi, and P.M. Jardine. 1989. Spatial variability of saturated hydraulic conductivity of the subsoil of two forested watersheds. Soil Sci. Soc. Am. J. 53: 679-685.

Wilson, G.V., P.M. Jardine, and J. P. Gwo. 1992. Modeling the hydraulic properties of a multiregion soil. Soil Sci. Soc. Am. J. 56: 1731-1737.

Wilson, G.V., P.M. Jardine, J.D. O'Dell, and M. Collineau. 1993. Field-scale transport from a buried line source in variably saturated soil. J. Hydrol. 145: 83-109.

Zachara, J.M., C.C. Ainsworth, C.E. Cowan, and C.T. Resch. 1989. Adsorption of chromate by subsurface soil horizons. Soil Sci. Soc. A. J. 53: 418-428.

Zachara, J.M., P.L. Gassman, S.C. Smith, and D.L. Taylor. 1995. Oxidation and adsorption of Co(II)EDTA^{2-} complexes in subsurface materials with iron and manganese oxide grain coatings. Geochimica et Cosmochimica Acta 59: 4449-4463.

Vita

Melanie Anna Mayes was born in Lebanon, Missouri on June 15, 1972. She attended public school, until graduation from Lebanon High School in May, 1990. She entered the University of Missouri at Columbia, Missouri in August of 1990 to pursue a journalism degree, but an introductory geology class piqued her interest in the geological sciences. Her study of geology culminated with a Bachelor of Science in December of 1995, with an emphasis on hydrology and geochemistry. Following graduation, she moved to Tennessee to participate in the Science and Engineering Research Semester, sponsored by the Department of Energy at Oak Ridge National Laboratory. In August of 1996, she entered the Master's program in Geological Sciences at the University of Tennessee, Knoxville. She conducted research in contaminant transport with subsurface materials, receiving her Master of Science degree in May of 1999. Her plans for the immediate future include a postgraduate internship at ORNL to continue research in contaminant transport.